Predicting Circulation and Dispersion Near Coastal Power Plants: Applications Using Models TEA and ELA

by

E. Eric Adams
and
Douglas J. Cosler

Energy Laboratory Report No. MIT-EL 87-008
December 1987

Predicting Circulation and Dispersion Near Coastal Power Plants: Applications Using Models TEA and ELA

by

E. Eric Adams

and

Douglas J. Cosler

Energy Laboratory

and

R. M. Parsons Laboratory
for
Water Resources and Hydrodynamics
Department of Civil Engineering

Massachusetts Institute of Technology
Cambridge, Massachusetts 02139

Sponsored by

Northeast Utilites Service Company
and
New England Power Company

under

M.I.T. Energy laboratory Electric Utility Program
Energy Laboratory Report No. MIT-EL 87-008

December 1987

Abstract

This report describes how a pair of two-dimensional numerical models (TEA and ELA) have been coupled to simulate thermal plume dispersion in the vicinity of coastal power plants. The work follows previous study by Kaufman and Adams (1981), but differs from most previous studies in that near field mixing is represented explicitly by specifying entrainment and mixed discharge fluxes as model boundary conditions. The models have been applied to two power plants—Brayton Point Generating Station and Millstone Nuclear Power Plant. Comparison against field data shows generally good agreement in both cases, and computational costs are reasonable. Several areas for additional research have been identified.

ACKNOWLEDGMENTS

The work described in this report was performed in connection with the project "Numerical Models of Coastal Circulation and Dispersion with Application to Power Plant Discharges" through the MIT Energy Laboratory Electric Utility Program. The authors wish to thank Northeast Utilities Service Company and New England Power Company for their generous support both of this project and its predecessor, "Near and Far Field Interactions of Thermal Discharges." These two projects, along with MIT Sea Grant, helped support the development of the models TEA and ELA upon which this work was based. We also wish to thank the project steering committee members Ernesto Lorda. Linda Bireley, William Renfro, and Andrew Aitken for their close cooperation in this work, as well as Keith Stolzenbach, Joannes Westerink, Antonio Baptista, Rick Kossik, and others at MIT who were influential in various phases of model development. Finally, we appreciate the assistance of Read Schusky in the preparation of the final report.

CONTENTS

I INTRODUCTION

The general objectives of our research have been to develop and apply improved numerical models to simulate thermal plumes and intake recirculation from coastal power plants. Our approach is to model flow and temperature in the so-called intermediate and far fields (i.e., distance greater than several hundred meters from the source) and to parameterize the near-field mixing (occurring at distances from the source of less than a transition distance of several hundred meters) through prescribed flux boundary conditions. This approach was documented in Kaufman and Adams (1981), and Figure 1.1, adapted from their report, shows the model schematization and parameter definitions for application to a hypothetical power plant with surface discharge and shoreline intake. Note that in this schematization, waste heat is presumed to reside in an upper layer of constant thickness while water in the lower layer remains unheated; however lower-layer water may be entrained into the discharge plume or drawn into the power plant intake.

Kaufman and Adams (1981) applied this schematization to the Millstone Nuclear Power Station (on Long Island Sound, near Waterford, Conn.) and the Brayton Point Generating Station (on Mt. Hope Bay, near Somerset, Mass.) using the two-dimensional numerical models CAFE and DISPER. The technique worked, but was very expensive due to requirements of small time and space steps. Hence only limited model sensitivity and refinement could be undertaken.

Accordingly, in recent research jointly sponsored by the ELAB/EUP and the MIT Sea Grant Program, two new and fundamentally different programs were developed. The first, TEA (Tidal Embayment Analysis), replaces CAFE and computes 2-D currents while the second, ELA (Eulerian-Lagrangian Analysis), replaces DISPER and computes temperatures (or the concentrations of a passive tracer). This report describes the adaptation and application of these models to the same two power plant sites, as illustrated by the calculations

in the following two sections. Before proceeding, however, the models are briefly reviewed with emphasis on their application to the power plant schematization of Figure 1.1. Additional information can be found in the listed references.

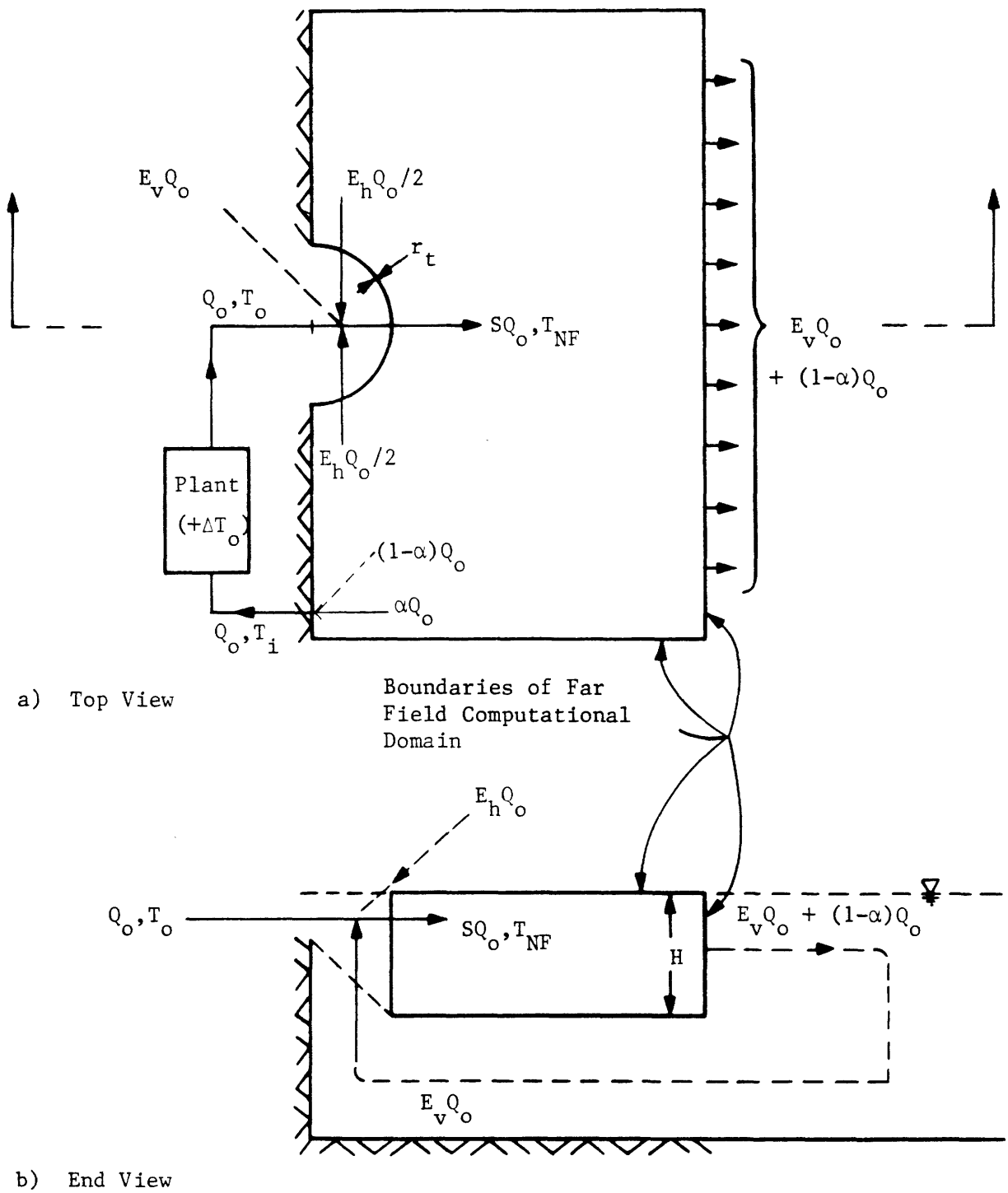

Figure 1.1 Description of surface jet parameters used in model schematization (adapted from Kaufman and Adams, 1981)

II BRIEF MODEL BACKGROUND

2.1 TEA

2.1.1 General

TEA is a two-dimensional harmonic finite element circulation model. Major references are Westerink et al. (1984, 1985), while additional references include Westerink et al. (1986a, b). In its complete non-linear form, TEA solves the following depth-averaged continuity and x and y momentum equations

$$\frac{\partial \eta}{\partial t} + \frac{\partial}{\partial x}[u(h+\eta)] + \frac{\partial}{\partial y}[v(h+\eta)] = 0 \tag{2.1}$$

$$\frac{\partial u}{\partial t} + u\frac{\partial u}{\partial x} + v\frac{\partial u}{\partial y} - fv = -g\frac{\partial \eta}{\partial x} + \tau_x^s/\rho(h+\eta) - \tau_x^b/\rho(h+\eta) \tag{2.2}$$

$$\frac{\partial v}{\partial t} + u\frac{\partial v}{\partial x} + v\frac{\partial v}{\partial y} + fu = -g\frac{\partial \eta}{\partial y} + \tau_y^s/\rho(h+\eta) - \tau_y^b/\rho(h+\eta) \tag{2.3}$$

where h(x,y) is mean water depth, η(x,y,t) is water surface elevation above the mean, u(x,y,t), v(x,y,t) are x and y velocity components, f is the Coriolis parameter, g is the acceleration of gravity, τ_x^s, τ_y^s are the x and y components of surface (wind) stress, $\tau_x^b = \rho c_f |u| u$, $\tau_y^b = \rho c_f |u| v$ are the x and y components of bottom friction, and $|u| = (u^2+v^2)^{\frac{1}{2}}$.

The model can be driven by prescribed elevations on open (ocean) boundaries, by prescribed fluxes (e.g., rivers or plant flows) on land boundaries, and by prescribed shear stress on the surface. Because the model is harmonic, all forcing functions are presumed to be the sums of periodic components. (Note that steady forcing can be modeled as a periodic forcing with zero frequency.) When the model is driven by forces of a particular frequency, the primary response in the interior is at the same frequency. However, because of non-linearities, responses at additional frequencies are also created. Through an iterative procedure,

the full non-linear model allows any number of such frequencies to be generated. However, the model may also be run in a linear mode in which non-linear terms are dropped (bottom friction is linearized) and hence the model responds only at the forcing frequency.

2.1.2 Application to Power Plants

In computing circulation from power plant discharges, two basic TEA runs have been superimposed. The first is tidal circulation, computed over the *entire* water depth, by specifying sinusoidal tidal elevations along open boundaries. In all applications to date, a single frequency ω, representing the M_2 tide, has been used. The second run simulates the plant-induced circulation, computed over the *upper layer*, by specifying steady fluxes representing i) diluted plant discharge *into* the upper layer (along the central portion of the transition circle) with total flow rate SQ_0, where S is the volumetric near-field dilution; ii) intake flow *out of* the upper layer (at the shoreline) with total flow αQ_0 where α ($0 \leq \alpha \leq 1$) is the fraction of intake flow drawn from the upper layer; iii) horizontal entrainment flow *out of* the upper layer (distributed along the outer portions of the transition circle) with total flow rate $E_h Q_0$, where E_h is the near-field horizontal entrainment rate; and iv) a downwelling flow necessitated by mass conservation flow *out of* the upper layer (distributed along distant regions of the shoreline) with total flow rate $[E_v + (1 - \alpha)]Q_0$, where E_v is the near-field vertical entrainment rate. Note that $S = 1 + E_h + E_v$.

Formulae for the near-field parameters E_h, E_v, S, and α, as well as the radius of the transition circle r_t, and the thickness of the upper layer h, have been developed from the Stolzenbach-Harleman surface jet model (Jirka et al., 1981) and are presented in Kaufman and Adams (1981). Site-specific values for Millstone and Brayton Point applications are given in the following sections. In principle these parameters vary with the tidal stage as does the spatial distribution of fluxes along the transition circle (e.g., the near-field plume may be deflected to the left during flood tide and to the right during ebb tide, or vice-

versa). Much of this variation may be approximated, in principle, by fitting time-varying fluxes, at frequencies ω and 2ω, to the computed tidal variations (at frequency ω) of near-field parameters.

It should be mentioned that, while we have used the non-linear version TEA, we have encountered instability when including the non-linear momentum terms. We believe this instability is due to the very large velocity gradients that occur due to prescribed near field boundary fluxes. Hence all results shown are without momentum terms. The consequence of this approximation is that predicted flow probably recirculates (toward the power plant intake and the near-field entrainment zone) faster than would occur in nature. However, comparison of measured and predicted temperatures suggests that this assumption is not too bad. Furthermore, the neglect of the momentum terms can be justified, in part, by the fact that computations begin in the intermediate field—after the relatively high momentum of the near field has been diluted.

2.2 ELA

2.2.1 General

ELA is a 2-D transport model which can be coupled with TEA to solve the advection-diffusion equation.

$$\frac{\partial c}{\partial t} + u\frac{\partial c}{\partial x} + v\frac{\partial c}{\partial y} = \frac{1}{h}\frac{\partial}{\partial x}\left[hD_{xx}\frac{\partial c}{\partial x} + hD_{xy}\frac{\partial c}{\partial y}\right] + \frac{1}{h}\frac{\partial}{\partial y}\left[hD_{yx}\frac{\partial c}{\partial x} + hD_{yy}\frac{\partial c}{\partial y}\right] + \theta \qquad (2.4)$$

where c(x,y,t) is concentration, D_{xx}, D_{xy}, D_{yx}, and D_{yy} are dispersion coefficients, and θ represents sources, sinks, and vertical boundary fluxes. ELA solves Eq. 2.4 using a split operator technique involving the backwards method of characteristics (a Lagrangian proce-

dure) for advection, a conventional implicit Galerkin finite element scheme (an Eulerian procedure) for dispersion, and local explicit calculations for source and sinks.

The treatment of advection is what makes ELA both more accurate and efficient than many previous transport models. In essence, advection is computed in two steps. In the first, characteristic lines are computed by integrating the velocity field backwards in time over a time step Δt from each node. The feet of the characteristic lines are then used as a basis for interpolating nodal concentrations from previous time steps. As part of this project, Baptista (1987) has studied, both theoretically and numerically, the accuracy of alternative Eulerian-Lagrangian schemes.

It should be mentioned that, for periodic flow fields (e.g., tidally driven at a single frequency, as we have assumed), tremendous savings are possible if the model time step in ELA is set to an integer fraction of the tidal period. In this way characteristic lines only need to be computed for each time step in the *first* tidal cycle. They can then be saved and used to interpolate concentration over succeeding tidal cycles. As a result, calculations lasting several weeks or more can be conducted at only a small additional cost over that of the first tidal cycle. Similar savings apply in applications using a steady flow field. Specific costs are discussed in the following sections concerning the Brayton Point simulation.

The major reference to ELA is Baptista et al. (1984), and additional references include Baptista et al. (1985, 1986) and Baptista (1987). An informal users' manual (Kossik et al., 1987) documents the combined use of TEA and ELA, including several computational improvements made to the model as part of this project.

2.2.2 Application to Power Plants

For power plant applications, Eq. 2.4 has generally been applied to the upper layer of constant depth h and concentration c has been replaced by excess temperature ΔT, which

is the difference between water temperature with and without plant operation. The sink term thus represents excess heat loss and is expressed as

$$\theta = -\frac{k\Delta T}{h} \tag{2.5}$$

where k is a surface heat loss coefficient (units of ℓ/t) computed from local meteorological data using formulae presented in Ryan et al. (1974). All calculations to date have used constant dispersion coefficients whereby $D_{xx} = D_{yy} = D$ and $D_{xy} = D_{yx} = 0$.

Excess heat enters the domain via the diluted power plant discharge in the middle of the transition circle and is represented by specifying an inflow (excess) temperature. The user may pre-specify steady or time-varying inflow temperatures or, more realistically, may allow the program to compute time-varying temperatures reflecting transient intake recirculation and near-field re-entrainment. The former are referred to as static heat budget calculations while the latter are termed dynamic heat budget calculations because the inflow temperatures are computed from a dynamic near-field energy budget using the instantaneous intake and entrainment temperatures. At open boundaries, excess temperature is assigned to be zero for both advection (on flood tide) and dispersion calculations.

Two features of our modeling that were introduced recently include simulations of wind drift and vertical diffusion. While a depth-averaged circulation model such as TEA can simulate the effects of surface wind stress, actual vertical velocity profiles resulting from wind stress are three-dimensional and near-surface velocities may bear little resemblance to depth-averaged velocities. This is true whether the full water depth or a constant depth surface layer is used. In order to analyze in a simple manner the effects of a surface wind shear on heat transport in the upper layer, a "wind drift" option was added to ELA. The influence of the wind can approximately be simulated by adding a drift velocity proportion-

al to the wind speed to the velocity field computed by the hydrodynamic model TEA. In this manner a three-dimensional effect is included in the sense that regions of implied upwelling and downwelling from a fictitious lower layer are introduced near boundaries. The excess temperature of upwelling water is assumed to be zero and heat associated with downwelled water is assumed to be lost from the system.

The option now exists in ELA to compute depth-varying concentrations (or excess temperature) due to vertical diffusion under certain limiting conditions. Consider a vertically uniform (2-D) flow field, u(x,y,t), v(x,y,t), large water depth (such that c = 0 on the bottom, z = h), spatially homogeneous horizontal and vertical diffusivities defined with respect to the (principal) coordinate axes, and internal loss represented by a first-order decay coefficient K. The 3-D transport equation (analogous to Eq. 2.4) for c(x,y,z,t) then becomes

$$\frac{\partial c}{\partial t} + u\frac{\partial c}{\partial x} + v\frac{\partial c}{\partial y} = D_{xx}\frac{\partial^2 c}{\partial x^2} + D_{yy}\frac{\partial^2 c}{\partial y^2} + D_{zz}\frac{\partial^2 c}{\partial z^2} - Kc \tag{2.6}$$

where the vertical coordinate z is defined positively downward from the water surface.

The zeroth and second vertical moments of the concentration distribution, $m_0(x,y,t)$ and $m_2(x,y,t)$ are defined as

$$m_0 = \int_0^h c\, dz \quad \text{and} \quad m_2 = \int_0^h cz^2\, dz \tag{2.7}$$

and the standard deviation $\sigma_z(x,y,t)$ of the vertical distribution is

$$\sigma_z \equiv \sqrt{m_2/m_0} \tag{2.8}$$

Multiplying each term of Eq. 2.6 first by z^0 and then by z^2 and integrating from top to bottom yields, after minor manipulations,

$$\frac{\partial m_0}{\partial t} + u\frac{\partial m_0}{\partial x} + v\frac{\partial m_0}{\partial y} = D_{xx}\frac{\partial^2 m_0}{\partial x^2} + D_{yy}\frac{\partial^2 m_0}{\partial y^2} - Km_0 \tag{2.9}$$

$$\frac{\partial \sigma_z^2}{\partial t} + u\frac{\partial \sigma_z^2}{\partial x} + v\frac{\partial \sigma_z^2}{\partial y} = D_{xx}\frac{\partial^2 \sigma_z^2}{\partial x^2} + D_{yy}\frac{\partial^2 \sigma_z^2}{\partial y^2} + 2E_z \tag{2.10}$$

Each of these transport equations is similar to the 2-D transport equation for c and is computed similarly by ELA. If a (half-) Gaussian vertical concentration distribution is assumed, then the computed values of the two dependent variables m_0 and σ_z^2 can be used to construct

$$c = \sqrt{\frac{2}{\pi}}\frac{m_0}{\sigma_z} e^{-z^2/2\sigma_z^2} \tag{2.11}$$

If, instead of internal loss, heat (or mass) is lost through surface exchange, an equivalent first-order decay coefficient can be computed as

$$K = \sqrt{\frac{2}{\pi}}\frac{k}{\sigma_z} \tag{2.12}$$

where k is the surface heat exchange coefficient defined in Eq. 2.5 and the decay coefficient is equivalent in the sense that the rate of heat loss is the same when integrated over the water column. In this case, the last term of Eq. 2.9 may be replaced by $(2/\pi)^{\frac{1}{2}}km_0/\sigma_z$ and Eqs. 2.9 and 2.10 now become mildly coupled. Note that these procedures are only approximate because the concentration distributions will not, in general, be Gaussian, especially under the influence of a surface loss mechanism.

III APPLICATIONS TO BRAYTON POINT GENERATING STATION

3.1 Site Description

The Brayton Point Generating Station is located in Somerset, Massachusetts, at the confluence of the Lee and Taunton Rivers at the northern end of Mount Hope Bay. See Figure 3.1. At low tide, Mount Hope Bay has an approximate length (along its north-south axis) of 7 mi, surface area of 15.6 mi^2, and volume of 8.3 billion ft^3. The average tidal range is 4.4 ft which results in a tidal prism volume of approximately 1.2 billion ft^3. Approximately 70% of the Bay area has an average depth of less than 18 ft at mean low water while the main shipping channels average 30 ft in depth at mean low water. With the exception of the abrupt increase in depth at the edge of the shipping channels and the rapid shoaling in the area of Spar Island, the bottom contours of much of the Bay are rather even, with a steady increase in depth from the head of the Bay to the two southerly passages.

Circulation in Mount Hope Bay is driven primarily by tides and secondarily by wind, and fresh water inflow from the Taunton River at the north end. Residence time within the bay has been estimated to be within the range of 6 to 12 days (MRI, 1978).

Temperatures within Mount Hope Bay vary with the tidal stage and are quite responsive to meteorological conditions due to the relative shallowness of the bay. In spring and summer, mild thermal stratification (3°-5° F) may be found while temperatures are generally vertically well mixed in the fall and winter. In mid-summer, surface and bottom temperatures beyond the influence of Brayton Point Station's thermal plume may reach into the high 70s while water temperatures during winter may occasionally reach the freezing point.

There are presently four generating units at Brayton Point with a combined capacity of about 1600 MWe. A once-through condenser cooling system is used. The intakes for Units

1, 2, and 3 are located on the eastern side of the plant site on the banks of the Taunton River while the intake for Unit 4 is to the west of the plant site on the banks of the Lee River. The discharge back to the bay is via a 3200-ft channel which terminates at the southern tip of the plant site at a venturi designed to promote mixing. Table 3.1 summarizes representative conditions associated with both 3- and 4-unit operation.

3.2 Site Schematization

Site schematization was similar to that described in Kaufman and Adams (1981). Figure 3.2a shows the finite element grid over Mt. Hope Bay. In accordance with the discussion in Section 2, for modeling the plant-induced flow, the domain had a constant depth of 11.5 ft corresponding to the estimated far-field plume thickness listed in Table 3.1. The depth was adjusted in shallow areas to account for depths less than 11.5 ft while for the tidal calculation the full depth was used. The near-field region was carved out of the domain in the region surrounding Brayton Point as shown in Figure 3.2b.

Table 3.1 summarizes the near field parameters used as boundary conditions. Note that, because of the relatively high discharge velocity, the plume intersects the bottom and the expected dilution is less than for deep water ($r_s < 1$).

Two different sets of discharge and entrainment fluxes were specified at the near-far field interface, corresponding to the simulation of three- and four-unit operation. In both cases, three nodal points at the bottom (southern end) of the interface had specified normal fluxes into the domain representing diluted discharge. Using parameters in Table 3.1, the temperature of the diluted discharge above the intake temperature was calculated as $14.8^\circ F/(0.65\times7.8) \simeq 2.9^\circ F$ for three units and $15.7^\circ F/(0.52\times10.3) \simeq 2.9^\circ F$ for four units. The temperature that was actually specified depended on where static or dynamic heat budget calculations were performed. The nodes adjacent to the diluted discharge had zero

normal flux and all the remaining nodes had approximately equal specified entrainment fluxes out of the domain (and into the theoretical near-field jet region).

The intake for the first three units was simulated by removing flux from three nodes within the shipping channel inlet. The magnitude of the intake flux depended on the value of α describing how much of the intake that was drawn from the upper layer. (Values of both $\alpha = 0.5$ and 1.0 were used.) In the four-unit simulation, the intake for the fourth unit only was added to the west side of Brayton Point, or on the Lee River boundary, and drew entirely from the upper layer ($\alpha = 1$).

To simulate ambient circulation in the domain, the two strings of nodes along the bottom of the bay were designated ocean boundaries. These nodes had specified tidal amplitude of 2.9 ft (as determined from a tidal gauge at the station), period = 44640 sec, and no phase lag. In addition to the tide, an inflow of 435 cfs from the Taunton River was established. Surface heat loss was simulated by making use of actual meteorological measurements recorded during the time period of interest. Average values of the various meteorological inputs were obtained from the week preceding the day for which the plume field data were given (August 25, 1976). The average meteorological data were used to compute a surface heat transfer coefficient of 157 BTU/ft^2-°F-day. The corresponding first-order decay coefficient (k/h of Eqn. 2.5; equal to 2.5×10^{-6} sec^{-1}) was based on a water depth of 11.5 ft.

3.3 Results

A large number of simulations have been made covering a range of model parameters and options, plant operating conditions, and tidal phases; clearly, only some results can be presented. The output presented was chosen to illustrate model capabilities, emphasizing

simulations for three-unit discharge (so that they can be compared with field data) and output at one tidal phase (maximum ebb).

Figures 3.3a-d depict current vectors within the surface layer of Mt. Hope Bay for four tidal phases, produced by combining the output form two TEA runs: ambient currents created by tidal forcing and Taunton River inflow computed over the entire water column and three-unit plant-induced flows over the upper layer forced by prescribed inflows and outflows along domain boundaries. For the plant-induced flow, $\alpha = 1$ (i.e, intake flow drawn entirely from the upper layer), which is consistent with the assumption implied in Kaufman and Adams (1981).

Figures 3.4a-c depict corresponding pathlines simulated by ELA for three particles. A particle originating near the Taunton River is shown being entrained in the intake, a particle near the plume center is shown to be transported south and flushed form Mt. Hope Bay, and a particle on the eastern edge of the plume is shown being recirculated to the plant intake. Note that, because the power plant intake flow is presumed to come entirely from the upper layer ($\alpha = 1$), this represents a worst-case condition for recirculation.

Figures 3.5a-d show contours of excess temperature (in °F) averaged over the surface layer for four tidal phases, based on the above flow field. Calculations represent quasi-steady state condition (they are output after 18 tidal cycles) and were made with a dispersion coefficient of D = 1.0 m^2/s, a time step of $\Delta t = 31$ min, and no wind. The discharge does not reflect any effects of intake recirculation or near-field re-entrainment of previously discharged water; i.e., the discharge excess temperature at the end of the near field has been held constant at approximately 2.9°F, which equals the discharge temperature rise of 14.8°F divided by the effective (shallow water) dilution of 5.1 (equal to the product of r_s and S; see Table 3.1). This condition is termed a static heat budget.

Figures 3.6a–d, along with Figure 3.5b, indicate sensitivity of computed excess temperature at maximum ebb to horizontal diffusion coefficient in the range $0 < D < 30 m^2/s$. Clearly, increasing D decreases temperature gradients, resulting in generally lower temperature near the plume and higher temperature away from the plume. Based on a a qualitative comparison with field measurements (shown later), it appears that $D = 1\ m^2/s$ is reasonably appropriate for Mt. Hope Bay and this value is used in remaining simulations.

Figures 3.7a–d indicate sensitivity to time step, Δt, for a short run of elapsed time = 186 min and a diffusion coefficient of $D = 10\ m^2/s$ (first maximum ebb after initial high slack). The contours show that, as Δt increases, the "time-splitting" error increases, resulting in higher temperatures near the discharge. This error is caused by the fact that ELA performs the operations of diffusion, advection, and heat loss sequentially (in that order) during a time step. For water in the middle of the bay, which has been transported for many time steps, the order and the number of time steps make relatively little difference because each parcel of water will have experienced each operation a number of times. However, water near the discharge is "younger," and hence the effects are more important. (The analogy can be made with a baseball game: early in the game, which team is leading is likely to depend on whether it's the top or bottom half of the inning; conversely, later in the game, each team will have had nearly the same number (percentage-wise) of at-bats.) The present sequence of operations errs on the side of over-estimating temperatures near the discharge because water parcels that are less than one time step "old" have never been diffused, those whose "age" is between one and two time steps have been diffused for only one time step, etc. If the order of operations were reversed, a similar error would occur tending to underestimate near plume temperature. Note that the magnitude of the error increases with the size of the diffusion coefficient.

One way to minimize this error would be to change the order (make diffusion follow advection) and have the diffusion operation (for each node) be proportional to the age of the parcel (for those nodes within a travel distance one time step from a boundary). While this may be tried in the future, the solution for present was to select Δt based on a trade-off between accuracy (dictating small Δt) and computational efficiency (suggesting large Δt). The chosen value of $\Delta t = 31$ min (used in all remaining simulations) is identically 1/24 of an M_2 tidal period, preserving the capability to save the feet of the characteristics for calculation with repeating (tidal) flow fields. The magnitude of the overestimate in plume temperature using $\Delta t = 31$ minutes can be gauged by comparing Figures 3.7a and 3.7c.

Figure 3.8 illustrates time-varying diluted jet temperature and various heat fluxes when the near-field temperature boundary condition *is varied* to reflect recirculation and re-entrainment. In particular, Figure 3.8a shows the jet temperature, while Figure 3.8b shows various heat flux terms including the mixed jet inflow into the domain, and the following fluxes out of the domain: 1) surface heat loss, 2) horizontal entrainment, 3) intake withdrawal, and 4) boundary loss used to account for vertical entrainment. The small difference between the jet influx and the sum of the four fluxes out of the domain represents heat loss through the open boundaries at the bottom of the domain.

These calculations are termed a dynamic heat budget calculation. Note that the time to adjust to quasi-steady conditions depends on the distance from the source, and that intermediate field temperatures seem to reach quasi-steady state after about 3–4 cycles at temperatures about 50% higher than without recirculation or re-entrainment. Thus, due to model linearity, results for no recirculation or re-entrainment (static heat budget calculation) could be scaled to include these effects by multiplying by a factor of about 1.5. Figure 3.9 shows excess temperature contours with recirculation and re-entrainment for maxi-

mum ebb, which corresponds to Figure 3.5b. Because the power plant intake flow is presumed to come exclusively from the upper layer ($\alpha = 1$), the simulated recirculation and re-entrainment (i.e, the factor of 1.5) are probably over-estimated..

To test sensitivity to the intake withdrawal, TEA and ELA were re-run using $\alpha = 0.5$ (i.e., half of the intake flow from the upper layer and half from the lower layer). The velocity vectors (not shown) indicate somewhat less (re-)circulation near the intake, but are otherwise similar to those shown in Figure 3.3. Figure 3.10 shows the corresponding excess temperature contours at maximum ebb. Over most of the domain contours simulated with $\alpha = 0.5$ (Figure 3.10) and 1.0 (Figure 3.9) are very similar, though near the discharge and intake, differences of up to about 0.5° F are apparent.

Figure 3.11a shows the time series of heat fluxes for $\alpha = 0.5$ and Figure 3.11b shows the time series of discharge, intake, and diluted jet temperatures (obtained from Figure 3.11a) by dividing by the approximate volume flow rate. Figure 3.11b indicates that simulated intake recirculation varies from about 0.8 to 1.3° F depending on tidal phase. Note that this includes both the effects of direct recirculation and far-field temperature build-up. As discussed in §2.1.2, the simulated recirculation should be viewed as an upper bound because the simulations of circulation with TEA do not include momentum effects, thus tending to exaggerate near field recirculation. Based on the water depths near the intake, $\alpha = 0.5$ is probably realistic, but some of the remaining calculations have been made with $\alpha = 1.0$.

Figures 3.12a-b illustrate the effect of wind for conditions otherwise similar to Figure 3.5b which has no wind drift. Part a) is for a steady westerly wind of 3 m/s while part b) is for a time-variable wind based on measurements leading up to August 25, 1976. (At the time of maximum ebb, the wind speed being simulated in part b) is the same as that assumed in part a).) In both cases, the wind drift has been taken as 0.5% of the wind speed.

Figures 3.13a and b reflect our three-dimensional ELA calculations showing excess temperatures at a depth of 0 and 3.5 m (11.5 ft) below the water surface for conditions of $E_z = 0$ (zero vertical diffusion). Figure 3.14a shows normalized measured vertical temperature profiles at several locations identified on Figure 3.2a and Figures 3.14b and c show simulated normalized profiles for two values of vertical diffusion. (Considering all phases of the tide and instances from the source representative of the measurements, it appears that zero vertical diffusion best represents the data.)

Figures 3.15a - 3.18a show measured excess temperature averaged over a depth of 11.5 feet at four tidal stages on August 25, 1976. These data are the same as presented by Kaufman and Adams (1981) but, in the present analysis, the ambient temperature used to establish excess temperatures has been computed differently. (Unlike the former analysis, where a unique background temperature was selected for each tidal phase, a constant ambient temperature equal to the lowest observation was used.)

Figure 3.15b - 3.18b show simulated excess temperatures plotted to the same scale, for comparison with the measurements. The simulations assume a dynamic heat budget, without wind drift, and are made with D = 1 m^2/s and $\alpha = 1.0$. In general, agreement is reasonably good and the tendency for the simulations to exaggerate excess temperature near the intake would diminish if lower values of α and Δt were used.

Finally, Figures 3.19 to 3.21 pertain to the present four-unit discharge, using parameters found in Table 3.1. Figures 3.19a and b show the upper layer velocity vectors based on output from TEA using $\alpha = 0.5$. Part a) is for only the power plant (steady state) forcing while part b) includes the tide and is presented at a phase of maximum ebb. Figure 3.20 shows excess temperature at maximum ebb using output from ELA assuming no wind, D = 1 m^2/s, and including a dynamic heat budget. Time series of the various fluxes are shown in Figure 3.21a, while discharge, intake, and diluted jet temperatures are shwn in Figure

3.21b. Referring to Table 3.1, because the four-unit discharge temperature rise (ΔT_0 = 15.7° F) and shallow water dilution ($r_s S$ = 5.4) are similar to corresponding values for three units (ΔT_0 = 14.8° F and $r_s S$ = 5.1), maximum plume temperatures for three and four units are similar. However, because the four-unit flow rate (Q_0) and heat rejection (proportional to $Q_0 \Delta T_0$) are approximately 40% and 50% higher, respectively, than for three units, the size of the isotherms for four units is somewhat larger.

Figure 3.21b indicates that simulated recirculation for four units ranges from about 1.7 to 2.2° F above ambient depending on tidal phase. The difference from the three-unit recirculation shown in Figure 3.11b (ranging from 0.8 to 1.3° F) reflects, primarily, the greater heat loading and the fact that the intake for unit 4 is drawn entirely from the upper layers, whereas the intake for units 1-3 are assumed to draw equally from upper and lower layers ($\alpha = 0.5$).

3.4 Computational Details

Calculations were performed on a MicroVax II and required the following approximate CPU times. To compute circulation over a repeated 12.4-hr tidal cycle, TEA requires 15-75 minutes, depending on the number of iterations and harmonics. For calculation with only one frequency, but iterating to simulate non-linear bottom (interfacial) friction, CPU time is approximately 15 minutes. To compute excess temperatures over the first tidal cycle, using a time step of 31 minutes, ELA required 38, 58, or 90 minutes as the specified tolerance governing the accuracy of the tracking algorithm (value of EPS) was varied from 10^{-3} to 10^{-4} to 10^{-5}. (Most calculations were performed with EPS = 10^{-4}.) To simulate an additional 17 tidal cycles (saving the feet of the characteristics) required an additional 18 minutes. In total, then, a typical calculation takes about 1½ CPU hours. Similar times were required for the Millstone calculations presented in the following chapters.

As stated earlier, program efficiencies made to the tracking algorithm in ELA make it possible to use time steps ranging from minutes to hours. If dispersion coefficients are independent of time (our assumption) CPU times decrease modestly while storage requirements decrease tremendously as time step increases, providing strong motivation to increase the time step. (The motivation is even stronger if time-varying coefficients are used.) The effect of Δt on the accuracy of Eulerian-Lagrangian transport models in general was studied by Baptista (1987) as part of this project. While his study concentrated on transport of an initial concentration distribution, additional "time-splitting" effects come into play when considering the introduction of mass (or excess heat) through a boundary (e.g., a river of the near-field transition circle of our power plant examples). Based on the sensitivity study (described above), the choice of $\Delta t = 31$ minutes (1/24 of a 12.4-hr tidal cycle) was chosen as a compromise between the objective of large Δt, and the desire to maintain accuracy (insensitivity to Δt) near boundaries. It is anticipated that a significant increase in Δt could be made, allowing increase in efficiency with little decrease in accuracy, if the order of computing dispersion and advection in ELA were reversed (so that advection would be computed first), and if the dispersion calculations took into consideration fractional time steps for points near a flux boundary.

Table 3.1
Near-Field Parameters Computed for Brayton Point Simulation

Parameter	Symbol	3-unit values*	4-unit values*
Discharge flow rate	Q_0 (cfs)	1380	1960
Discharge temperature rise	ΔT_0 (°F)	14.8	15.7
Discharge velocity	u_0 (fps)	4.0 - 6.4	5.6 - 9.1
Discharge channel depth	h_0 (ft)	7.4 - 11.9	7.4 - 11.9
Discharge channel half-width	b_0 (ft)	14.6	14.6
Discharge channel characteristic length	ℓ_0 (ft)	10.4 - 13.2	10.4 - 13.2
Densimetric Froude no. (based on h_0)	$\mathbb{F}_0$	4.2 - 8.5	5.7 - 11.7
Channel aspect ratio	h_0/b_0	0.51 - 0.82	0.51 - 0.82
Densimetric Froude no. (based on ℓ_0)	$\mathbb{F}_0'$	4.0 - 7.2	5.5 - 10.0
Transition radius	r_t (ft)	790 - 1120 (1000)	1080 - 1550 (1000)
Near-field volumetric dilution	S**	5.6 - 10.1 (7.8)	7.6 - 13.9 (10.3)
Vertical mass entrainment	E_v**	3.6 - 7.4 (5.4)	5.4 - 10.7 (7.6)
Horizontal mass entrainment	E_h	1.0 - 1.6 (1.3)	1.3 - 2.2 (1.7)
Maximum plume depth	h_{max} (ft)	22.1 - 31.4 (23.0)	30.2 - 43.4 (23.0)
Far-field plume depth	h_{far} (ft)	11.1 - 15.7 (11.5)	15.1 - 21.7 (11.5)
Shallow water dilution correction	r_s	0.65	0.52

*Ranges given refer to variation over tidal cycle. Values in parentheses were used in simulation.

**These parameters were altered for model use to account for shallowness effects: $S_{actual} = r_s S$; $E_{V_{actual}} = E_v - (S - S_{actual})$.

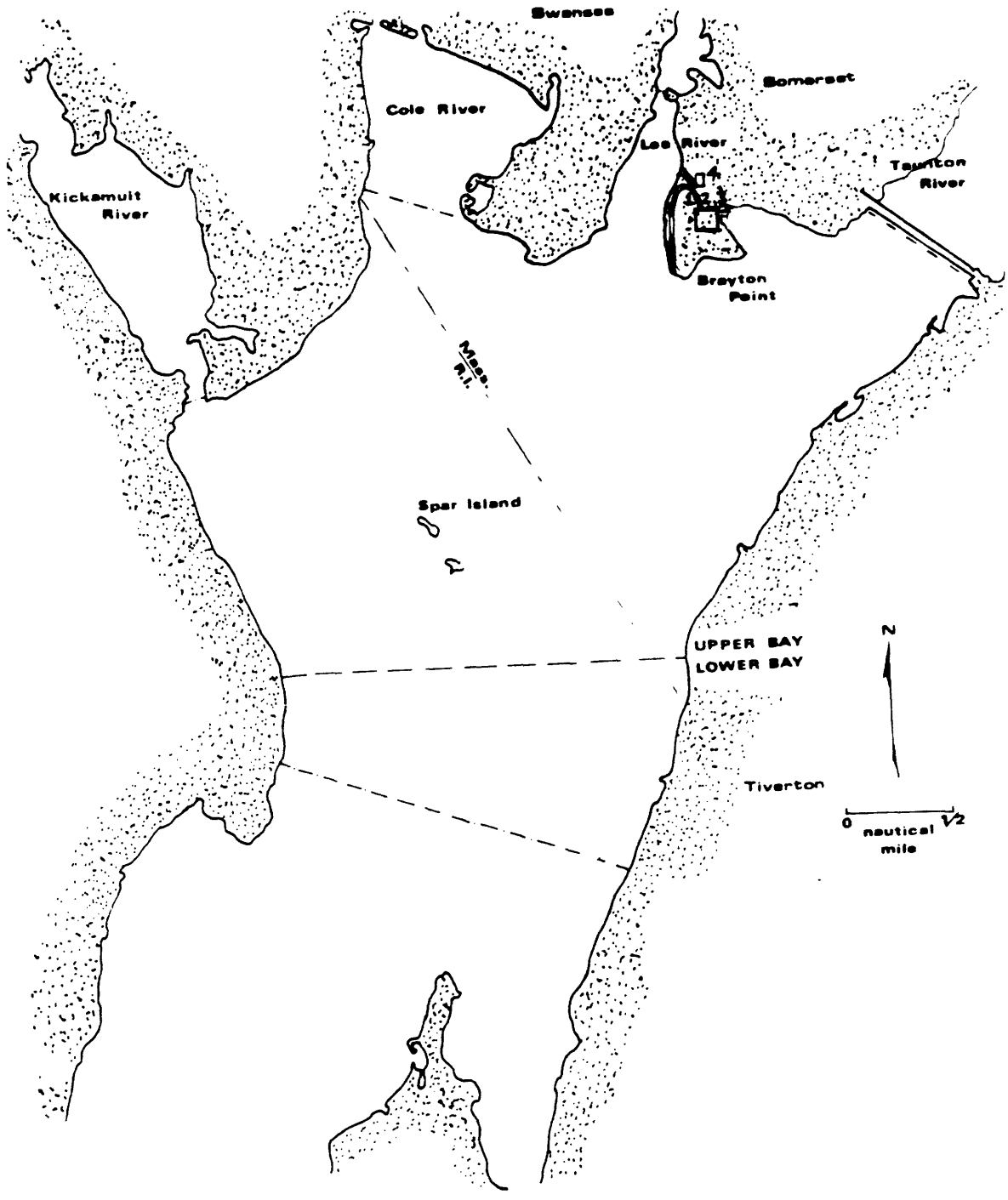

Figure 3.1 Site of Brayton Point generating station. (Note location of generating units 1, 2, and 3 and generating unit 4 on Brayton Point.)

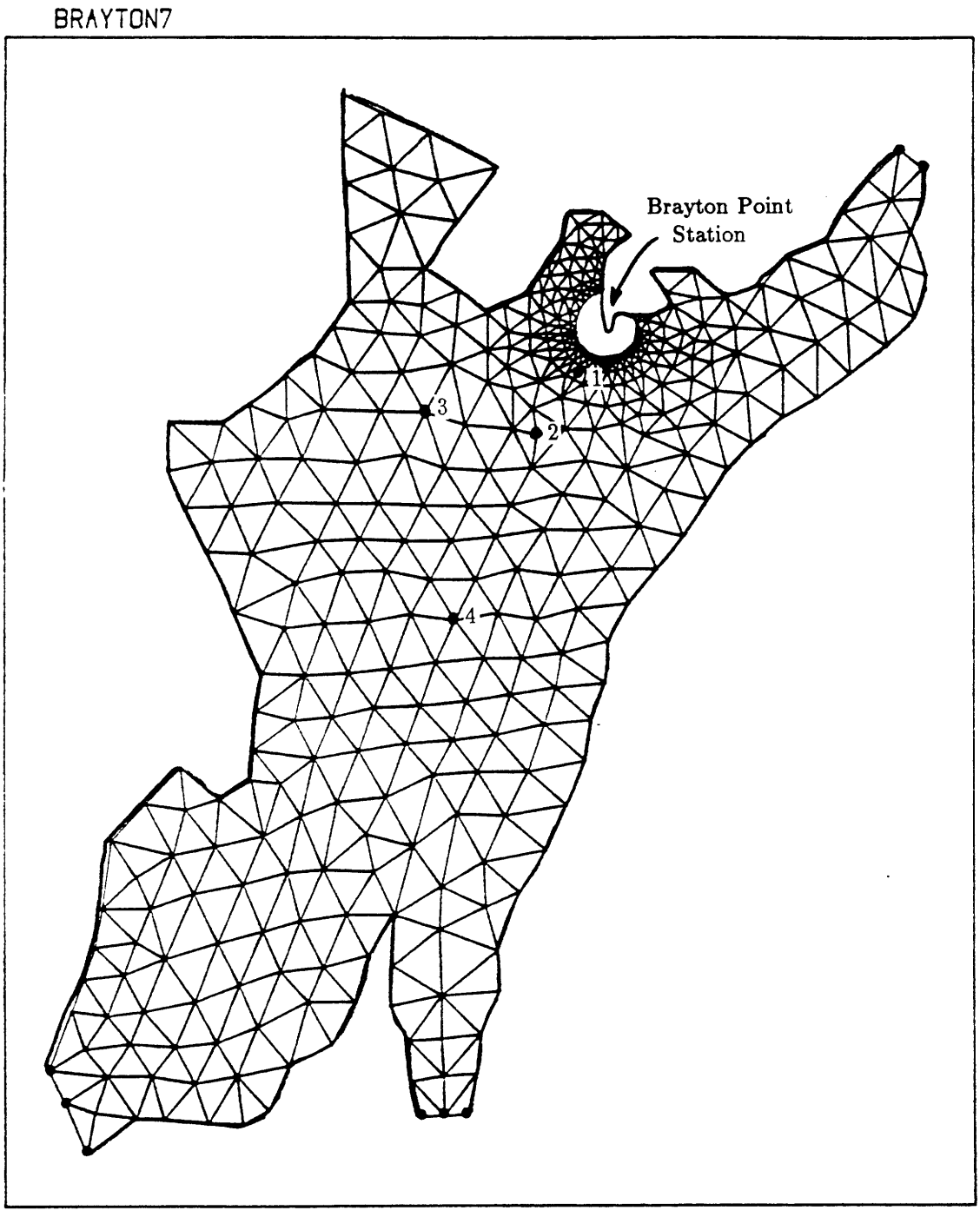

Figure 3.2 Finite element discretization of Mount Hope Bay
a) Entire bay

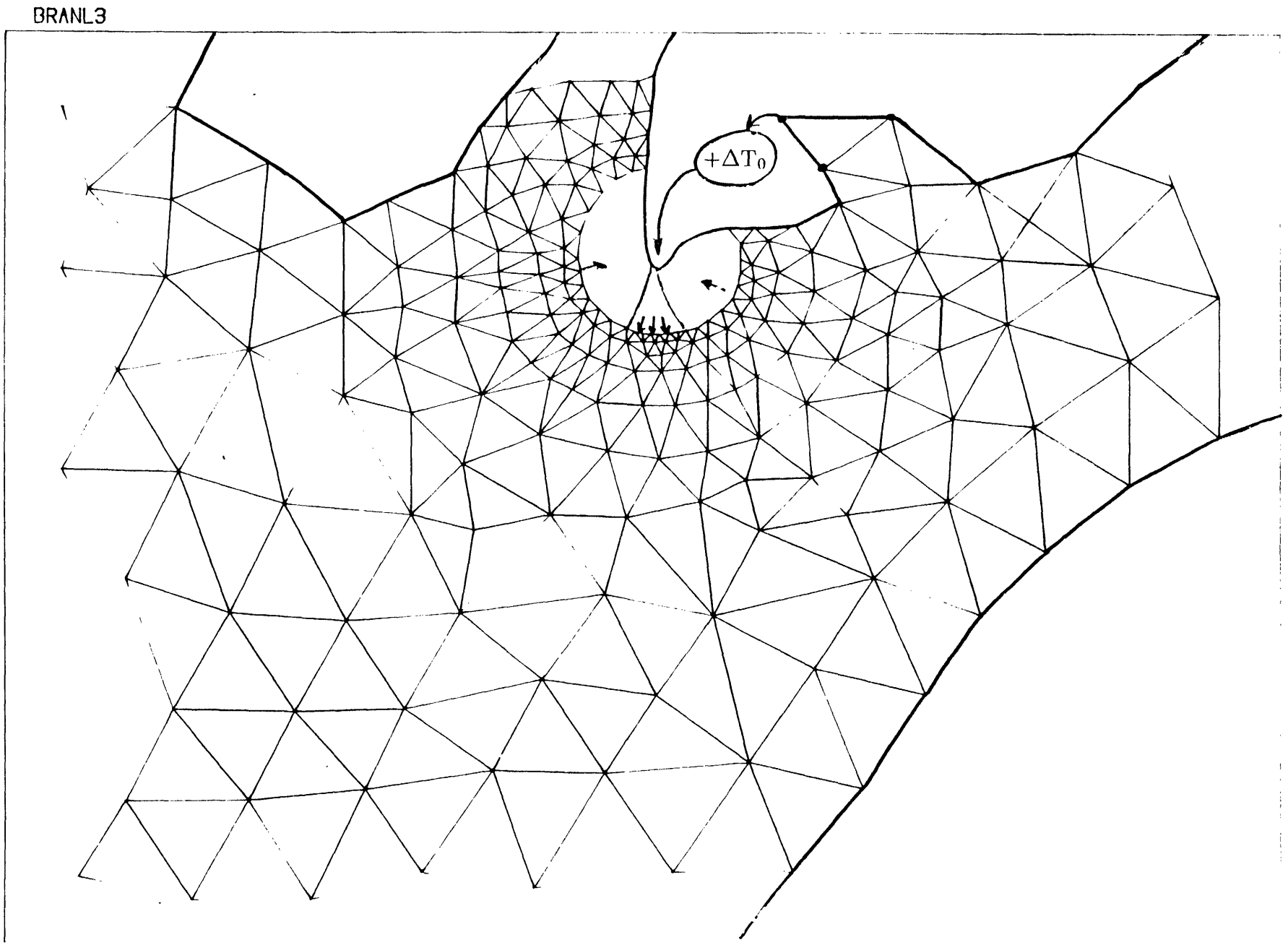

Figure 3.2b Details of near field showing entrainment and mixed discharge fluxes

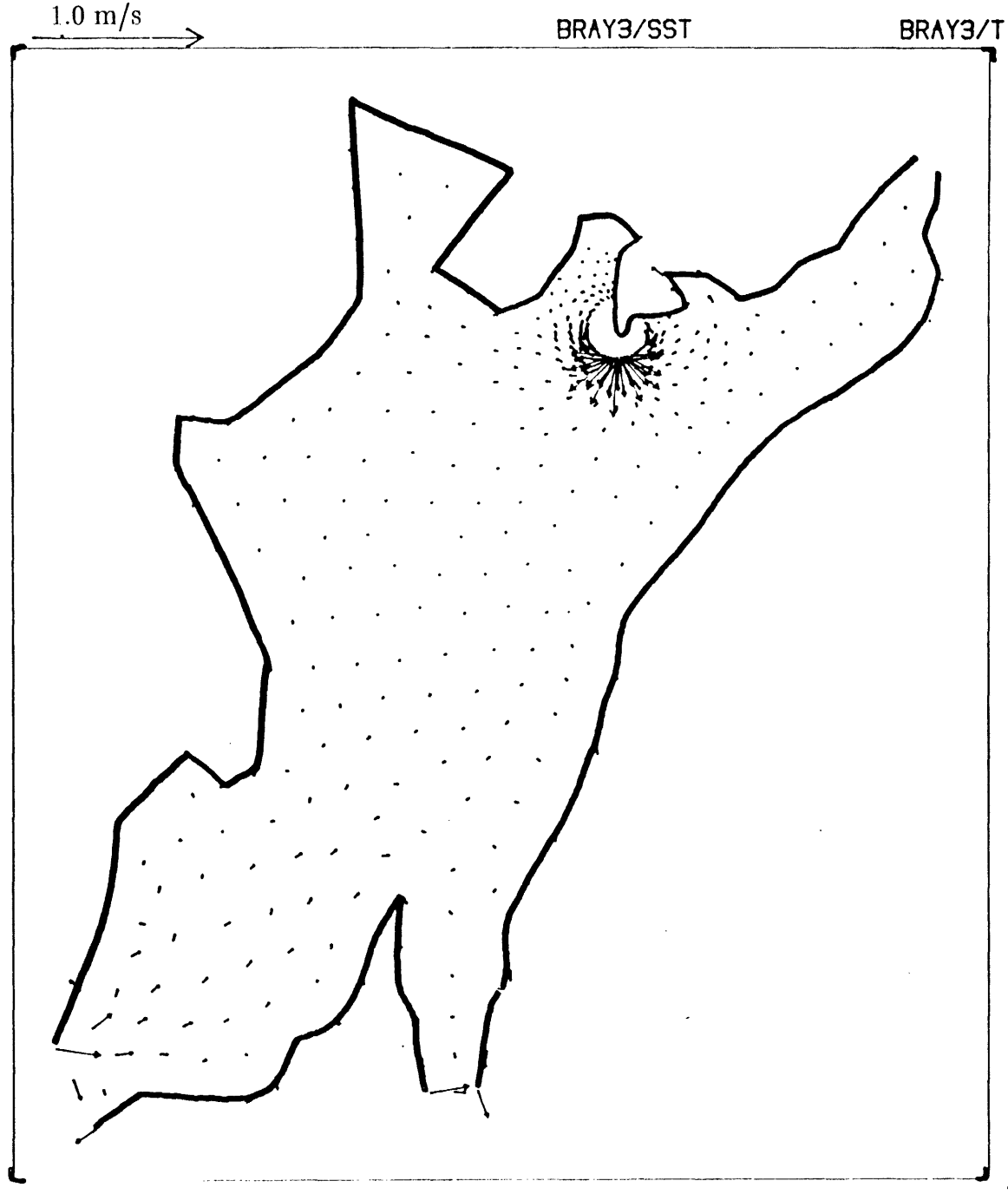

Figure 3.3 Computed surface velocities for three units
a) High slack

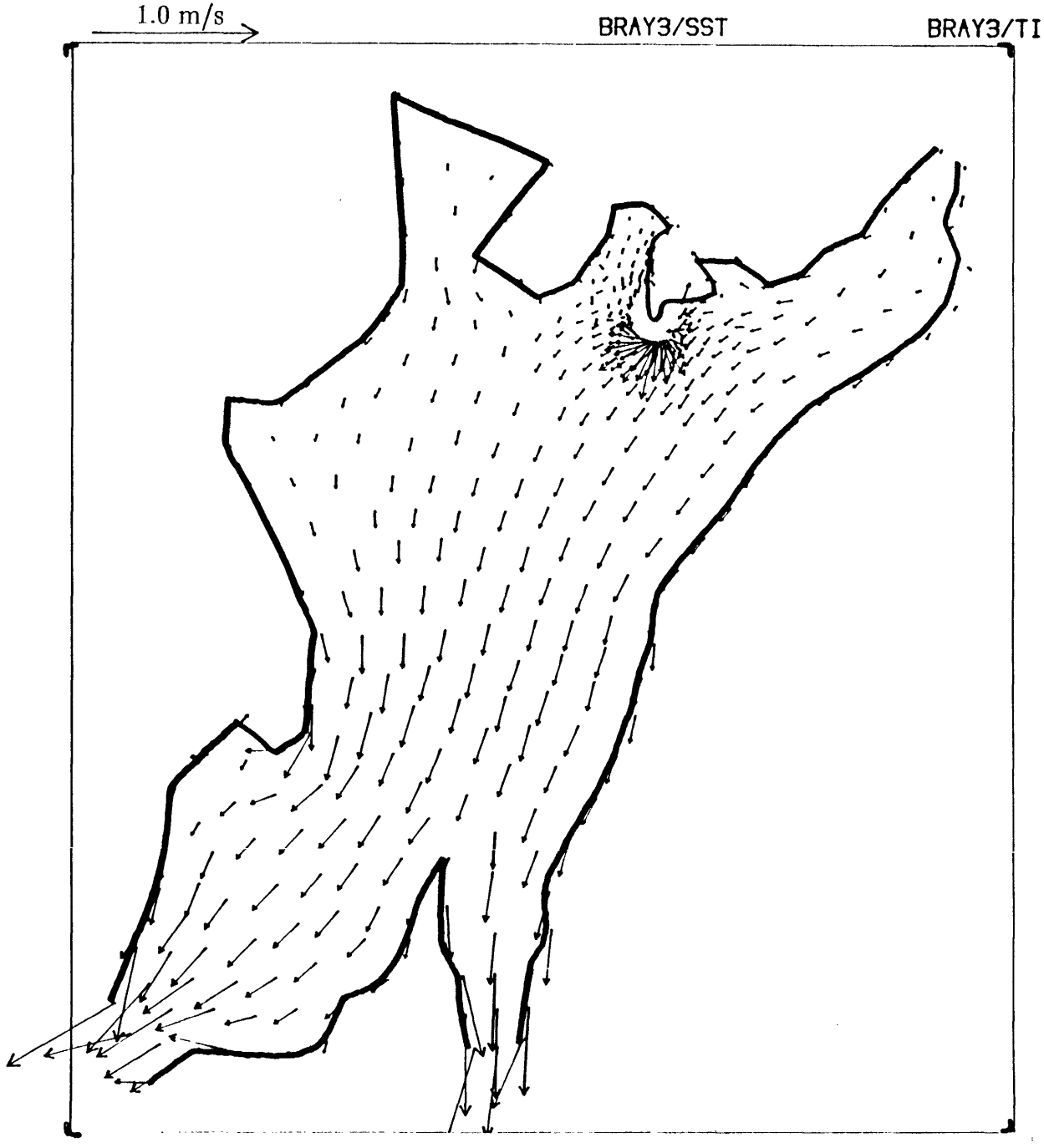

Figure 3.3b Maximum ebb

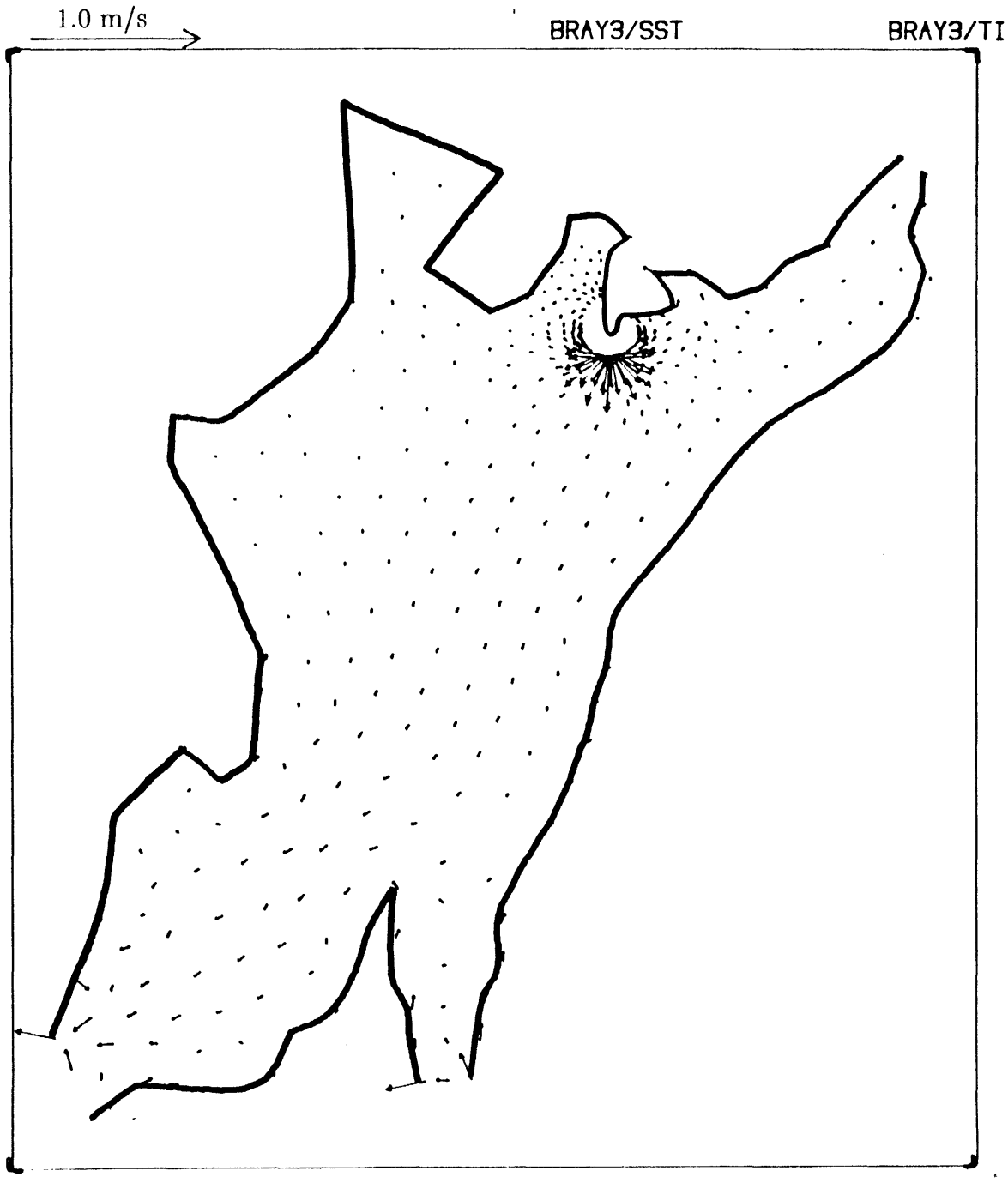

Figure 3.3c Low slack

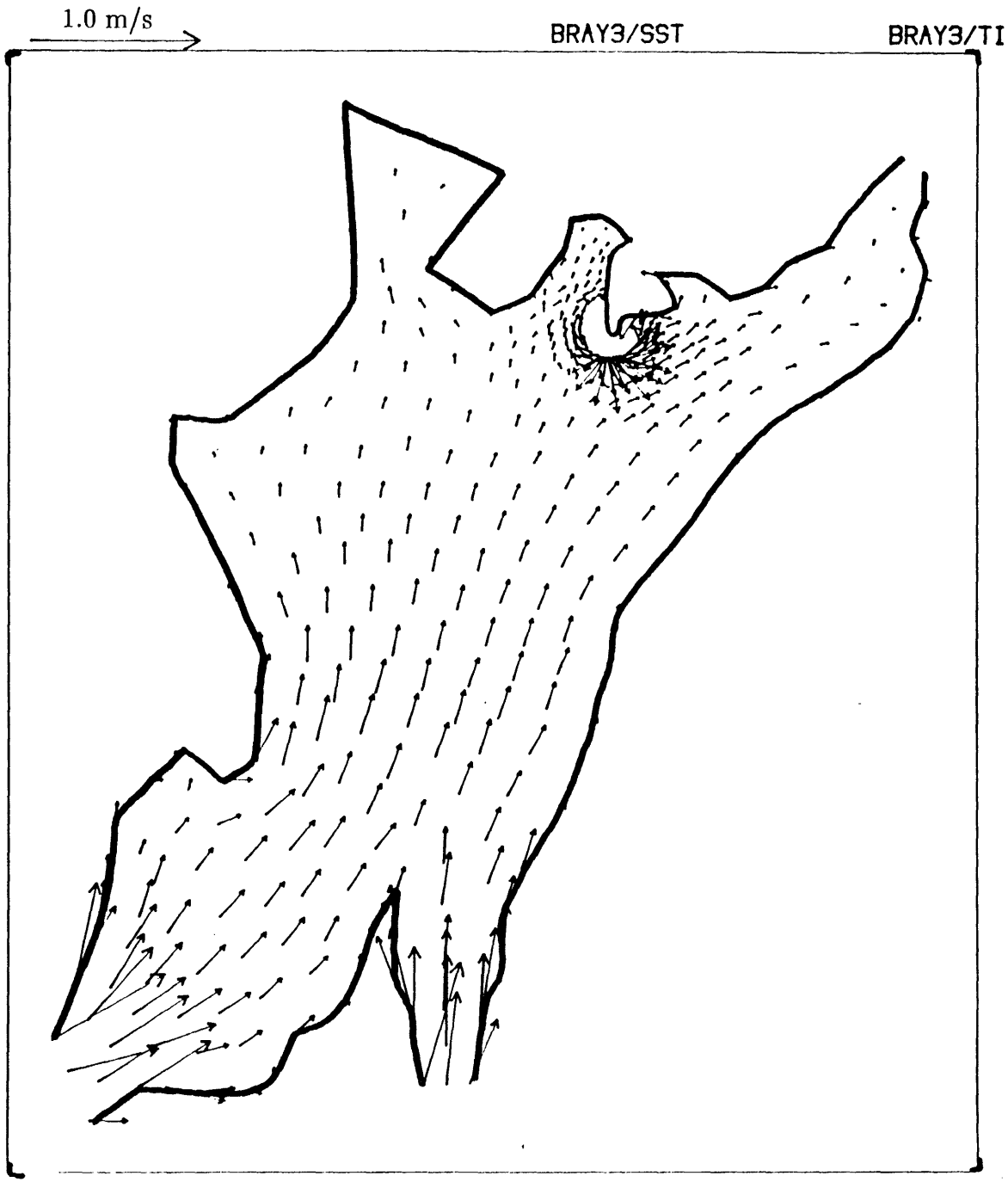

Figure 3.3d Maximum flood

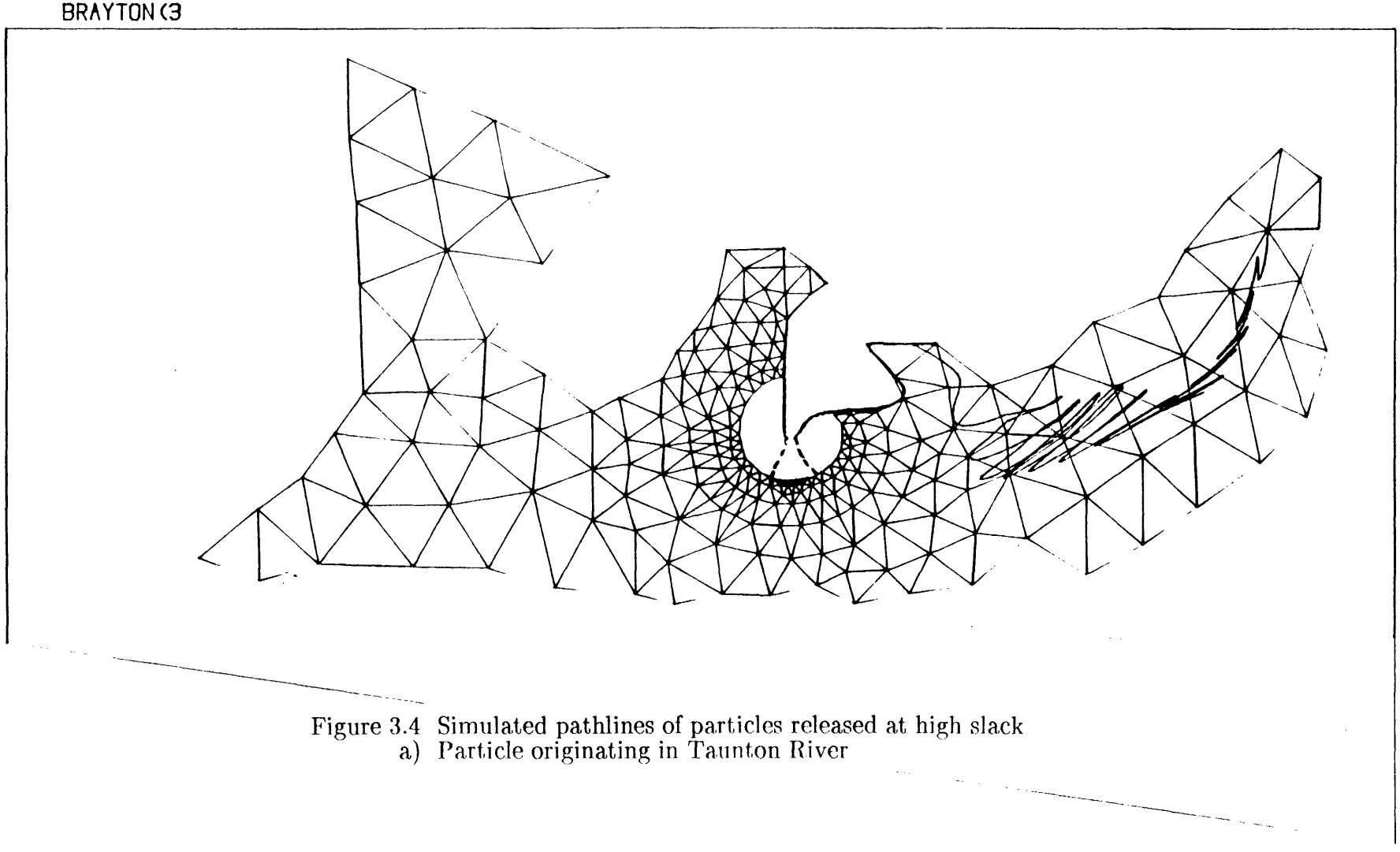

Figure 3.4 Simulated pathlines of particles released at high slack
a) Particle originating in Taunton River

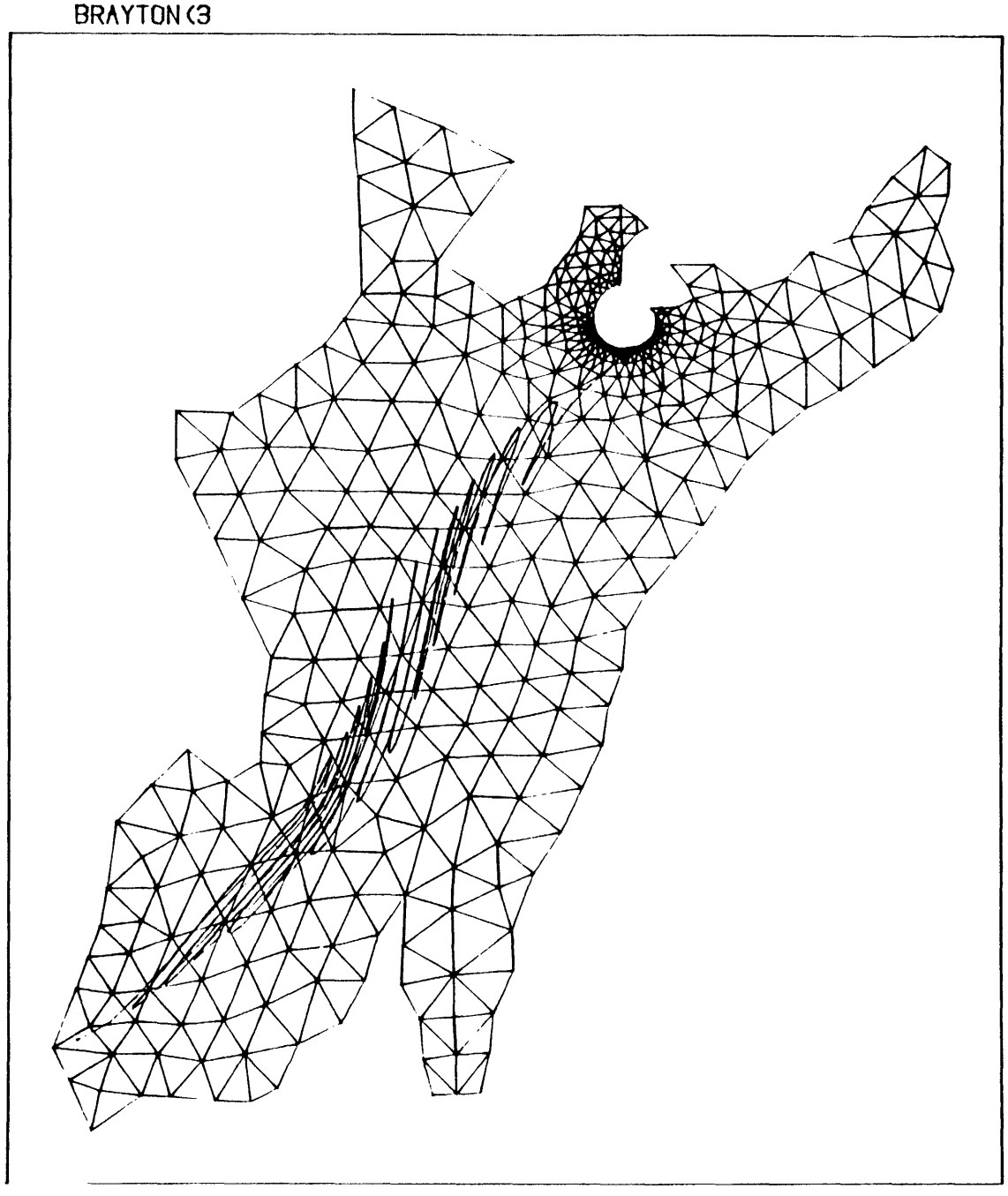

Figure 3.4b Particle originating at center of plume

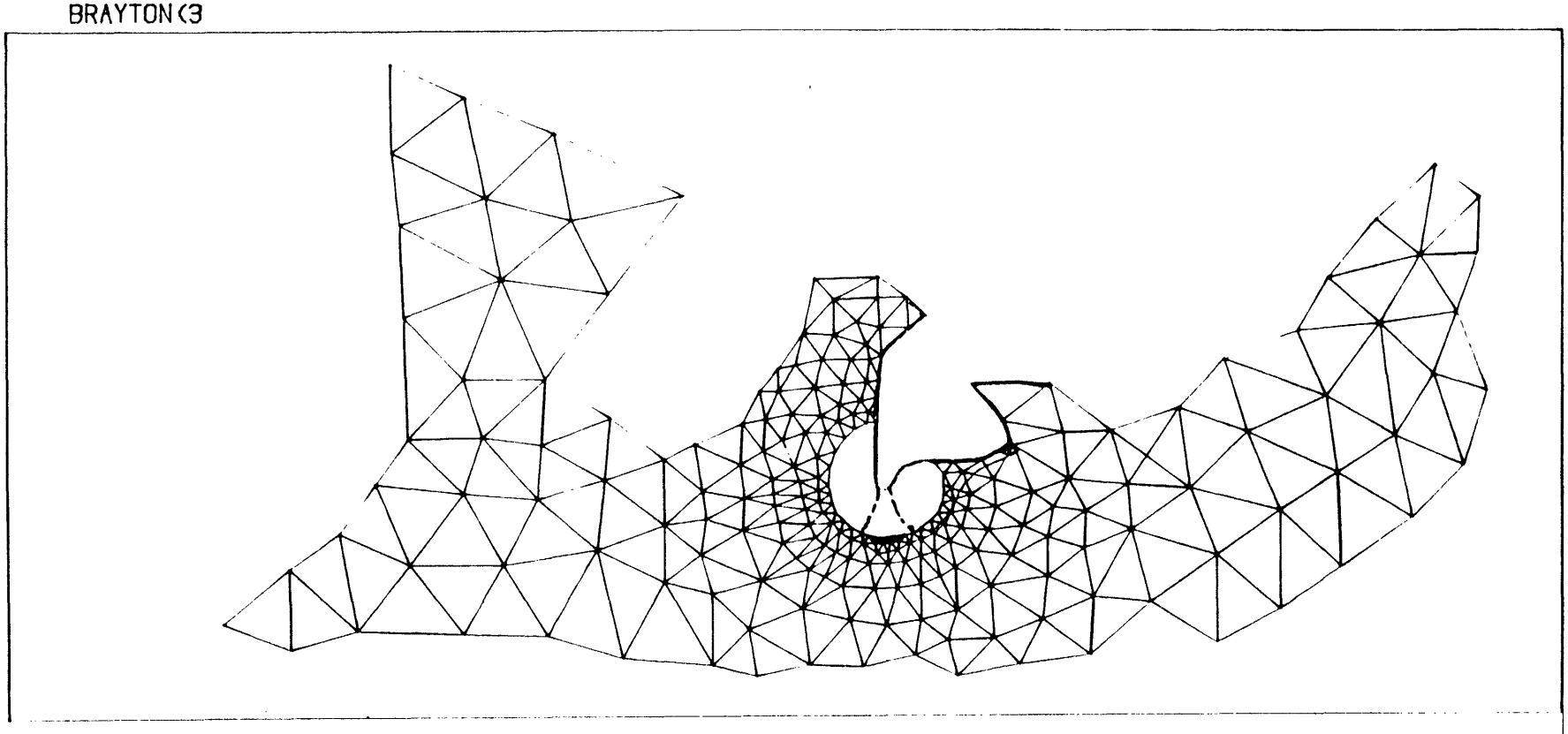

Figure 3.4c Particle originating at plume edge

Figure 3.5 Quasi-steady surface layer excess temperatures (°F) as a function of tidal stage (3 units, D = 1.0 m²/s, $\alpha = 1$, no wind, $\Delta t = 31$ min, static heat budget.)

a) High slack

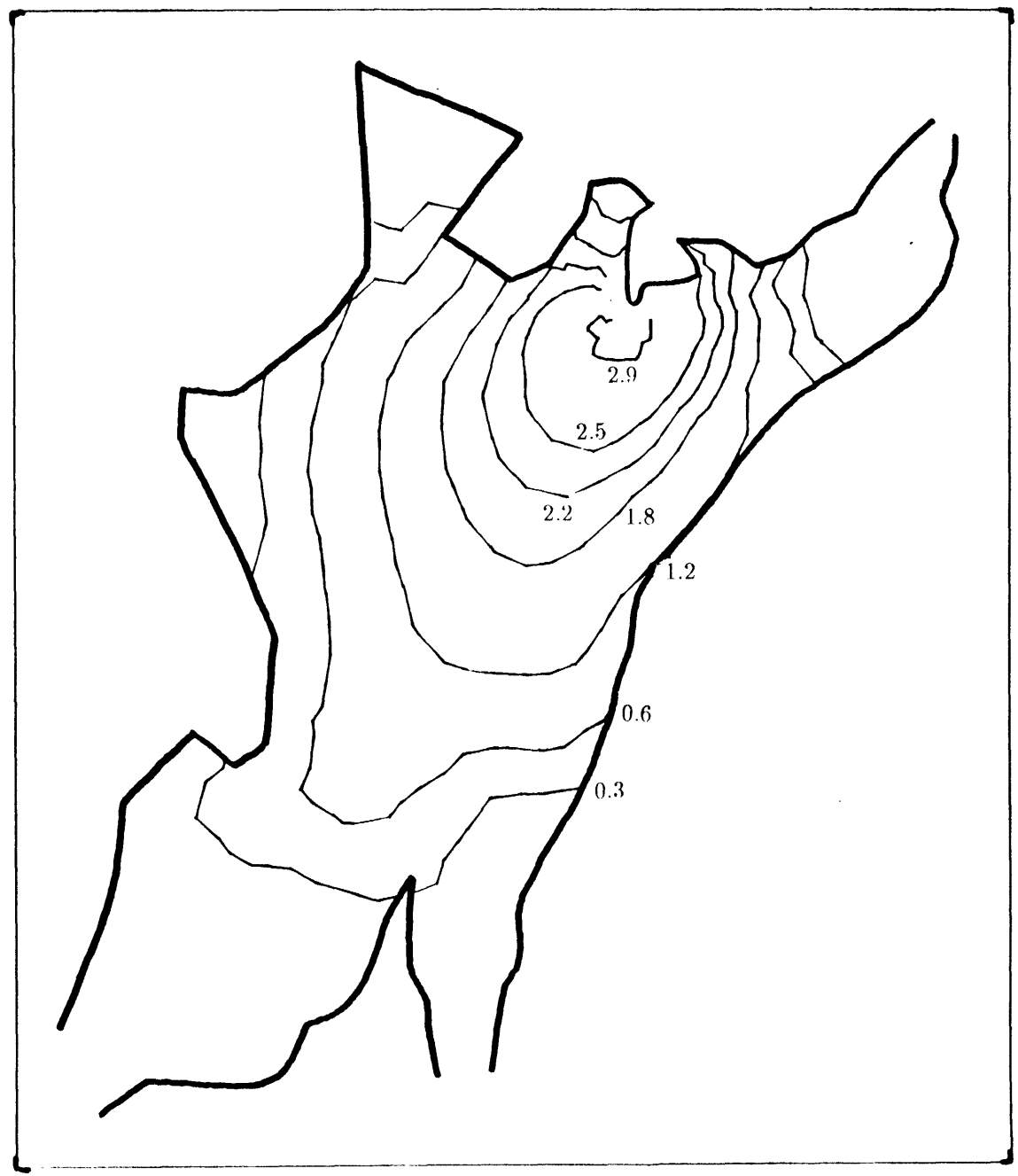

Figure 3.5b Maximum ebb

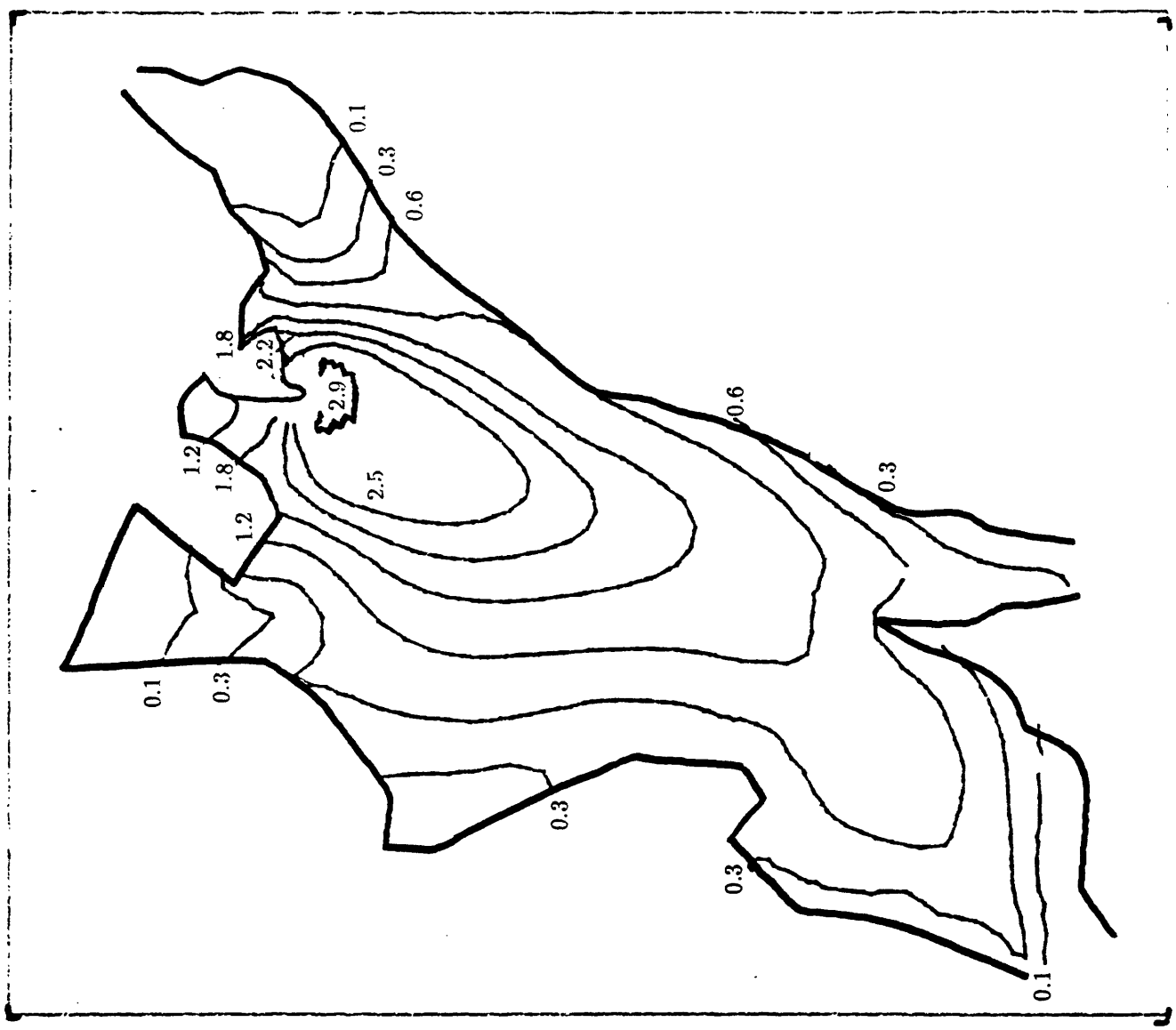

Figure 3.5c Low slack

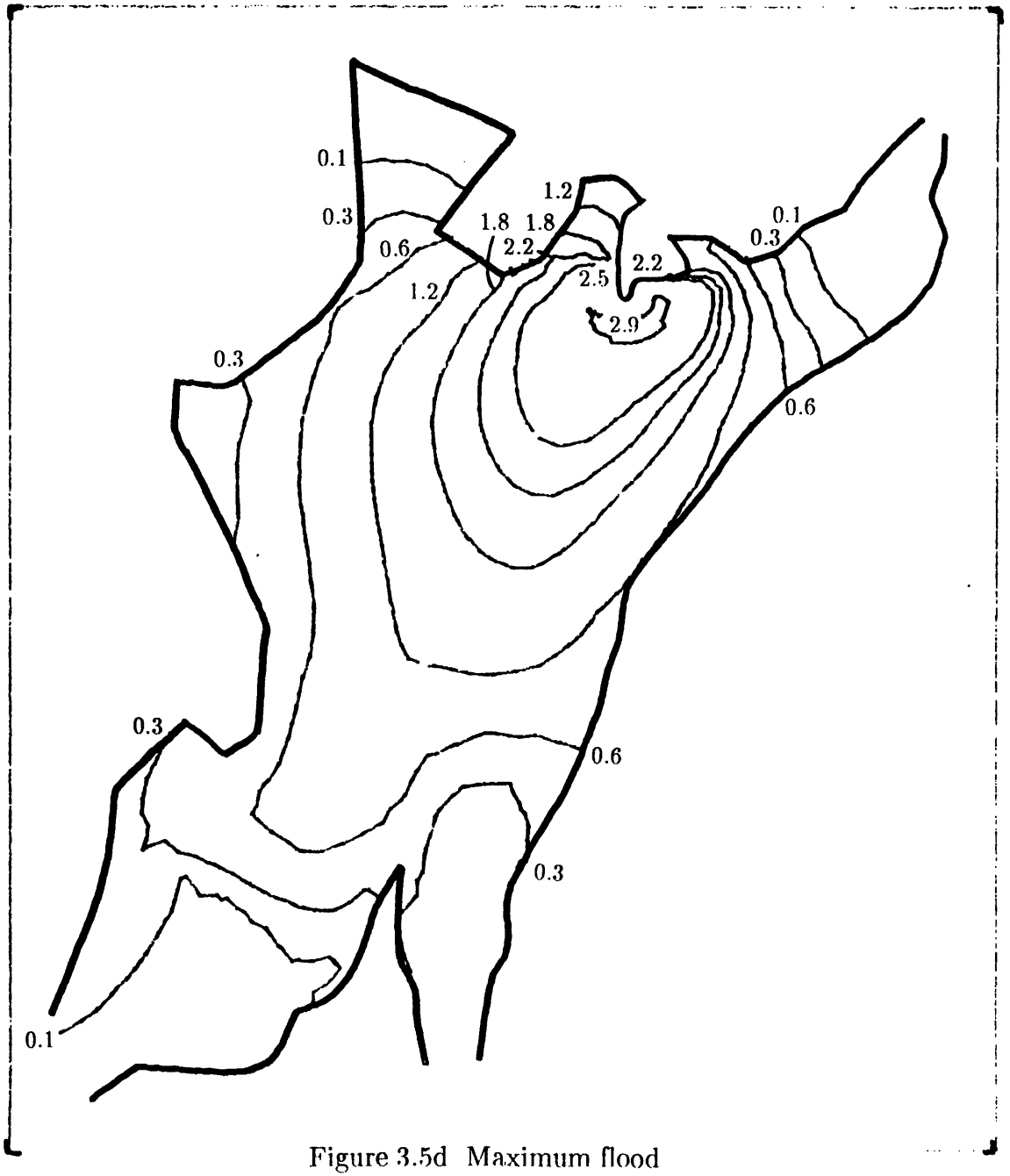

Figure 3.5d Maximum flood

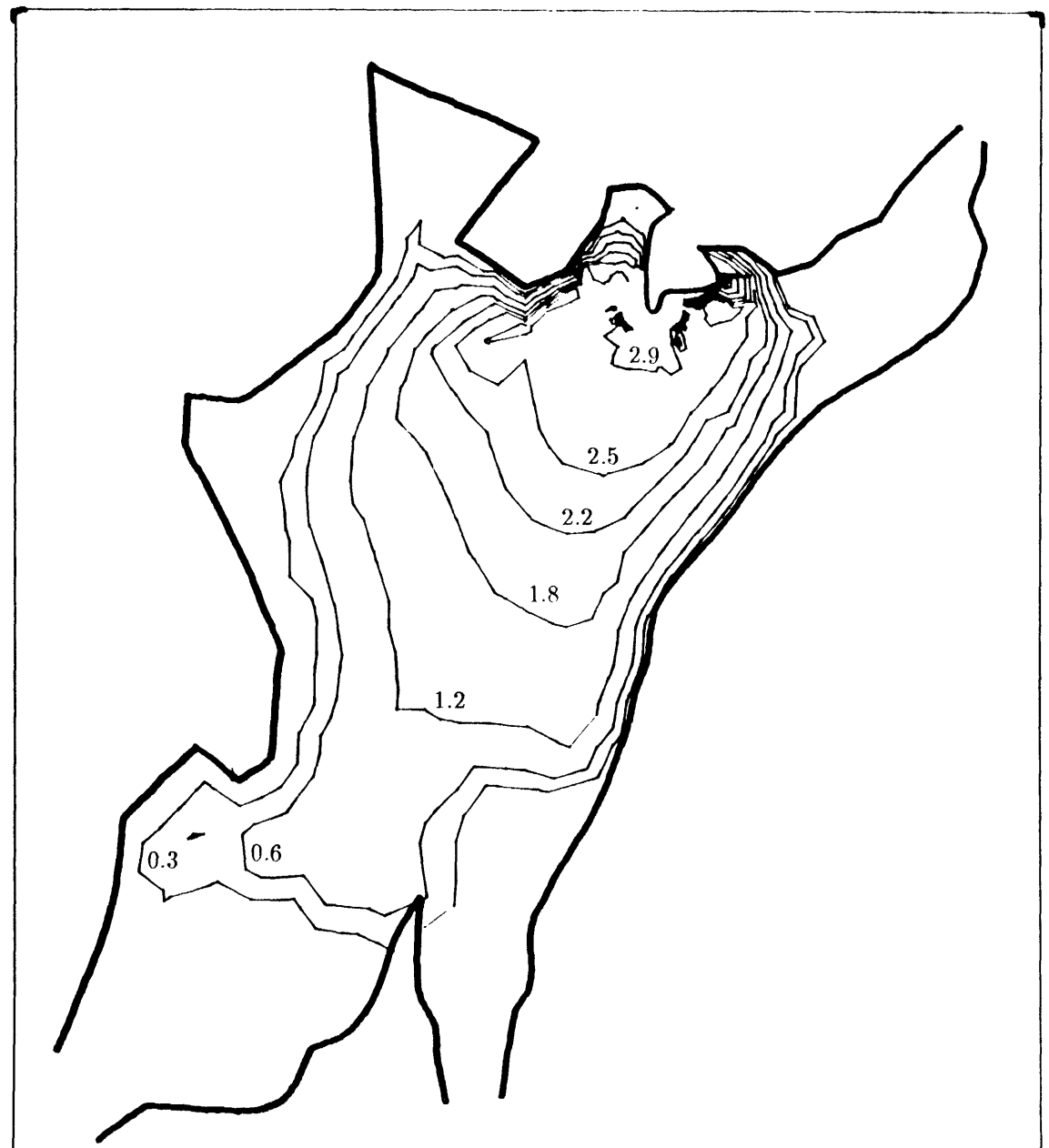

Figure 3.6 Quasi-steady surface layer excess temperatures (°F) as a function of diffusion coefficient (3 units, max. ebb, $\Delta t = 31$ min, $\alpha = 1$, static heat budget). Compare also with Figure 3.5b ($D = 1\ m^2/s$)
a) $D = 0\ m^2/s$

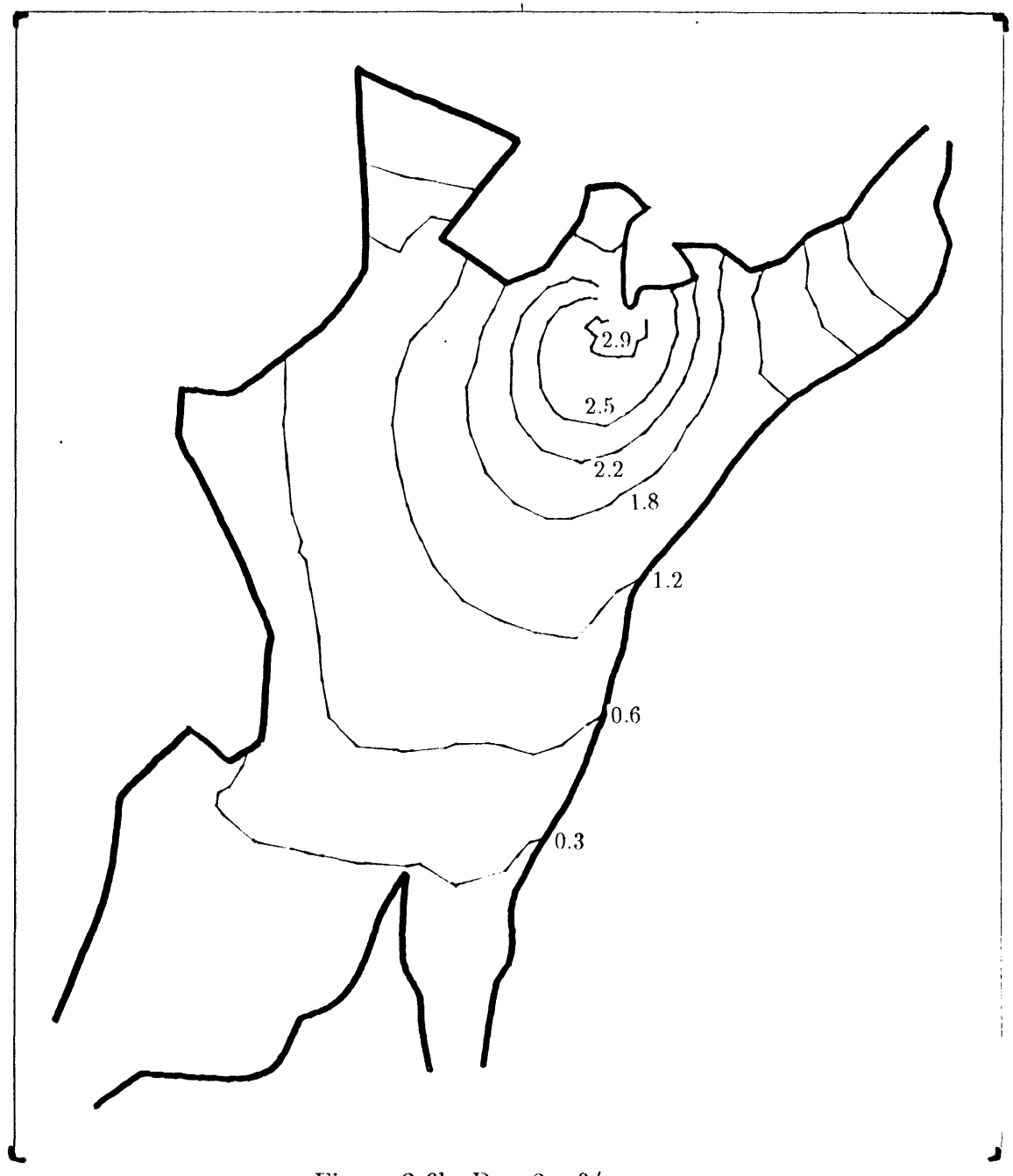

Figure 3.6b D = 3 m²/s

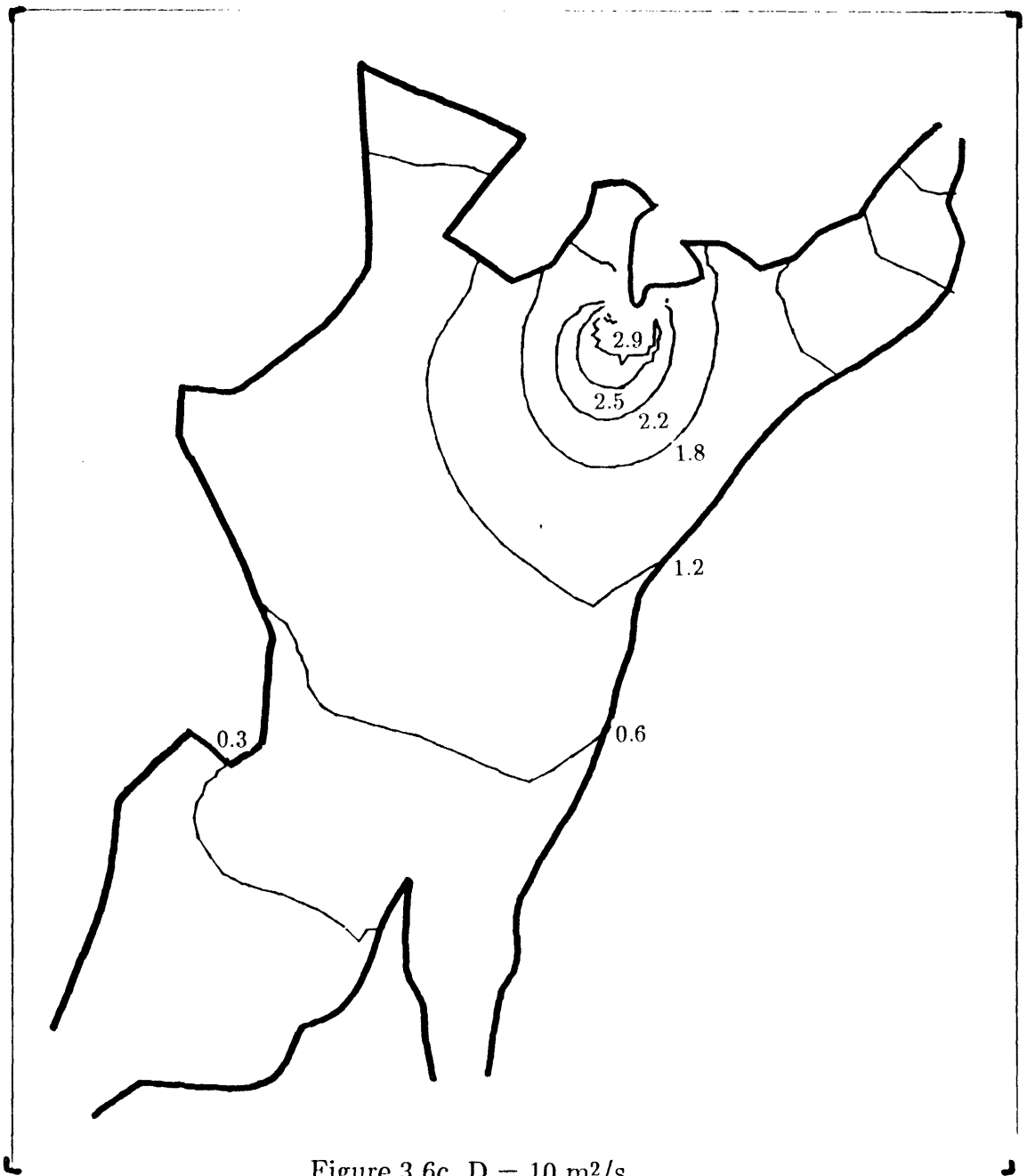

Figure 3.6c D = 10 m^2/s

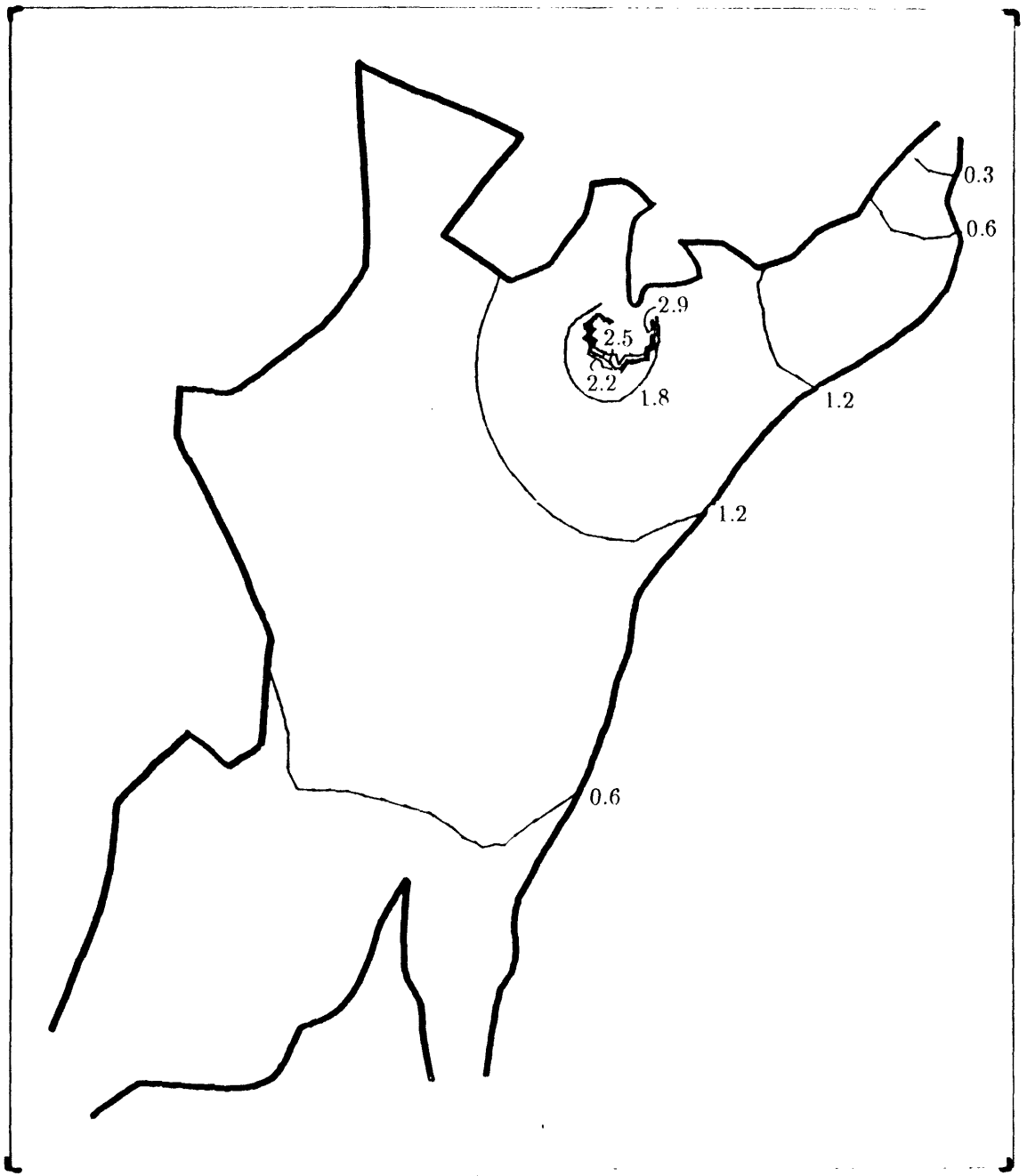

Figure 3.6d) D = 30 m²/s

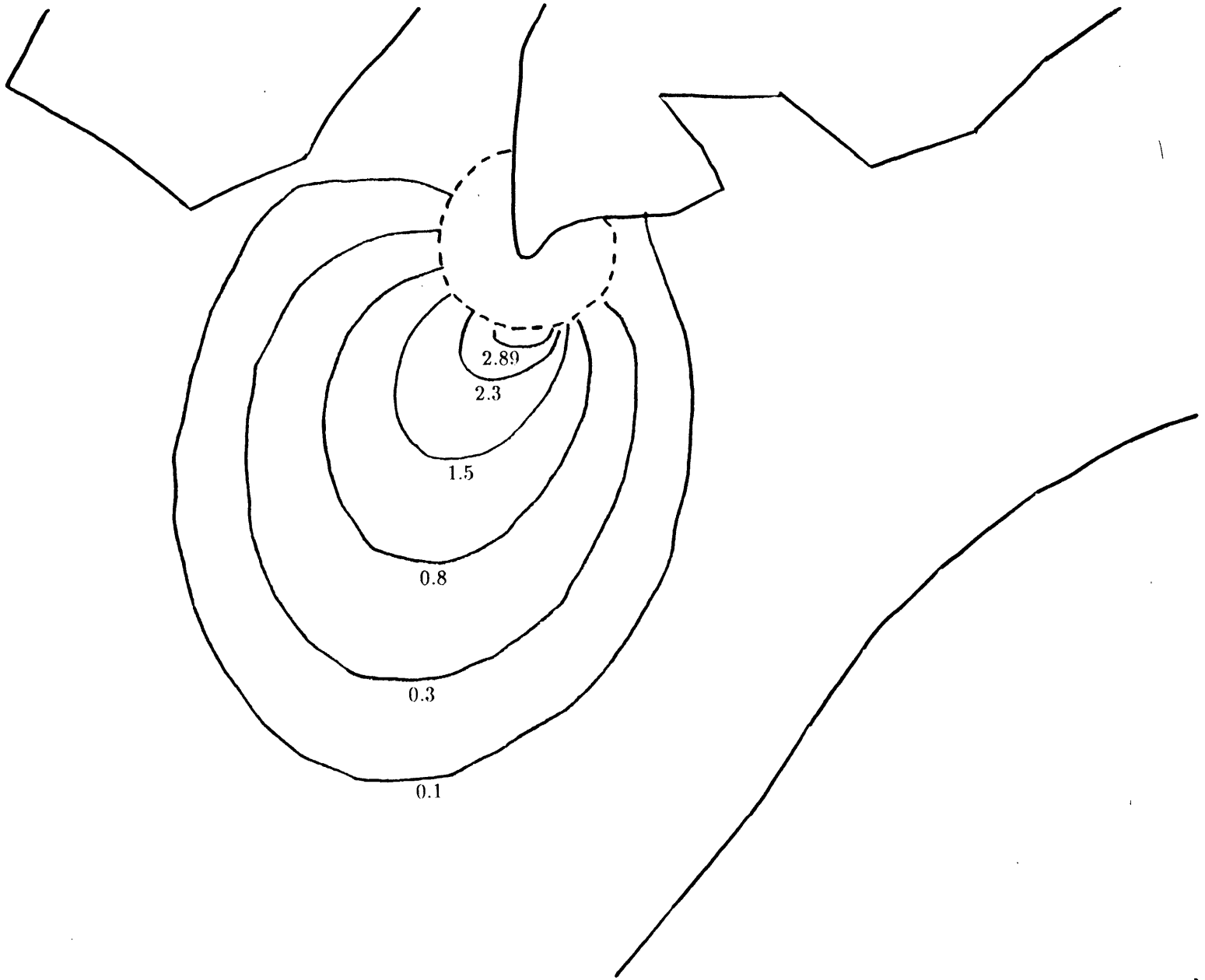

Figure 3.7 Transient surface layer excess temperatures (°F) as a function of time step (3 units, max. ebb, D = 10 m^2/s, $\alpha = 1$, no wind, static heat budget, elapsed time = 186 min)
a) $\Delta t = 6.2$ min

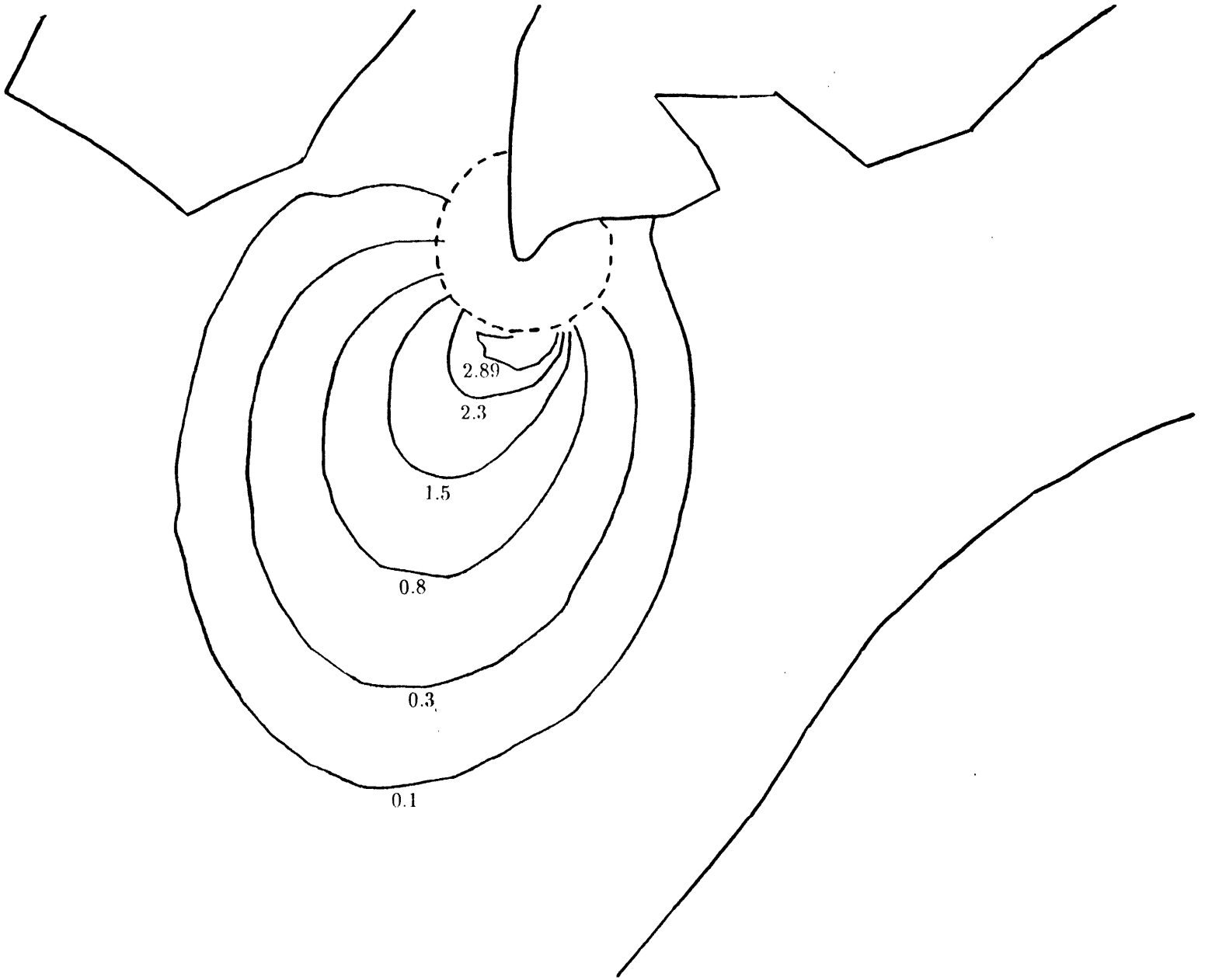

Figure 3.7b $\Delta t = 15.5$ min

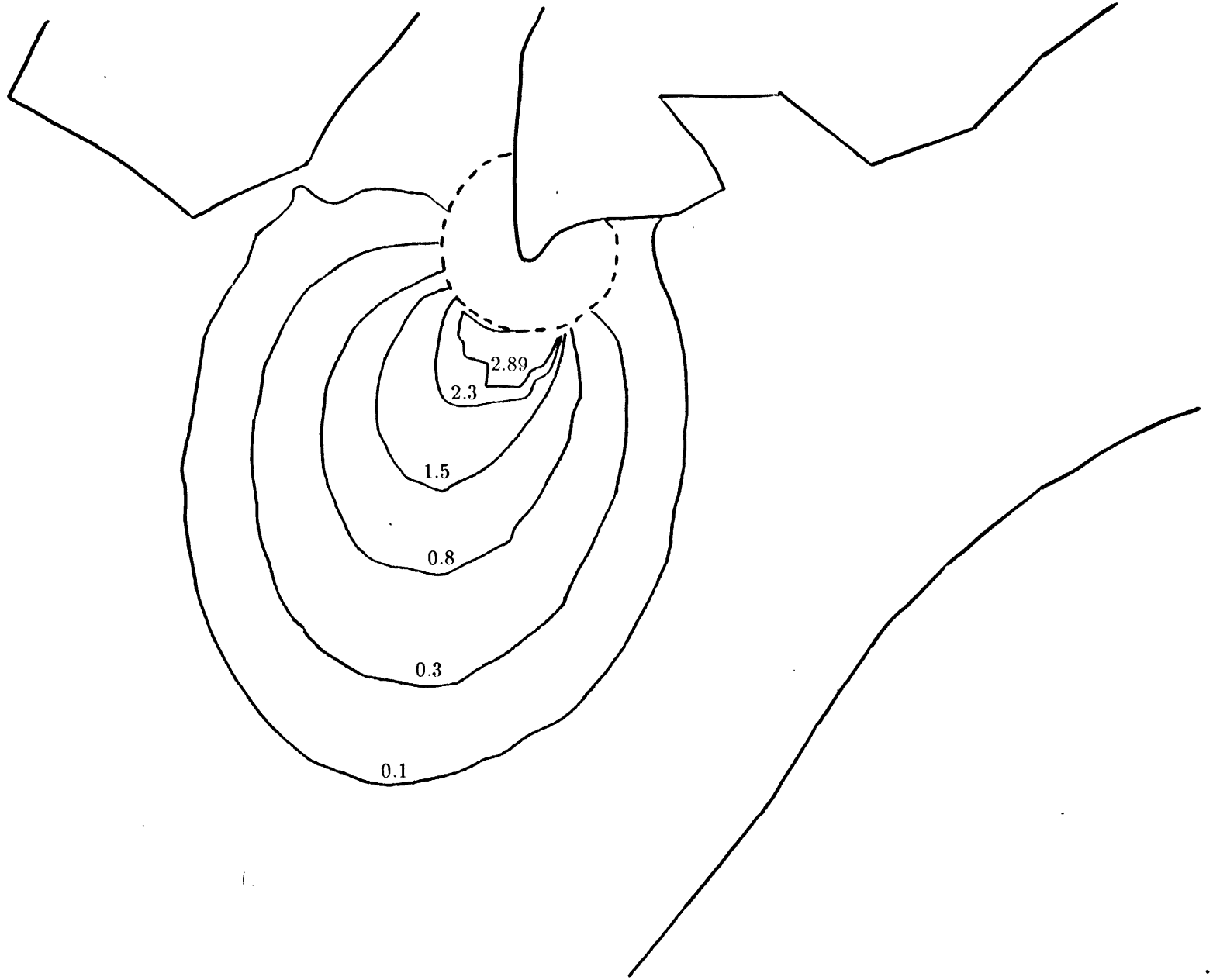

Figure 3.7c $\Delta t = 31$ min

Figure 3.7d $\Delta t = 186$ min

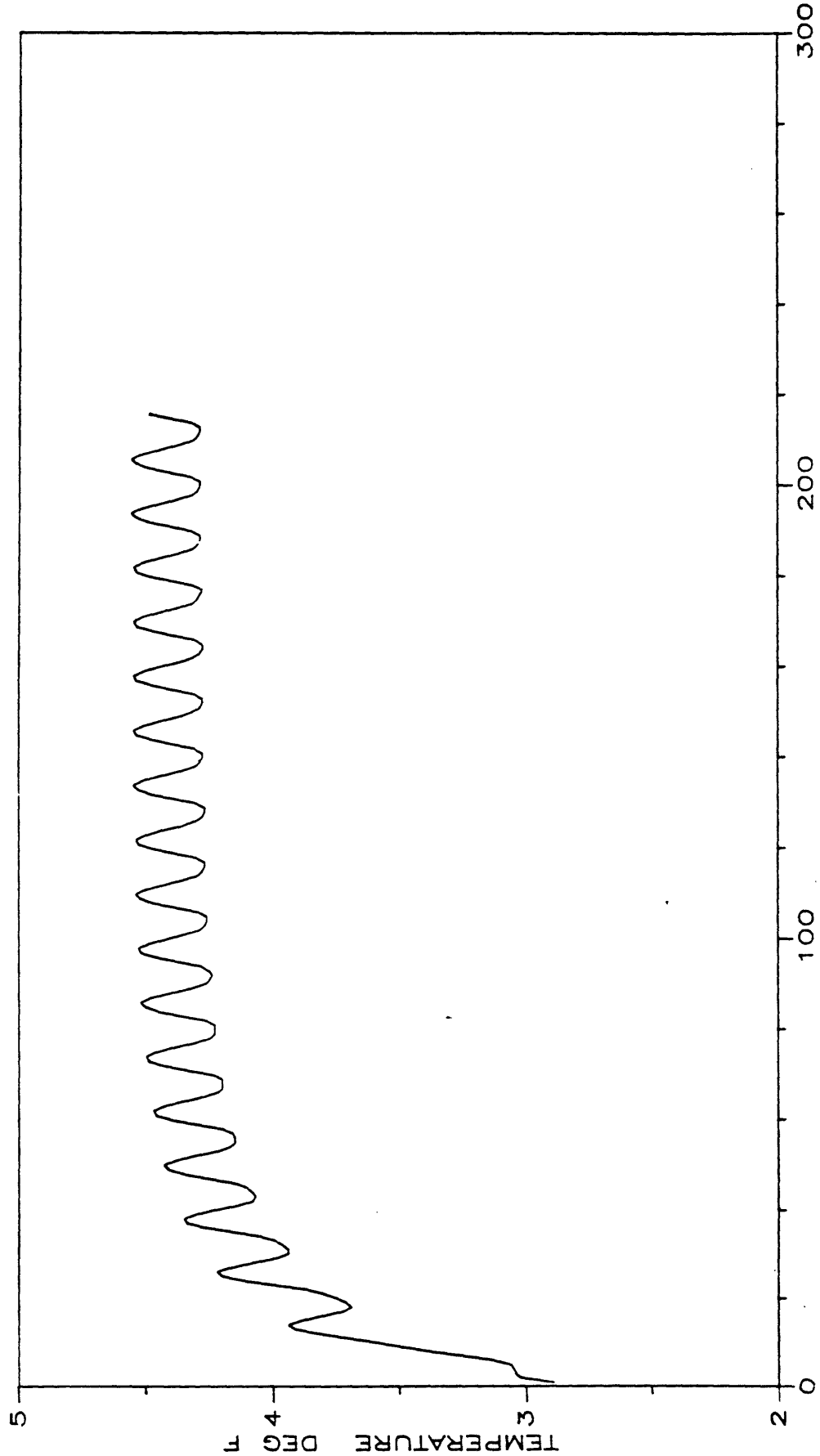

Figure 3.8 Time-varying parameters for dynamic heat budget calculations ($\alpha = 1$)
a) Discharge temperature

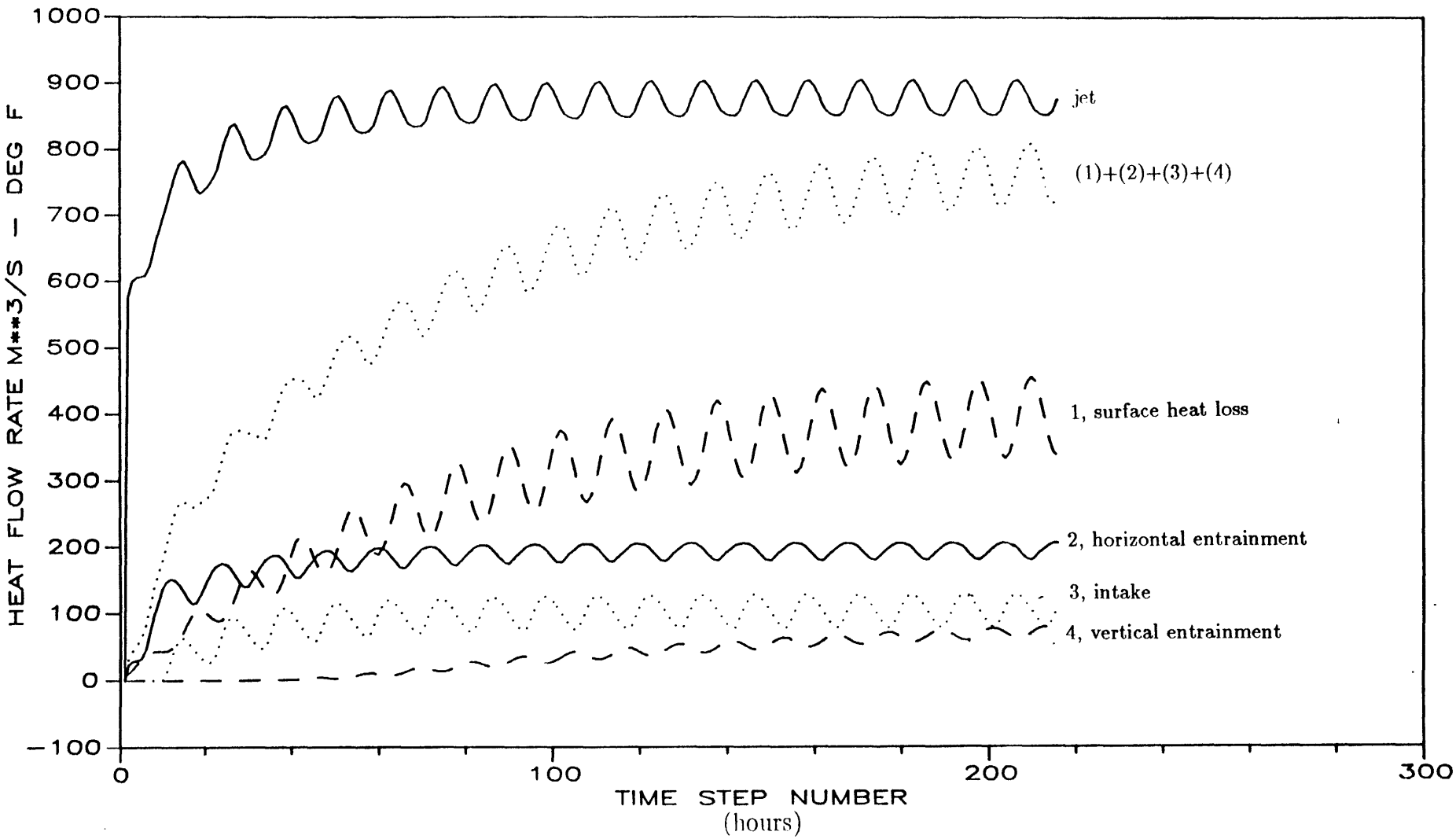

Figure 3.8b) Various heat fluxes

Figure 3.9 Quasi-steady surface layer excess temperatures (°F) using dynamic heat budget calculations (max. ebb, $\Delta t = 31$ min, no wind, $D = 1.0$ m^2/s, $\alpha = 1$). Compare with corresponding static heat budget calculations of Figure 3.5b.

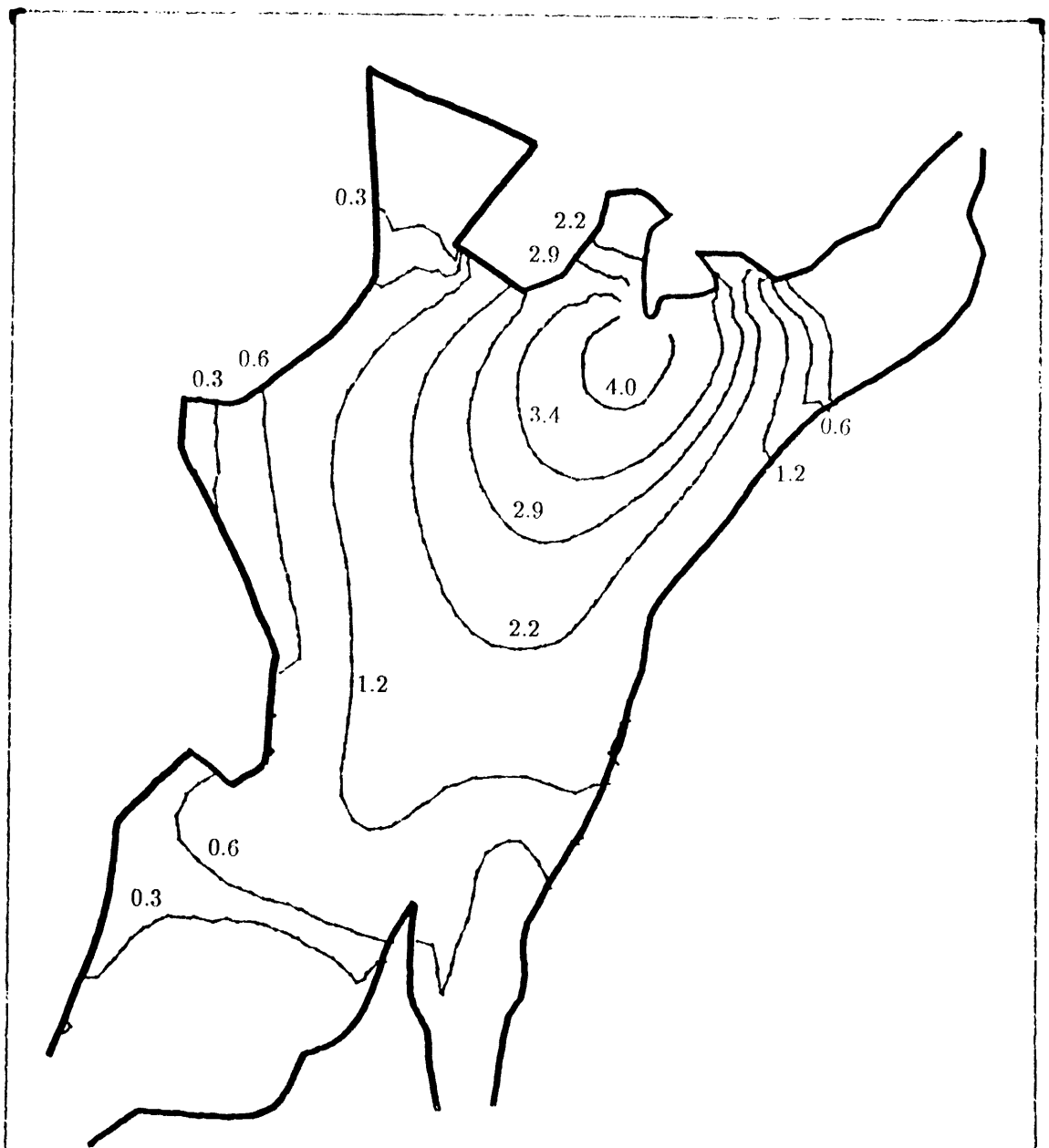

Figure 3.10 Quasi-steady surface layer excess temperatures (°F) using dynamic heat budget calculations with $\alpha = 0.5$ (max. ebb, $\Delta t = 31$ min, no wind, D = 1.0 m^2/s). Compare with corresponding calculations for $\alpha = 1$ shown in 3.9.

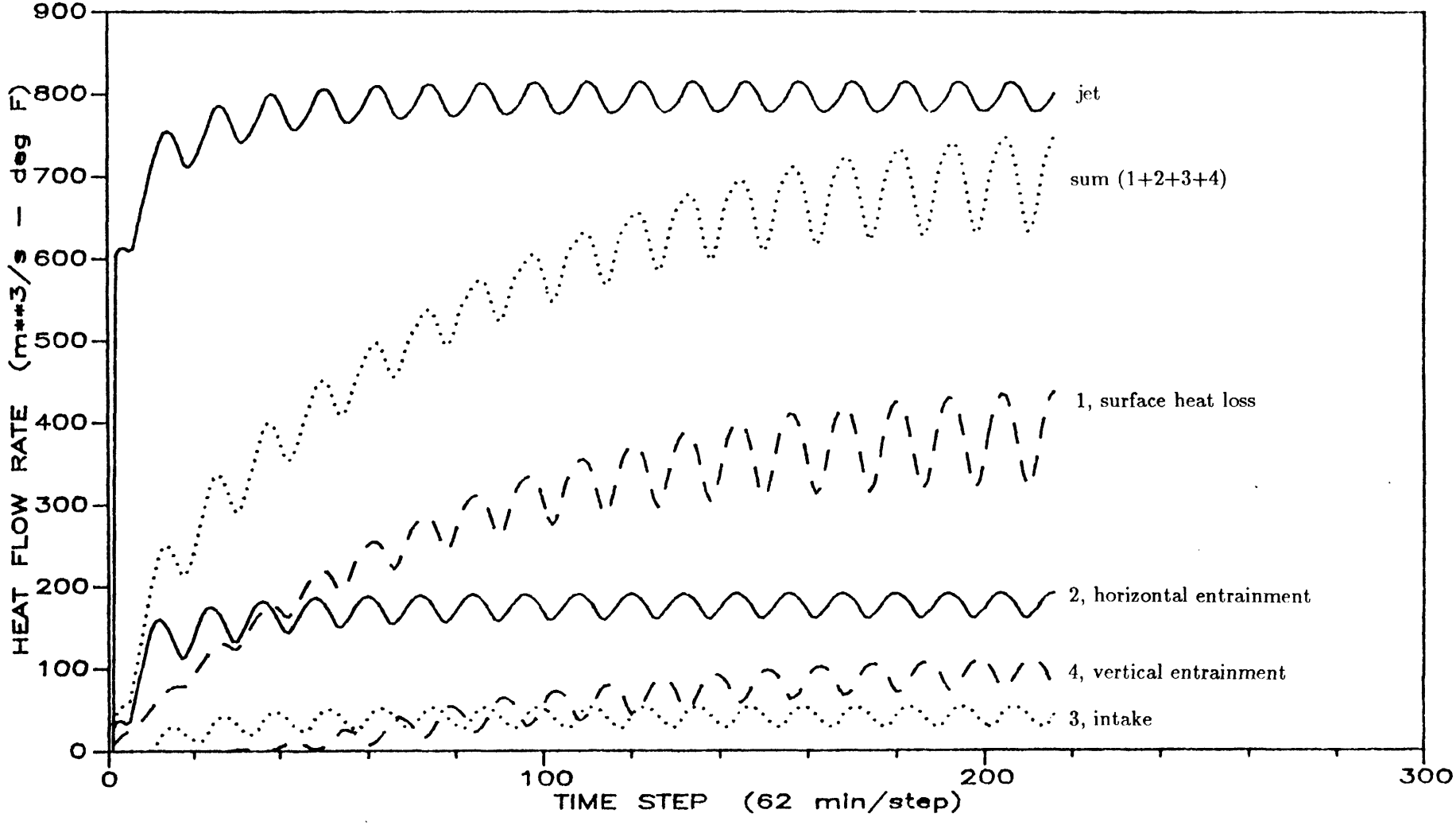

Figure 3.11 Time-varying parameters for dynamic heat budget calculations ($\alpha = 0.5$). Compare with corresponding fluxes with $\alpha = 1$ in Figure 3.8b.
a) Various heat fluxes

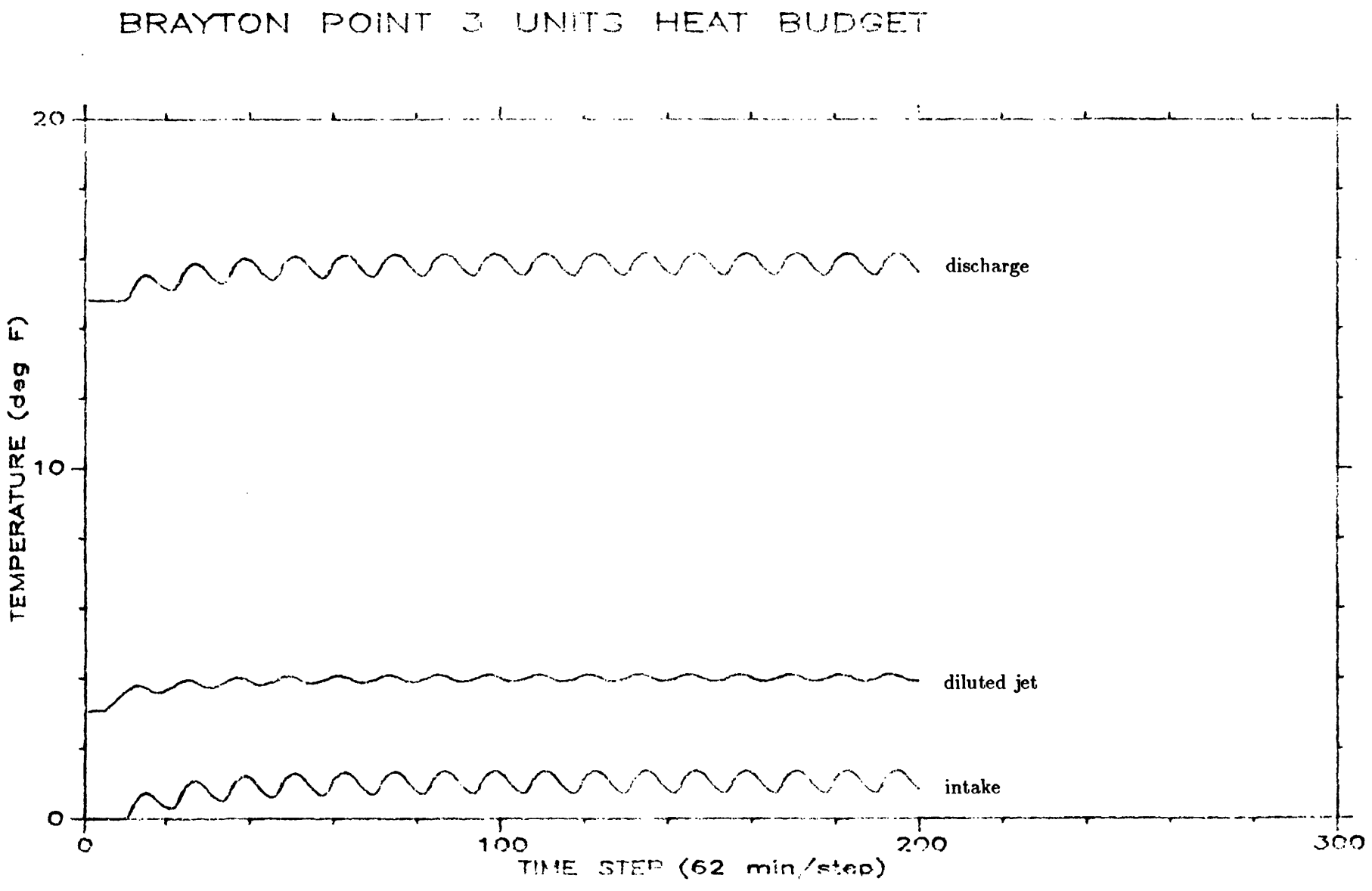

Figure 3.11b Discharge, intake, and diluted jet temperature

Figure 3.12 Surface layer excess temperatures (°F) under influence of surface wind drift (3 units, D = 1.0 m^2/s, $\alpha = 1$, $\Delta t = 31$ min, static heat budget). Compare with corresponding calculations without wind drift in Figure 3.5b.
a) Steady 3 m/s westerly wind

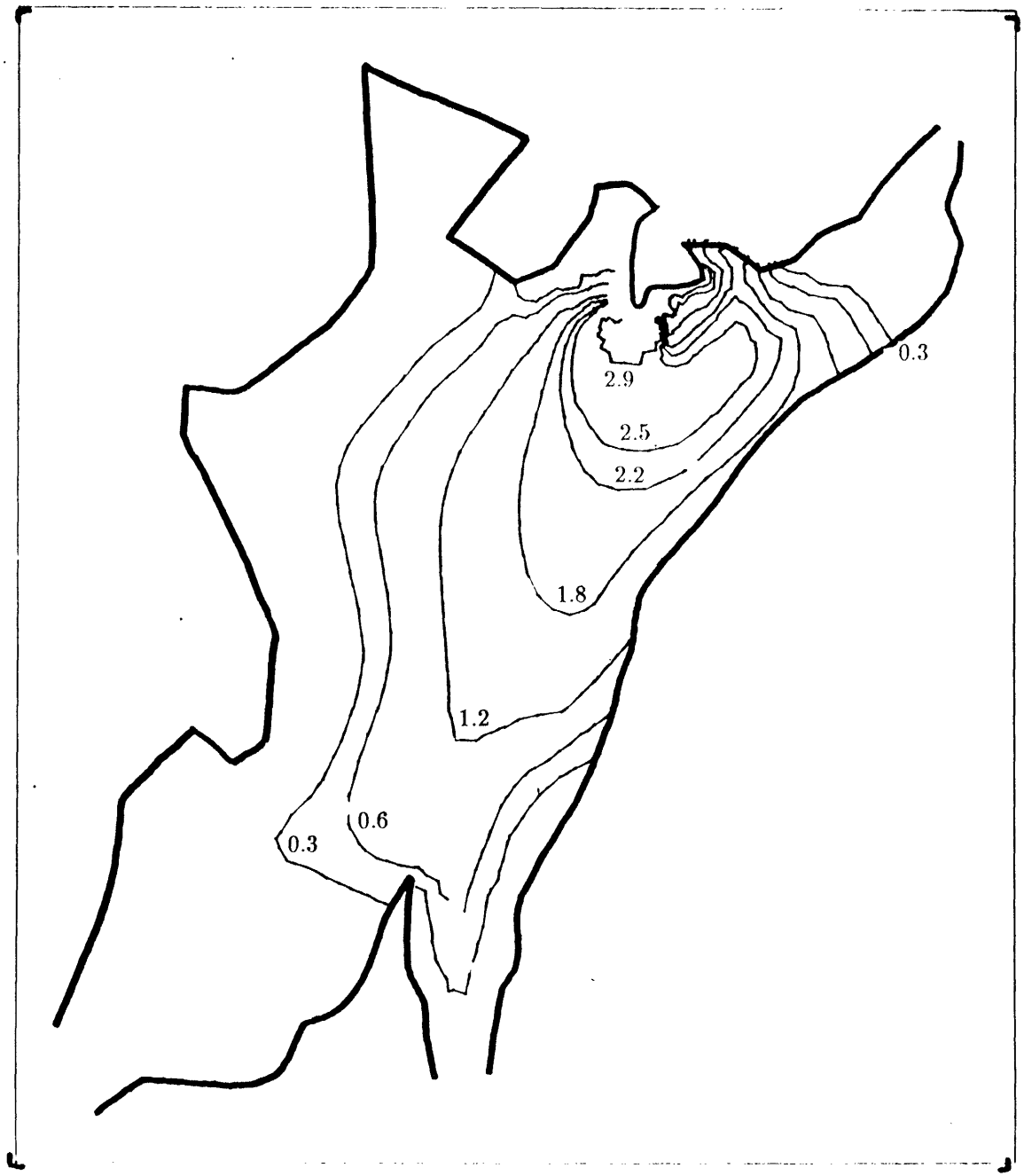

Figure 3.12b Variable wind

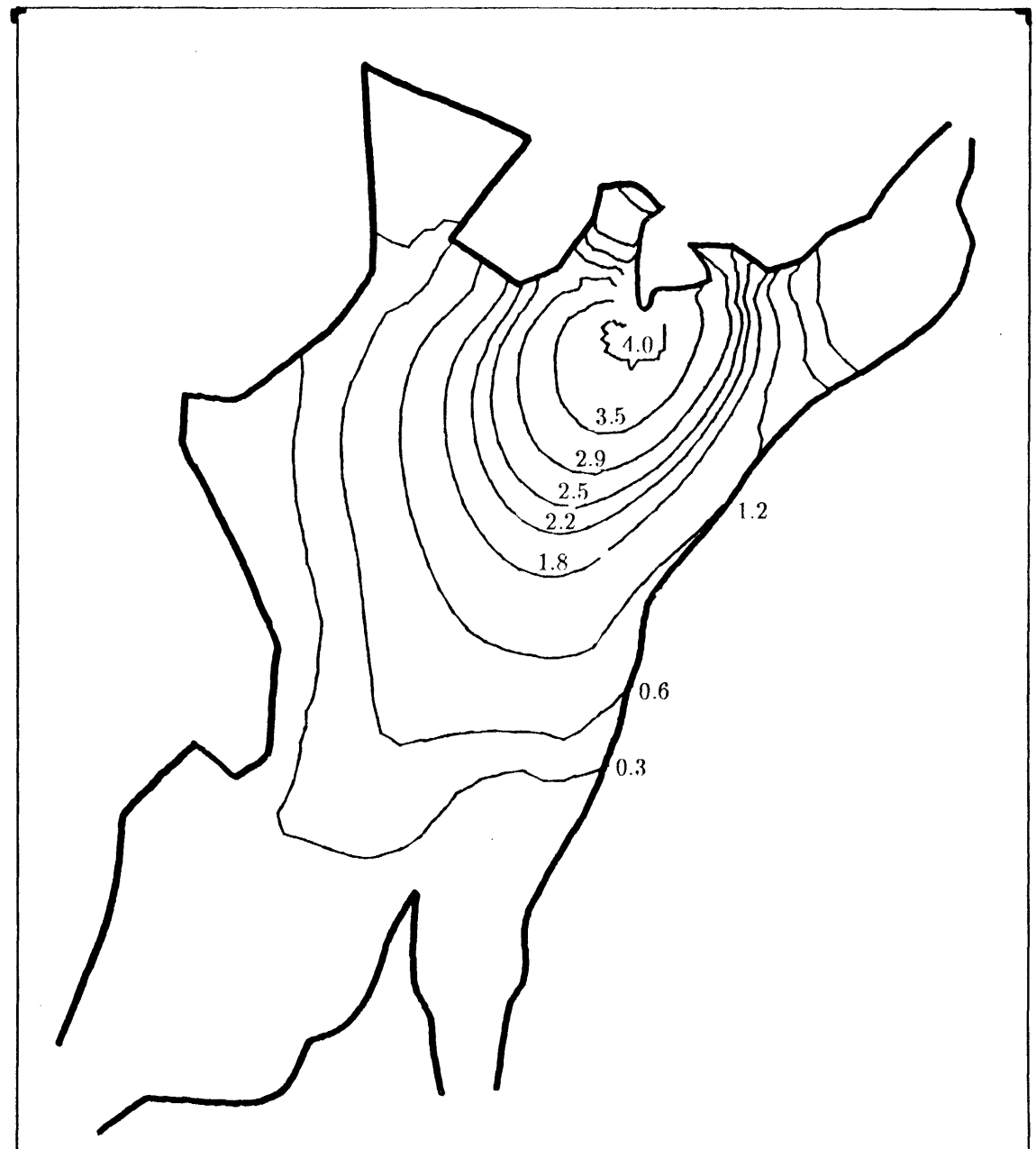

Figure 3.13 Computed 3-D excess temperatures (°F) as a function of depth (3 units, $D = 1.0\ m^2/s$, $\alpha = 1$, no wind, $\Delta t = 31$ min, static heat budget)
a) Surface

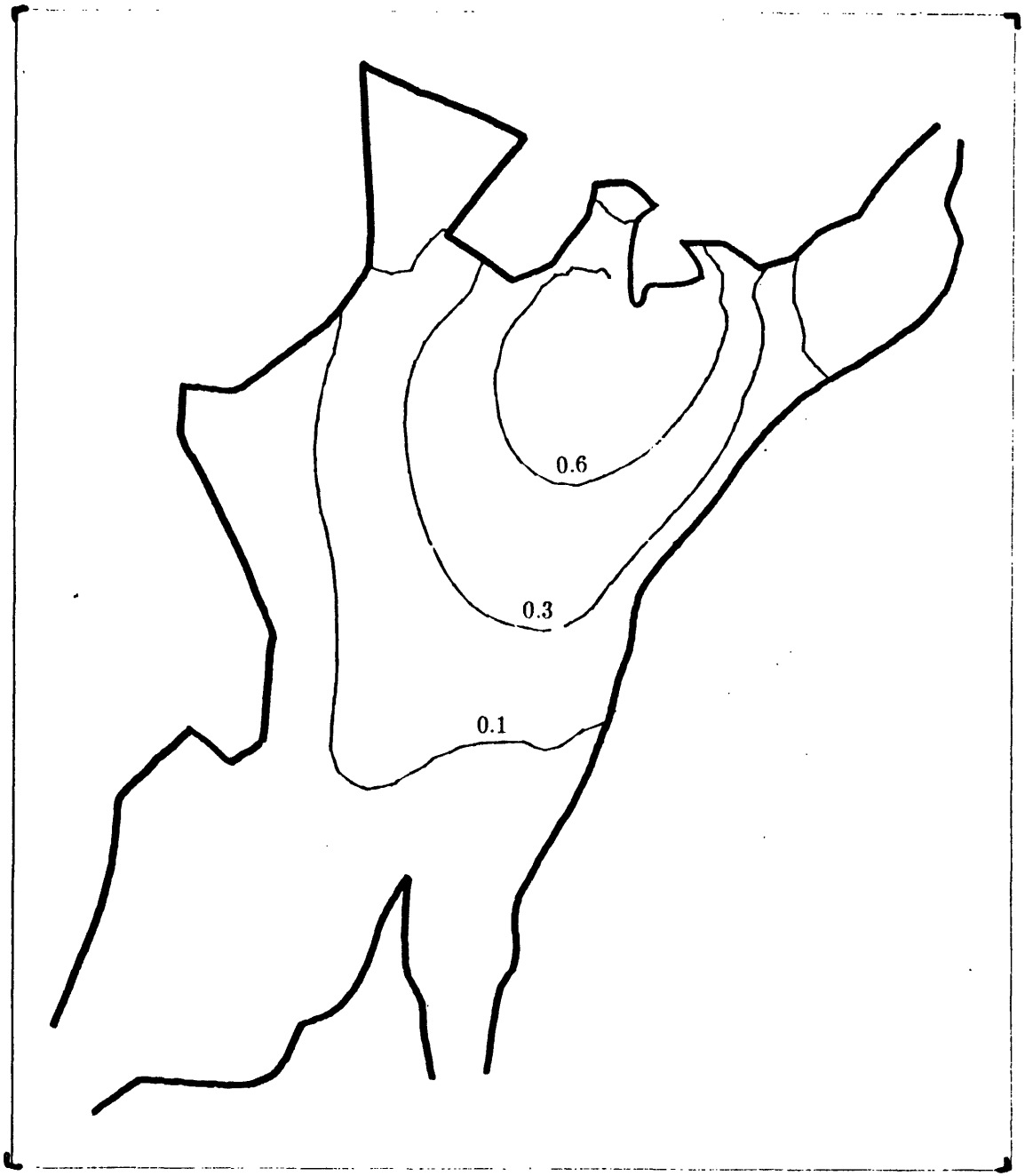

Figure 3.13b Depth = 3.5 m

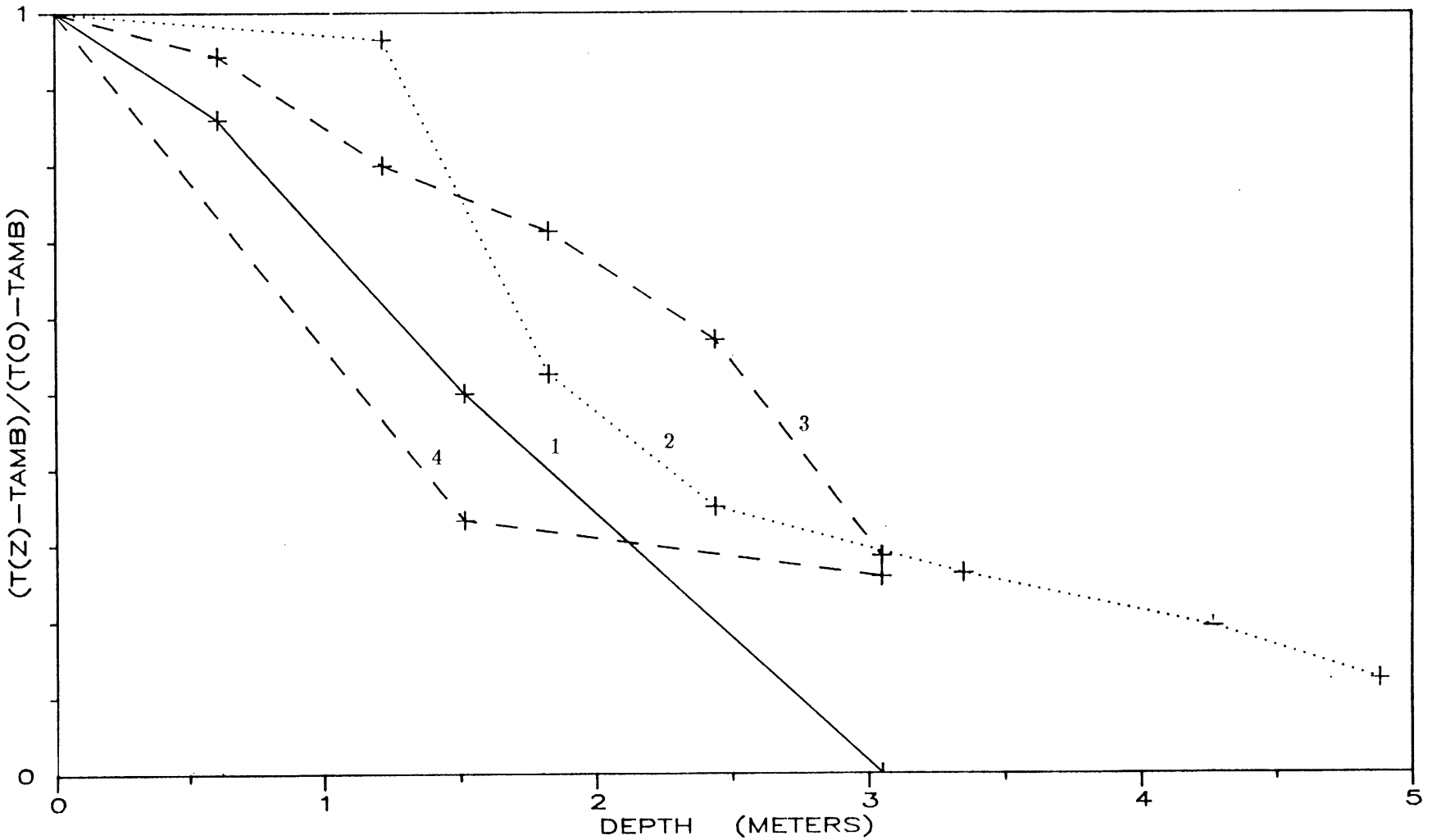

Figure 3.14 Vertical normalized excess temperature profiles
a) Measurements at four stations identified in Figure 3.2a

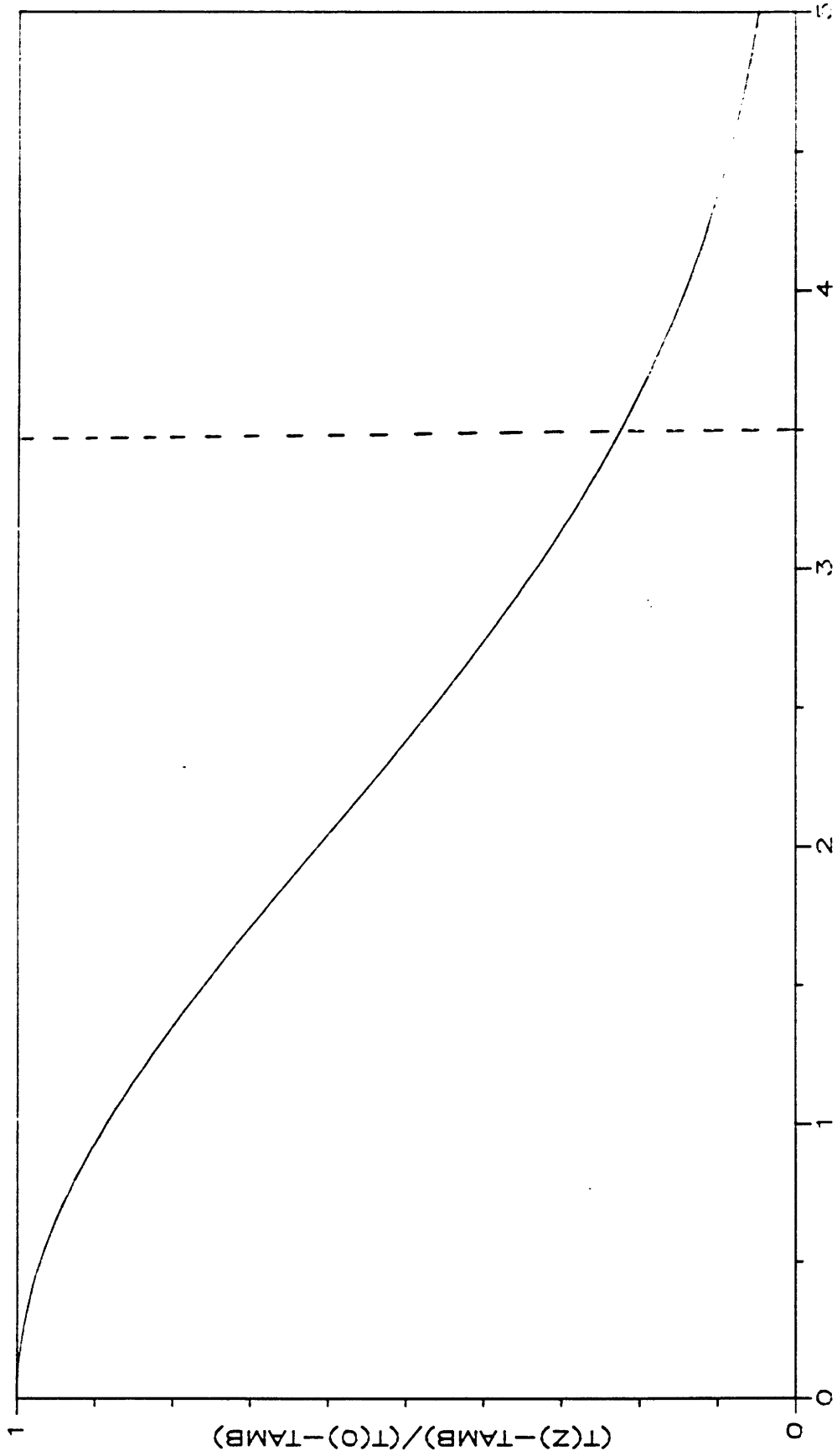

Figure 3.14b Simulation with $F_z = 0$

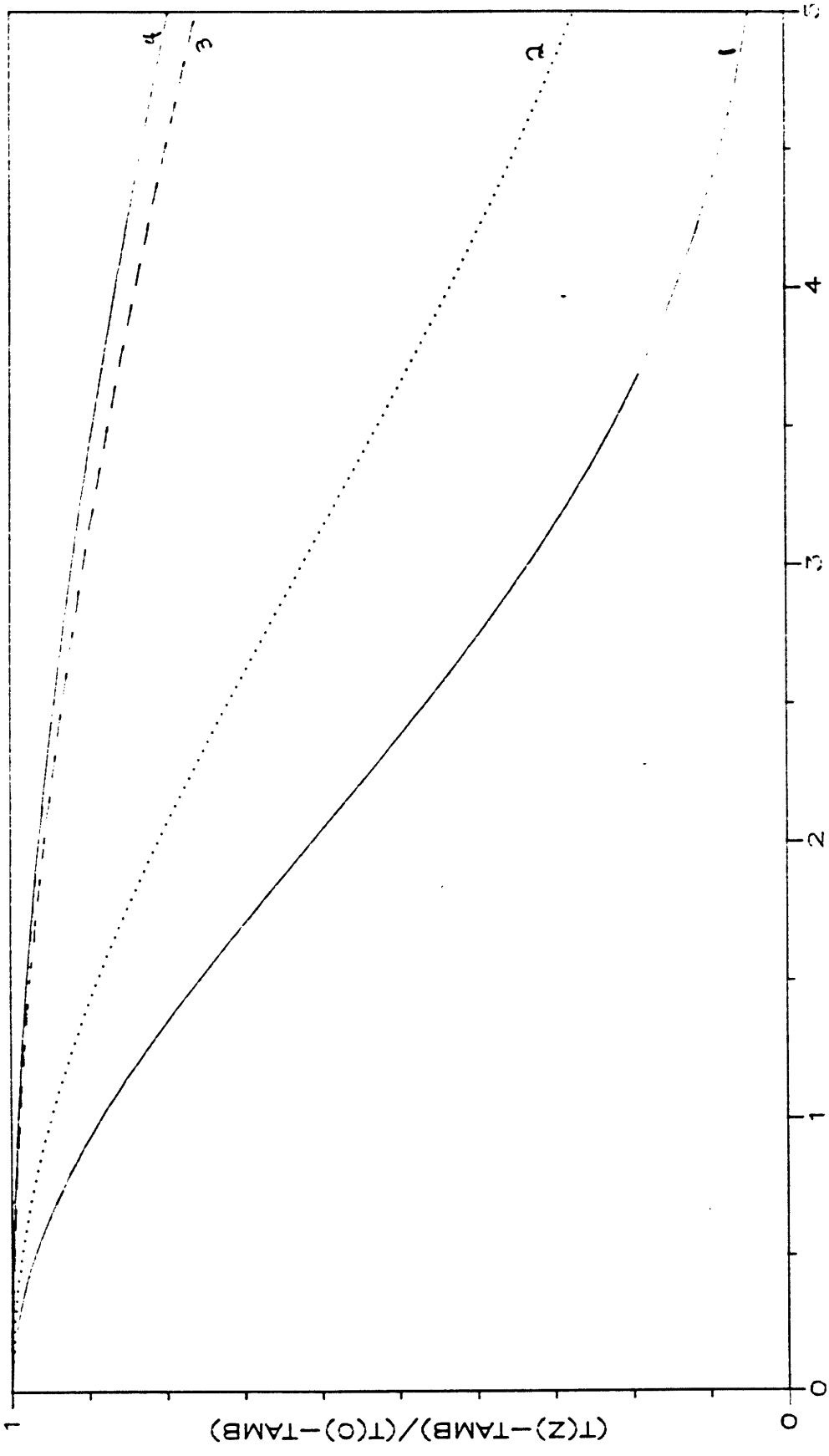

Figure 3.14c Simulation with $E_z = 0.0001$ m^2/s

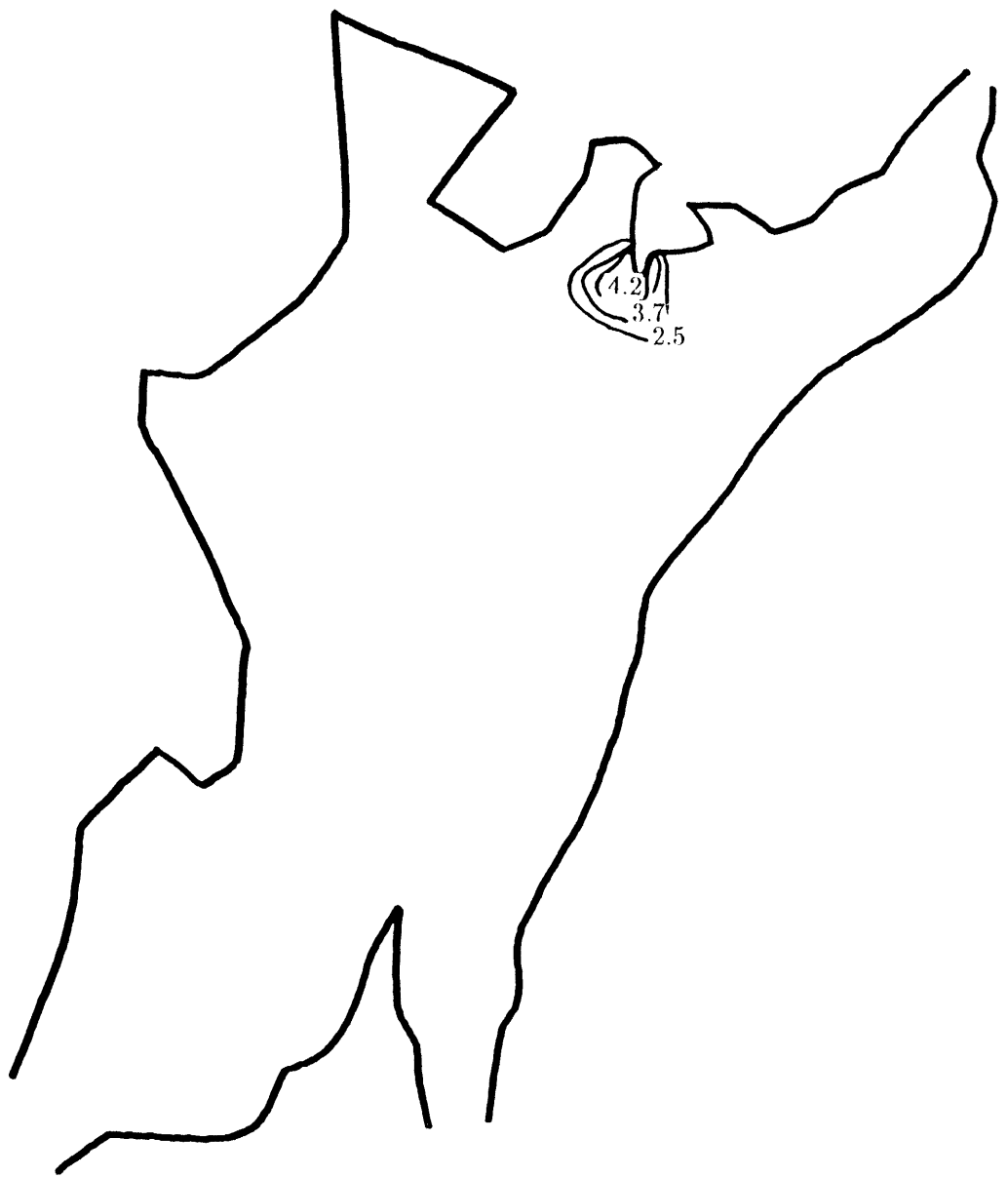

Figure 3.15 Surface layer excess temperatures (°F) at high slack on August 25, 1976
a) Measurements

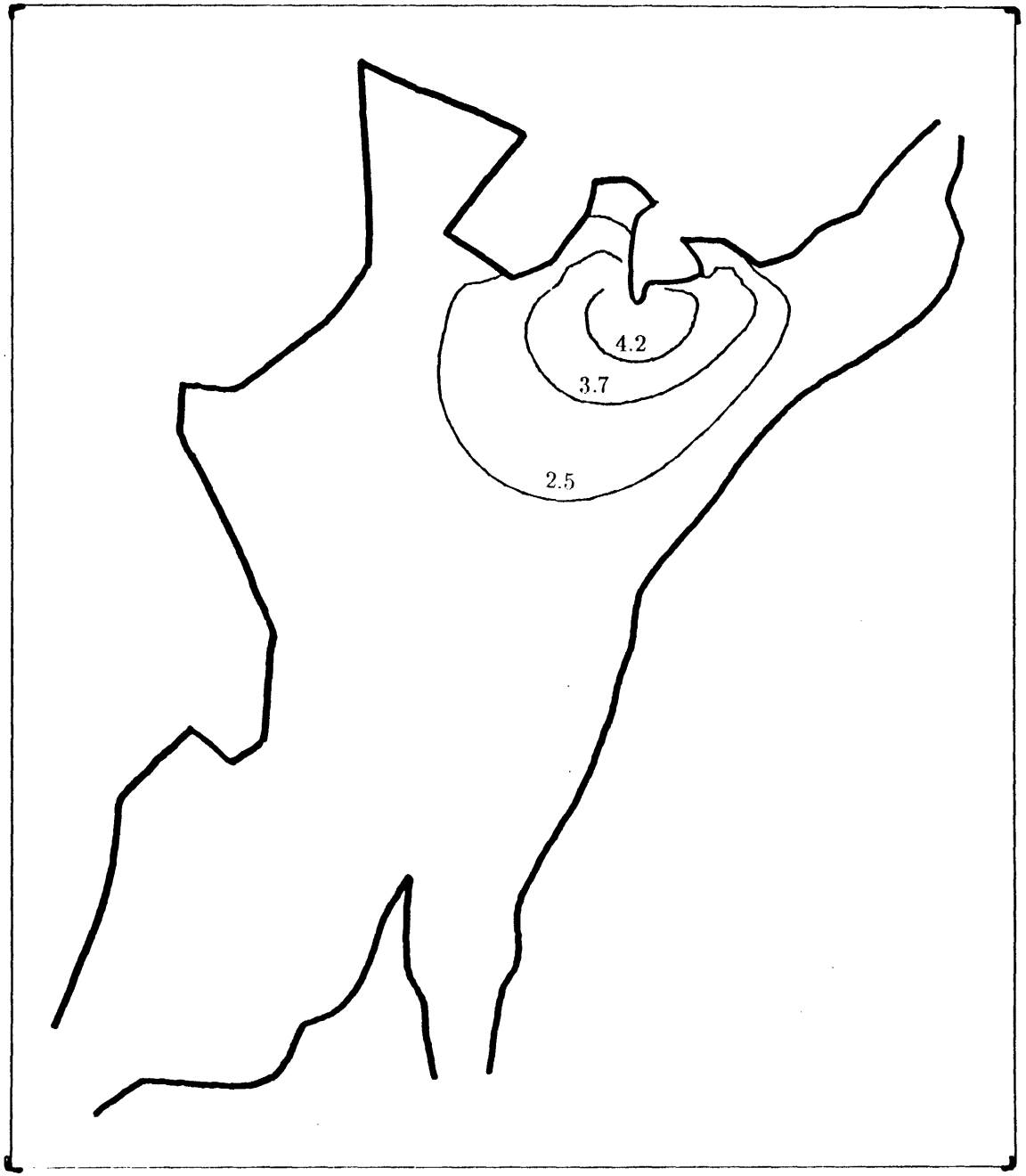

Figure 3.15b Simulation

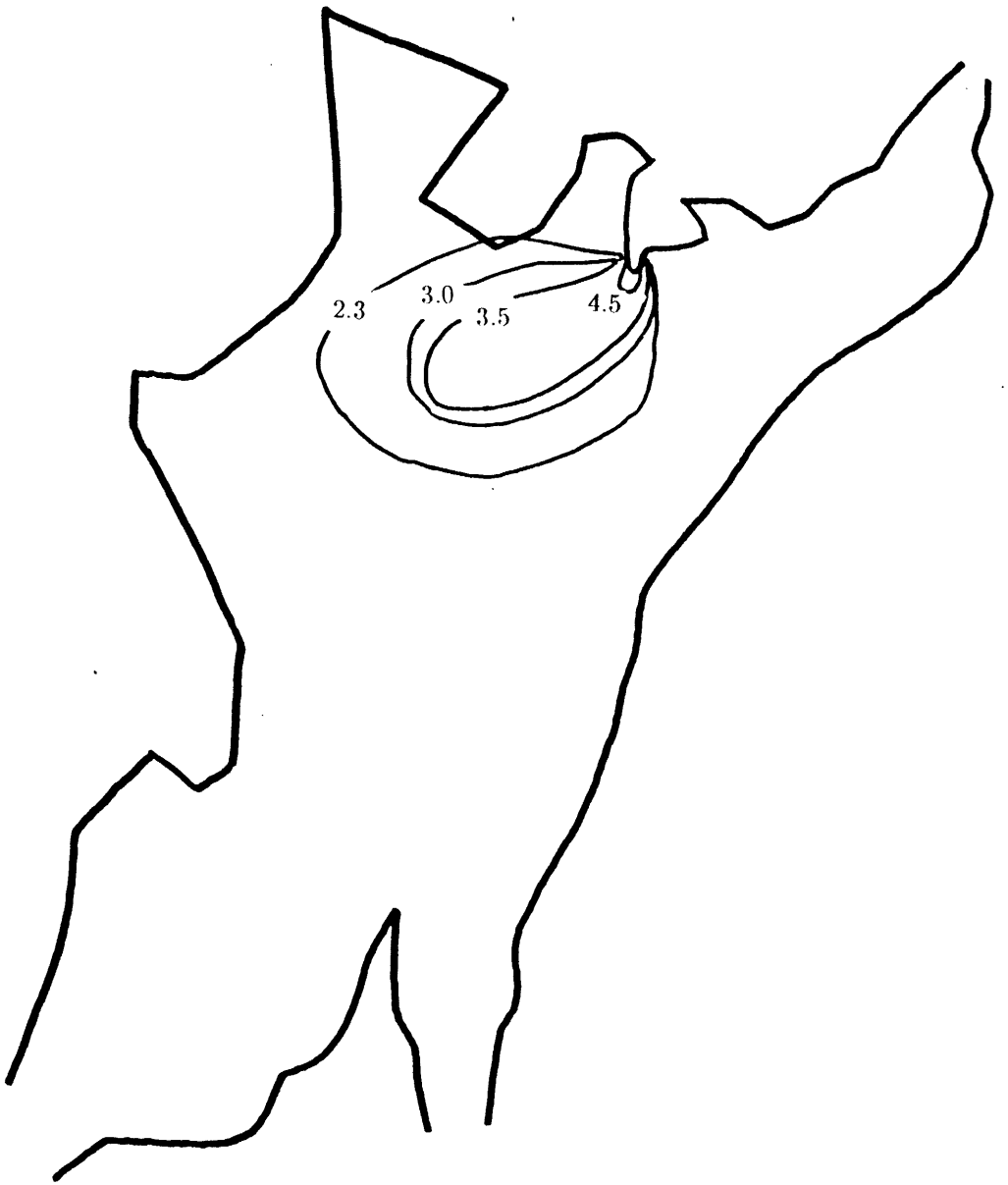

Figure 3.16 Surface layer excess temperatures (°F) at maximum ebb on August 25, 1976
a) Measurements

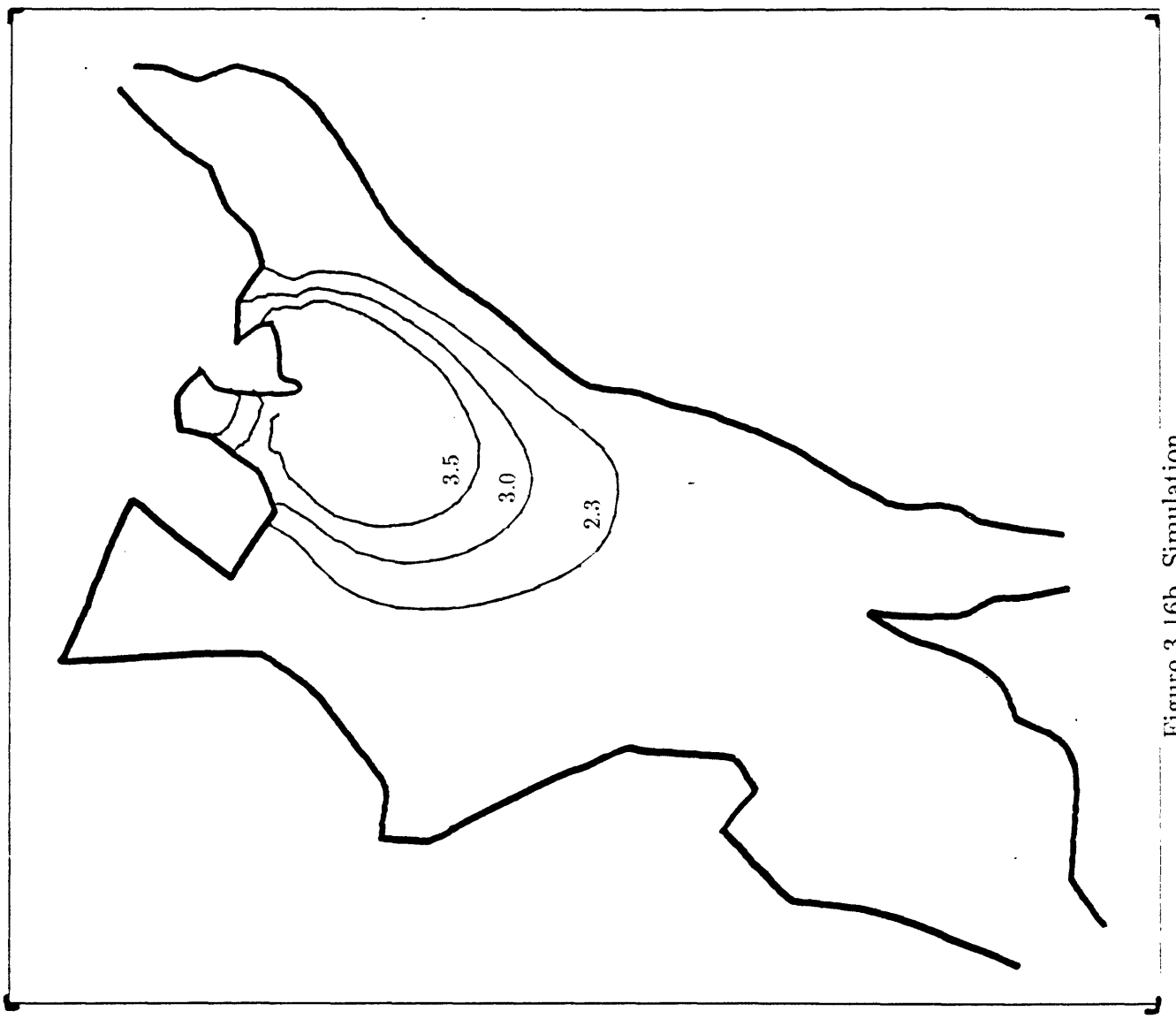

Figure 3.16b Simulation

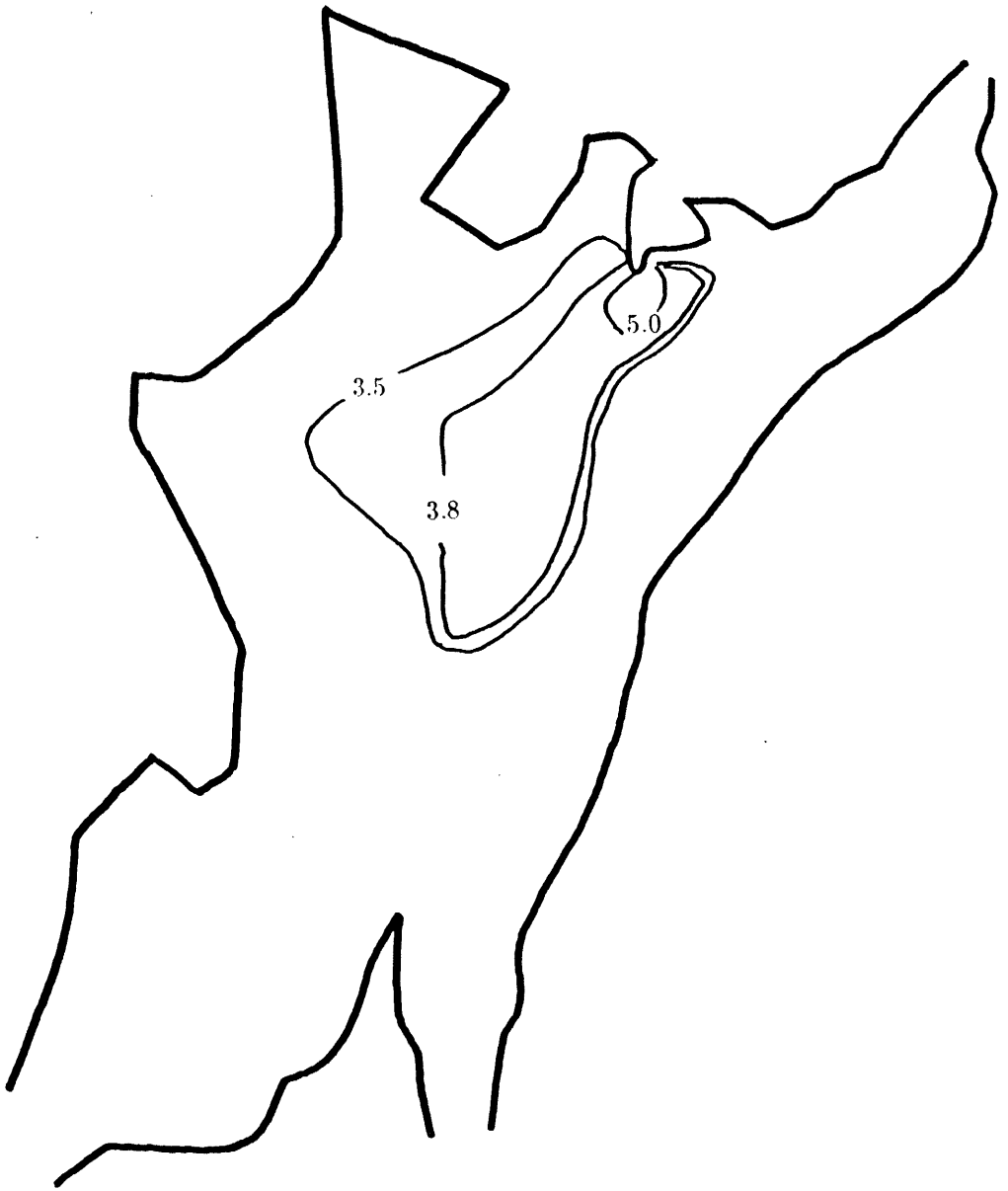

Figure 3.17 Surface layer excess temperatures (°F) at low slack on August 25, 1976
a) Measurements

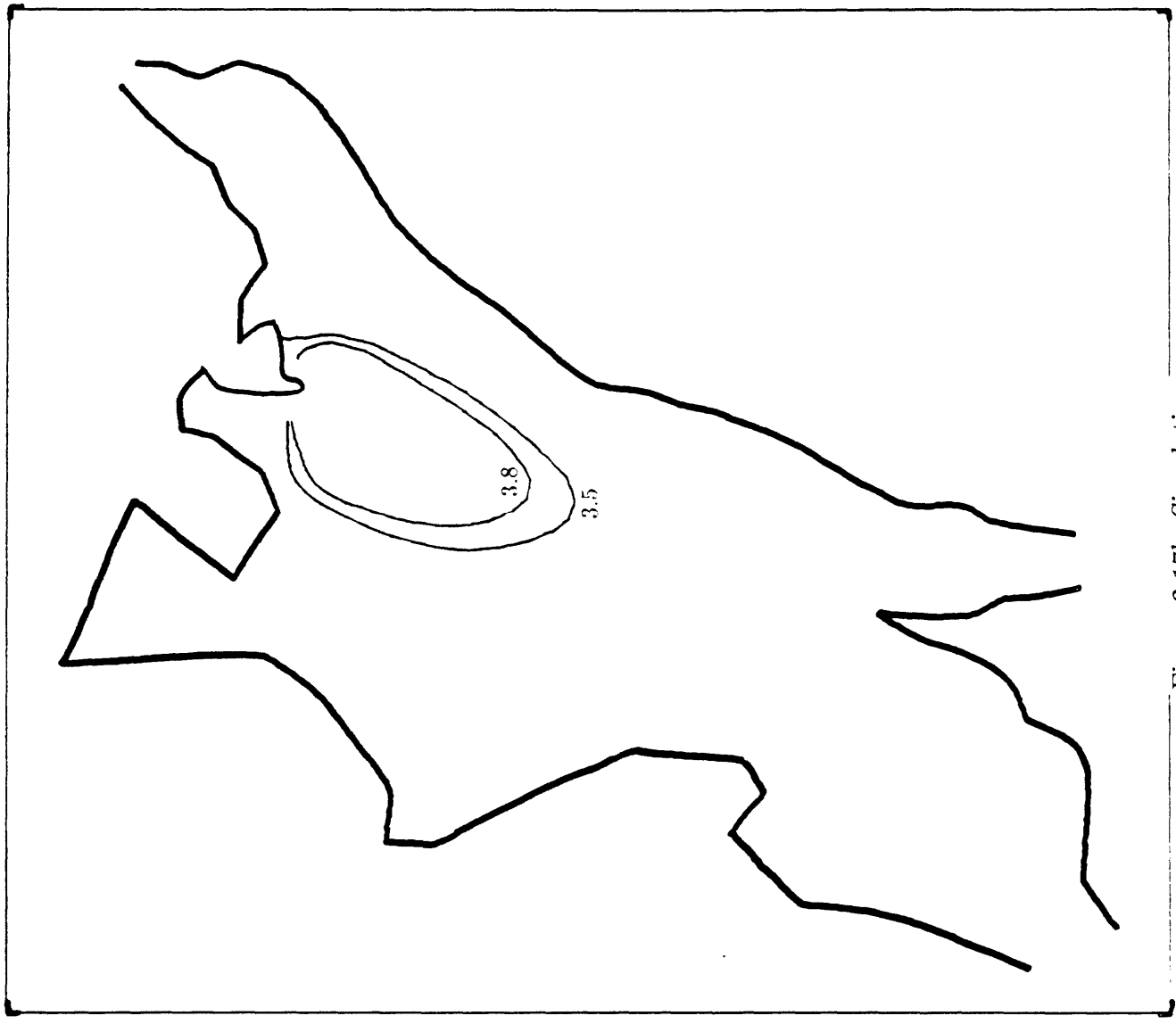

Figure 3.17b Simulation

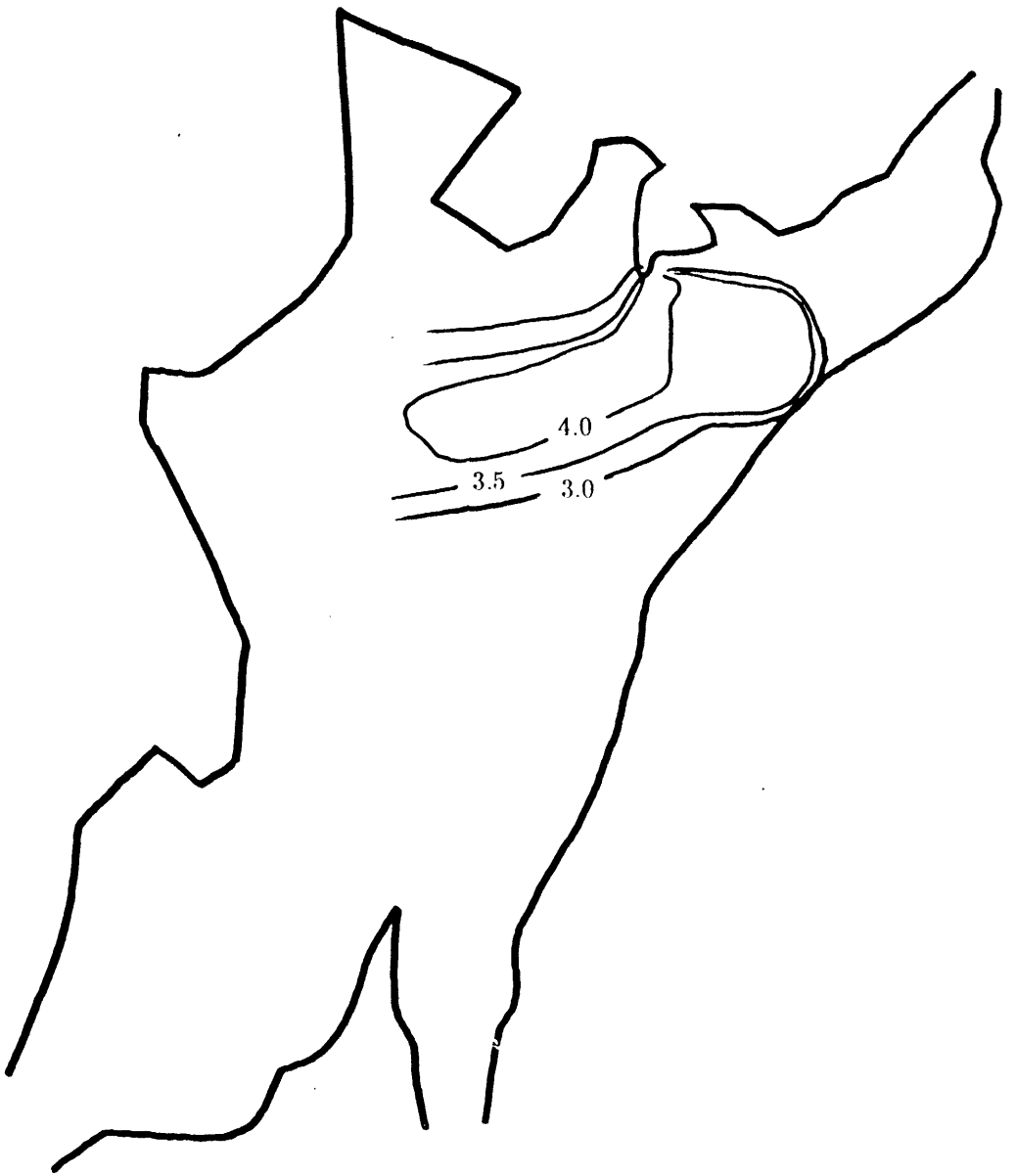

Figure 3.18 Surface layer excess temperatures (°F) at maximum flood on August 25, 1976
a) Measurements

Figure 3.18b Simulation

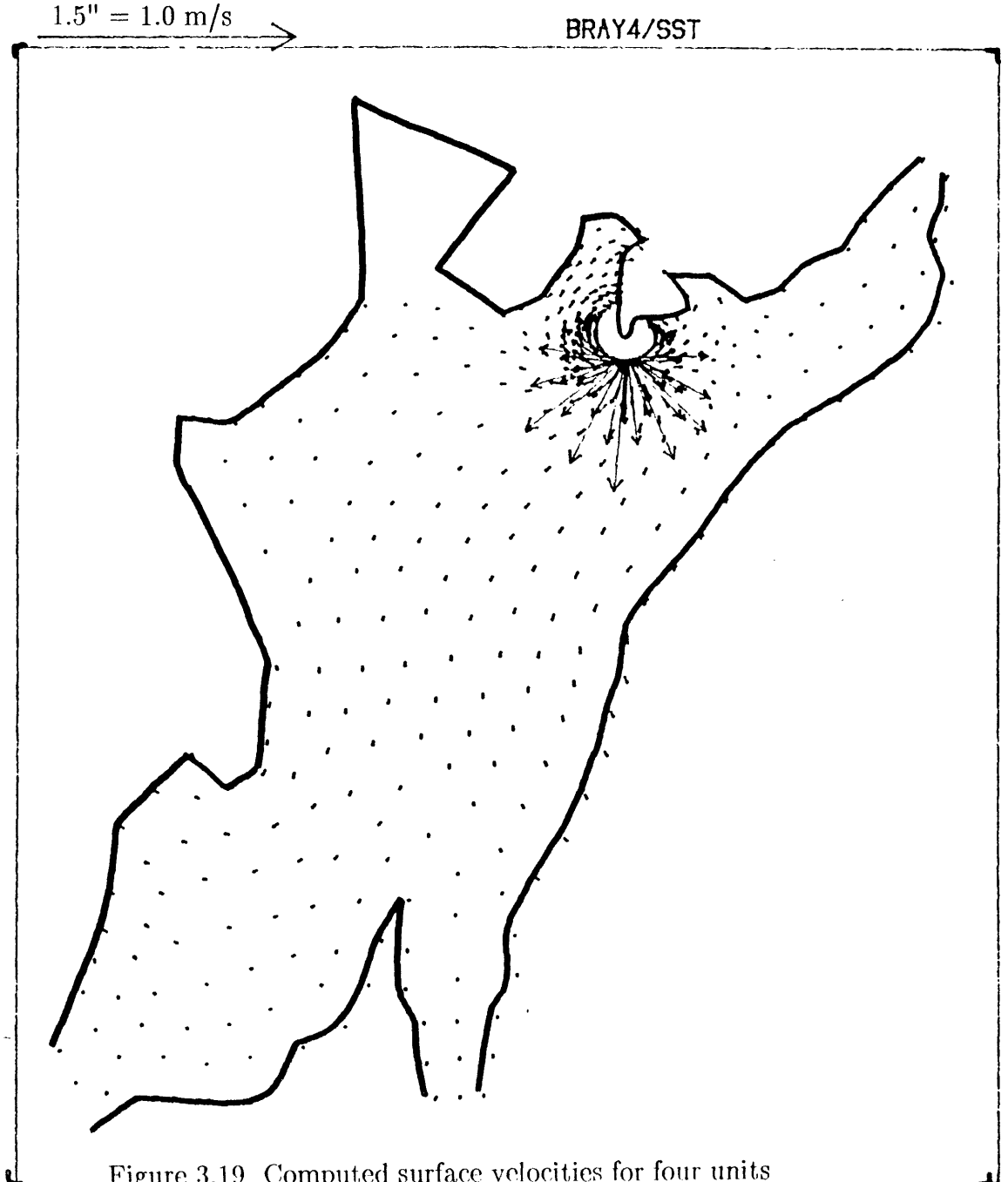

Figure 3.19 Computed surface velocities for four units
a) Steady state velocities reflecting power plant discharge

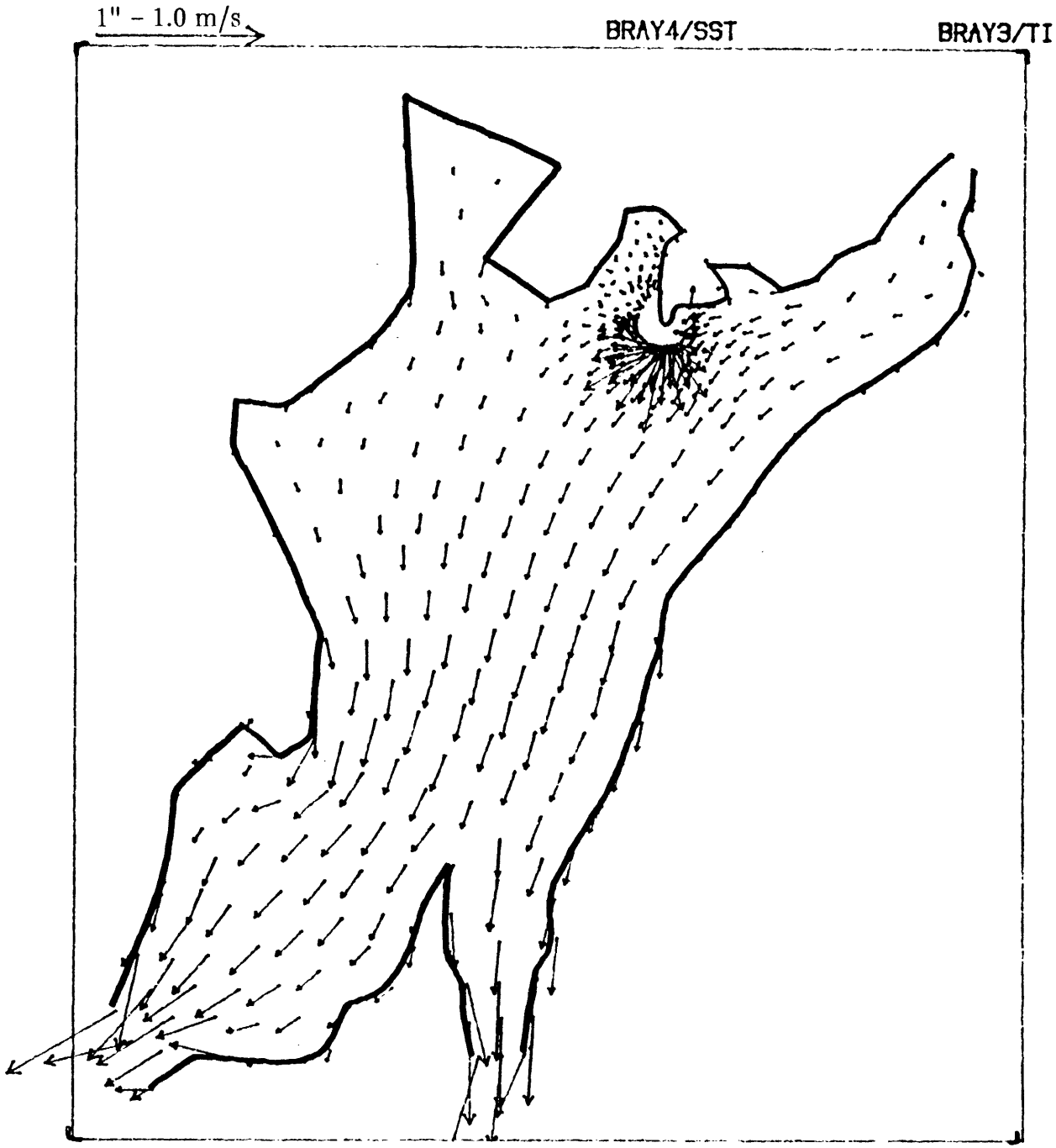

Figure 3.19b Tidal plus steady state velocities at maximum ebb

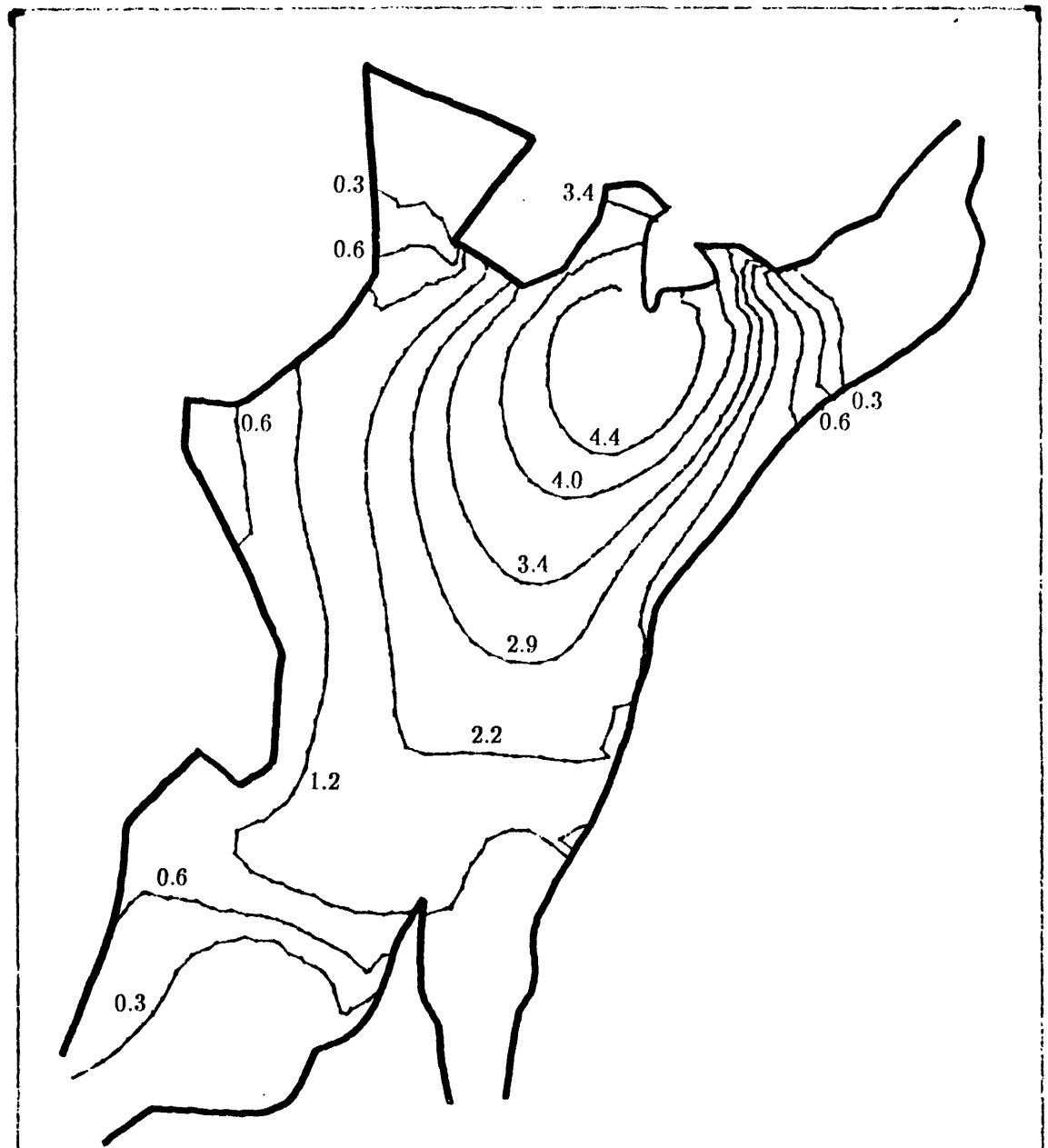

Figure 3.20 Quasi-steady surface layer excess temperatures (°F) for 4 units (max. ebb, $D = 1.0\ m^2/s$, $\alpha = 0.5$, no wind, $\Delta t = 31$ min, dynamic heat budget). Compare with corresponding calculations with 3 units in Figure 3.10.

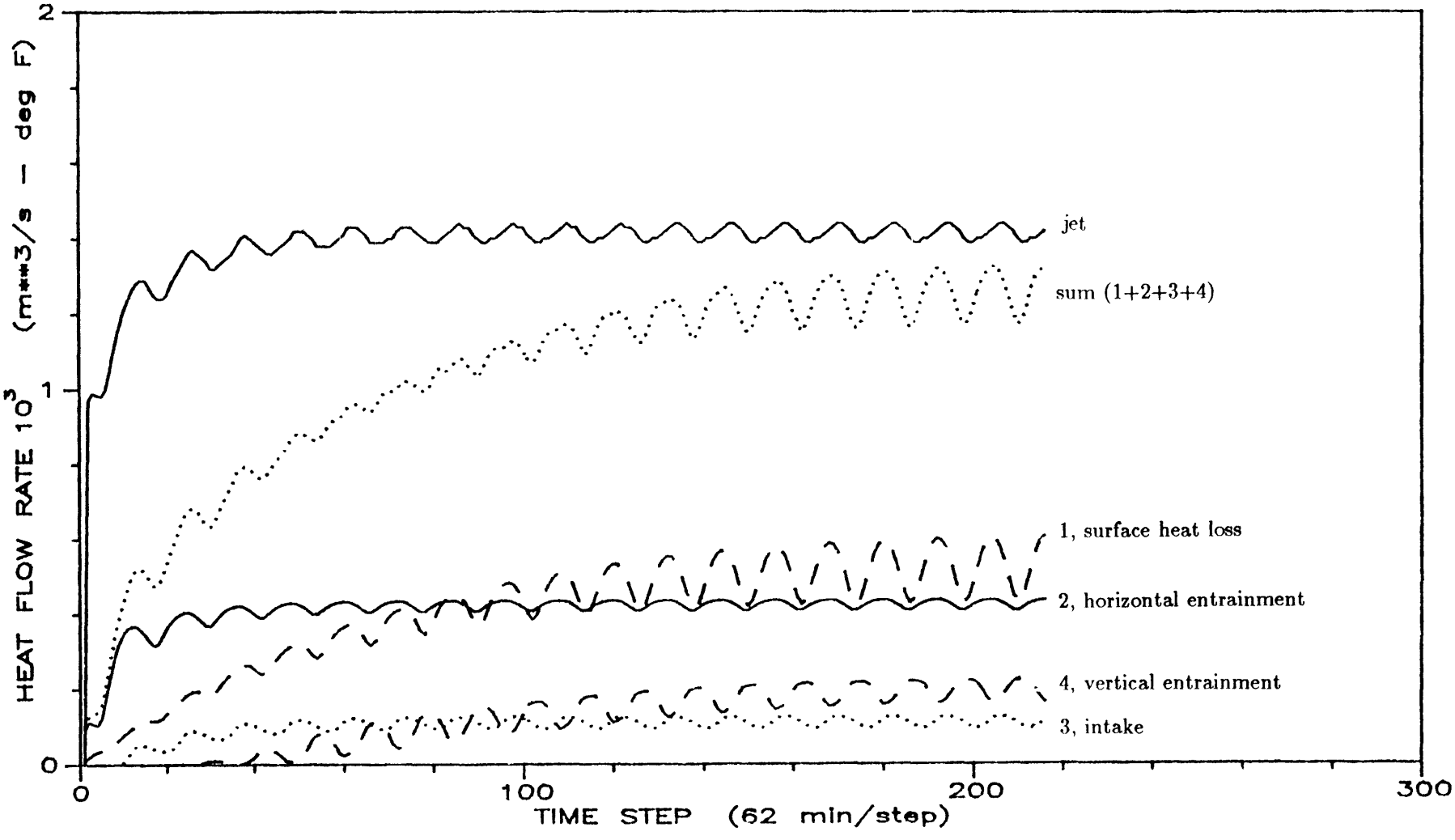

Figure 3.21 Time-varying parameters for dynamic heat budget calculations with 4 units ($\alpha = 0.5$). Compare with corresponding 3-unit calculations in Figure 3.11.
a) Various fluxes

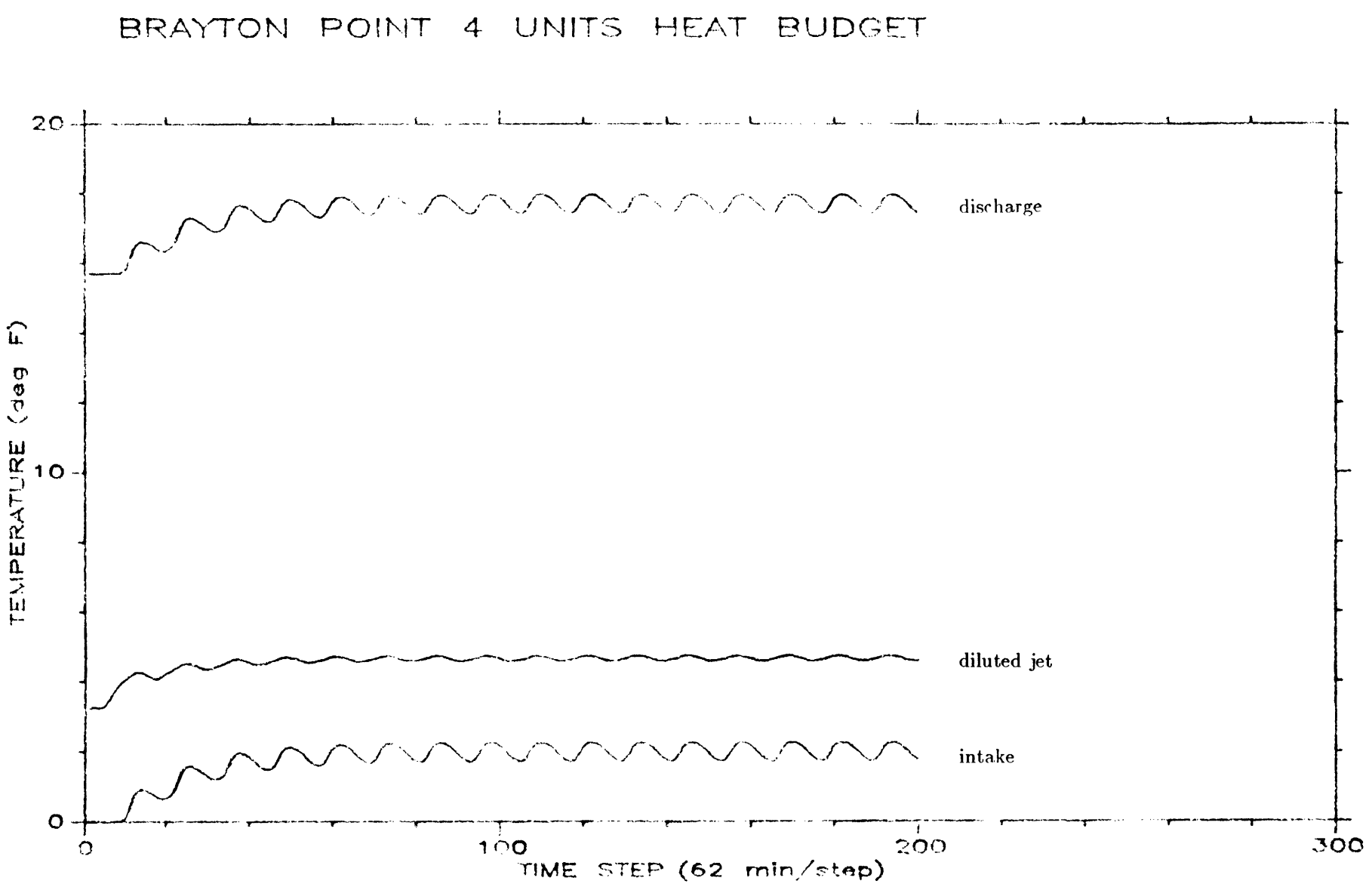

Figure 3.21b Discharge, intake, and diluted jet temperature

IV APPLICATIONS TO MILLSTONE NUCLEAR POWER STATION

4.1 Site Description

The Millstone Nuclear Power Station is located in Waterford, Connecticut, on the north shore of Long Island Sound. The area of the site is approximately 500 acres. The main station area of about 80 acres is sited on a point of land which is bounded on the east by Jordan Cove and on the west by Niantic Bay which forms the entrance to the Niantic River estuary (see Figure 4.1).

Tides in the Niantic Bay area are semi-diurnal with mean and spring ranges of 2.7 ft and 3.2 ft, respectively. Water depths range from several to 100 ft. Field data collected at the site indicate that tidal currents dominate natural water movement in the vicinity of the station. In particular, the flow into and out of Niantic Bay forms a strong current past the station along a line running from the plant site through Twotree Island Channel. Currents in Niantic Bay are also relatively strong as a result of flow into and out of the Niantic River. In contrast, the currents in Jordan Cove, even during the strength of ebb and flood tides, are relatively weak. Thermal- and salinity-induced stratification is not a significant factor in the vicinity of the plant site although considerable natural temperature variation is observed, particularly in shallower regions of the shoreline area.

The site consists of three nuclear units with a combined electrical output of approximately 2730 MWe. Open cycle cooling is employed with condenser cooling water entering the station through intake structures located on the west side of Millstone Point. After the water passes through the condensers, the heated water is discharged in a southeasterly direction through a 1200-ft-long 100-ft-deep quarry and then into Long Island Sound through a pair of 55-ft-wide channels.

4.2 Site Schematization

Figure 4.2 shows the finite element grid. With minor modifications, this grid and the site schematization are similar to those used by Kaufman and Adams.

For modeling plant-induced flow, the domain had a constant depth of 11.5 feet over most of its area corresponding to the estimated far-field plume thickness listed in Table 4.1. As with the Brayton Point Simulations, the depth was adjusted in shallow areas to account for depths less than 11.5 ft. For the tidal calculations, the full depth was used. As illustrated in Figure 4.2, a semi-circular near field region with radius of 475 feet was carved out of the domain at the tip of Millstone Point.

Near-field mixing parameters, based on the analysis of Jirka et al. (1981), are summarized in Table 4.1. Parameters are listed for both the existing three-unit and the previous two-unit conditions. Note that, at Millstone, the water depths surrounding the outfall are relatively deep resulting in negligible bottom effects on the discharge and entrainment (i.e., $r_s = 1.0$ for both two and three units).

Different magnitudes of discharge and entrainment fluxes were specified at the near-far field interface, corresponding to the simulation of two- and three-unit operation. As with the Brayton Point simulations, nodal points at the southern edge of the transition circle had specified normal flux into the domain representing the dilute discharge. Using parameters listed in Table 4.1, the temperature of the diluted discharge above the intake temperature was calculated as $23^\circ F/4.0 \simeq 5.8^\circ F$ for two units and $21.5^\circ F/3.0 \simeq 7.2^\circ F$ for three units. As with the Brayton Point simulation, the temperature that was actually specified depended on whether static or dynamic heat budget calculations were performed. The nodes adjacent to the diluted discharge had zero normal flux and all the remaining nodes had approximately equal specified entrainment fluxes out of the domain (and into the theoretical near-field jet region). The intake was simulated by removing flux from four nodes

on the western edge of Millstone point. For these calculations, $\alpha = 0.5$ indicating that half of the intake flow was drawn from the upper layer and half was drawn from the lower layer.

Ambient circulation was simulated by specifying time-varying water levels along the ocean boundary at the southern and eastern sides of the bay. To account for the spatial variation of tidal flow along this boundary, a phase lag was utilized causing the tide to propagate from east to west. The tidal period was 44640 sec, the amplitude was 1.35 ft, and the phase lag was 12 min between the top node on the eastern boundary and the far western node.

The remaining far-field parameters were selected in order to best match conditions observed during recent field measurements with three units reported by NUEL (1988). Measurements were conducted during Aug. 1987 during conditions of near constant (full-load) station operation and generally low winds. Hence near field parameters from Table 4.1 were used directly, with no wind drift. Vertical temperature profiles indicated little or no vertical differences and hence only 2-D simulations were performed. A horizontal dispersion coefficient of D = 50 m^2/s was used based on previous modeling of the two-unit plume by Stolzenbach and Adams (1979). This coefficient is significantly higher than the value used at Brayton Point (1.0 m^2/s) reflecting increased tidal mixing due to greater exposure at Millstone Point. Surface heat loss was simulated using a surface heat transfer coefficient of 157 BTU/ft^2-° F-day corresponding to a first-order decay coefficient of 2.5 × $10^{-6}sec^{-1}$ based on a water depth of 11.5 ft. These values are consistent with summertime meteorological conditions at the site.

4.3 Results

Simulations are presented for both two and three units. In each case the dynamic heat budget was used. Initial calculations showed significant sensitivity to time step (more so than at Brayton Point) and hence a value of 15.5 min was used. As discussed previously, the sensitivity to time step in ELA increases with the magnitude of diffusion coefficient, explaining the increased sensitivity at Millstone as compared with Brayton Point.

Figure 4.3 shows simulated plant-induced velocities while Figures 4.4a-d depict surface velocities for a combination of plant-induced and tidal circulation. The velocities were computed by TEA for conditions of two-unit discharge. Figure 4.5 depicts corresponding pathlines simulated by ELA for nine particles released within the domain at high tide. Depending on their point of release, some particles are entrained at the intake, some are entrained in the plume, some are flushed from the domain, and some remain in the domain.

Figures 4.6a-d show computed two-unit excess temperatures (in °F) averaged over the surface layer for four tidal phases, based on the above flow field. Figure 4.7a shows corresponding time-varying fluxes and Figure 4.7b shows time-varying values of discharge, intake, and diluted jet temperature over a period of 200 time steps, or a little more than four tidal periods.

Note in Figure 4.7a that the sum of the surface heat loss, horizontal entrainment, and intake temperature fluxes is significantly less than the diluted discharge heat flux. The major reason is that the downwelling flow, necessary to provide for vertical entrainment and lower layer intake flow, is not modeled explicitly, but is just advected out the open boundary. Also note that, by the end of the simulation, the diluted jet temperature has reached periodic steady state at a level of about 7-7.5°F depending on tidal stage. This is about 20 to 30% greater than the diluted discharge temperature for a static heat budget (5.8°F). Finally note that the intake recirculation varies between about 0.4 and 1.8°F

depending on tidal phase. In comparison with Brayton Pt., the effect of the tide in promoting direct recirculation (during flood phase) appears greater, while the effect of far field build up appears to be less.

Figures 4.8a - 4.11a show simulated surface layer excess temperature contours for three units, under conditions of maximum ebb, low slack, maximum flood, and high slack, respectively. Except for the different discharge conditions (as assigned from Table 4.1) these simulations are similar to those for two units presented in Figures 4.6a-d. The corresponding circulation field for three units (not shown) is similar to that for two units (Figures 4.3 and 4.4) except that the influence of the plant-induced circulation extends further into the domain.

In comparing temperatures for two and three units, note that the three-unit contours are higher than the two-unit contours throughout the domain. This is due to the fact that, not only is more heat being discharged, but the near field dilution is reduced (from S = 4.0 with two units to 3.0 with three units). The reduced near field dilution results from the fact that, with three units, discharge is through a *pair* of openings in the quarry. The resulting crossectional area of the discharge opening is thus twice as large for three units as for two units. The resulting decrease in discharge velocity combined with the increase in channel characteristic length scale (ℓ_0; see table 4.1) results in a lower Froude number and hence reduced near field mixing. Note that this situation is in contrast to that that occurred at Brayton Point where discharge from three and four units was through the same structure, leading to a small *increase* in dilution with the added units. It can also be mentioned that there was a transition period at Millstone where the second quarry cut had been opened but only two units were operational. In comparison with the original condition with two units and one cut, the transition condition resulted in much lower discharge velocities and mixing. These conditions explained the sudden increase in near field and intermediate field temperatures observed following the second cut (NUEL, 1987).

Figures 4.8b–4.11b show near-surface plume measurements under similar tidal phases, and plotted to the same scale as the corresponding simulations shown in part a) of each figure. Measurements were made by Ocean Surveys, Inc., and were reported by NUEL (1988). It should be noted that the measurements were of dye concentrations and were scaled to excess temperature. Agreement between measurements and simulations is reasonably good, although the following discrepancies can be noted.

First, the higher temperature contours (e.g., 6 and 8°F) are sometimes bigger in the simulations than the measurements (e.g., high slack). As discussed previously, this may be explained by the finite time steps and the sequence of diffusion and advection calculations in ELA that tend to overestimate temperature near the point of discharge.

Second, simulated contours near the open boundary (e.g., the 1.5°F contour for maximum ebb) are somewhat smaller than measured. This can be explained by the finite size of the computational domain combined with the assigned boundary condition of zero concentration. A somewhat larger 1.5°F contour would be simulated if the domain were larger.

Third, the simulated low slack isotherms extend considerably further to the east than the measured isotherm. This is explained by the fact that the measured plume, while nominally taken at low slack, was actually taken more than an hour into flood phase (NUEL, 1988).

Finally, the simulated plumes are somewhat rounder (less elongated) than the measured contours. In part this is due to the formulation of linear TEA which omits the momentum terms, leading to exaggerated near field circulation. It may also be due to the method of plume measurement and/or presentation. For example, dye measurements at the Unit 1 intake indicate recirculation of the order of 1.2 to 1.4°F. If the intake were drawing equally from an upper (thermally influenced) and a lower (ambient) layer—consistent with the

assumed value of $\alpha = 0.5$—then upper-layer excess temperature adjacent to the intake would range from 2.4 to 2.6° F. Yet the measured contours imply that surface temperatures near the intake are less than 1.5° F for all tidal phases. Certainly during high slack one would expect to see some residual heat (dye) build-up in Niantic Bay.

Figure 4.12a shows time-varying heat fluxes and Figure 4.12b shows corresponding discharge, intake, and diluted discharge temperatures for three units. Note that the diluted discharge temperature, which ranges from about 8.5 to 9.5° F, is higher than the corresponding temperatures for two units (approximately 7 to 7.5° F) due mainly to the decreased near field dilution. The intake recirculation shown in Figure 4.12b ranges from 0.6 to 2.3° F. These values are similar, on average, but greater in range than the values of 1.2-1.4° F reported (by NUEL, 1988) based on dye measurements.

Table 4.1
Near-Field Parameters Computed for Millstone Simulation

Parameter	Symbol	2-unit values*	3-unit values*
Discharge flow rate	Q_0 (cfs)	2290	4150
Discharge temperature rise	ΔT_0 (°F)	23	21.5
Discharge velocity	u_0 (fps)	3.6 - 4.5	3.1 - 3.9
Discharge channel depth	h_0 (ft)	9.2 - 11.7	9.2 - 11.7
Discharge channel half-width	b_0 (ft)	27.5	57.5
Discharge channel characteristic length	ℓ_0 (ft)	15.9 - 17.9	23.0 - 25.9
Densimetric Froude no. (based on h_0)	$\mathbb{F}_0$	3.0 - 4.3	2.6 - 3.8
Channel aspect ratio	h_0/b_0	0.33 - 0.42	0.16 - 0.20
Densimetric Froude no. (based on ℓ_0)	$\mathbb{F}_0'$	2.4 - 3.3	1.8 - 2.4
Transition radius	r_t (ft)	655 - 782 (475)	700 - 830 (475)
Near-field volumetric dilution	S	3.4 - 4.6 (4.0)	2.5 - 3.4 (3.0)
Vertical mass entrainment	E_v	1.7 - 2.7 (2.2)	0.9 - 1.7 (1.3)
Horizontal mass entrainment	E_h	0.7 - 0.9 (0.8)	0.6 - 0.7 (0.7)
Maximum plume depth	h_{max} (ft)	18.3 - 21.9	19.4 - 23.2
Far-field plume depth	h_{far} (ft)	9.2 - 11.0 (11.5)	9.7 - 11.6 (11.5)
Shallow water dilution correction	r_s	1.0	1.0

*Ranges given refer to variation over tidal cycle. Values in parentheses were used in simulation

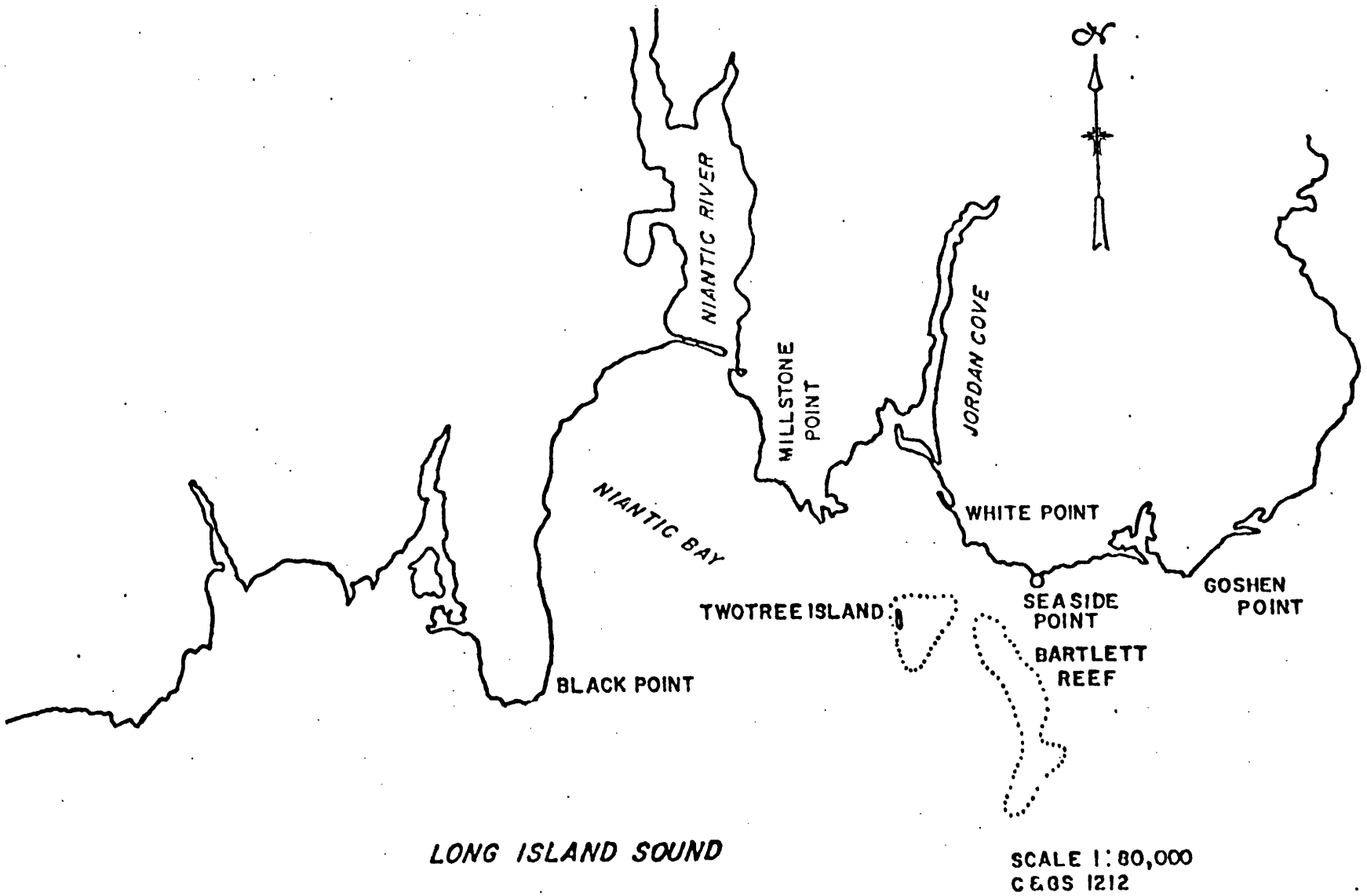

Figure 4.1 Site of Millstone Nuclear Power Station

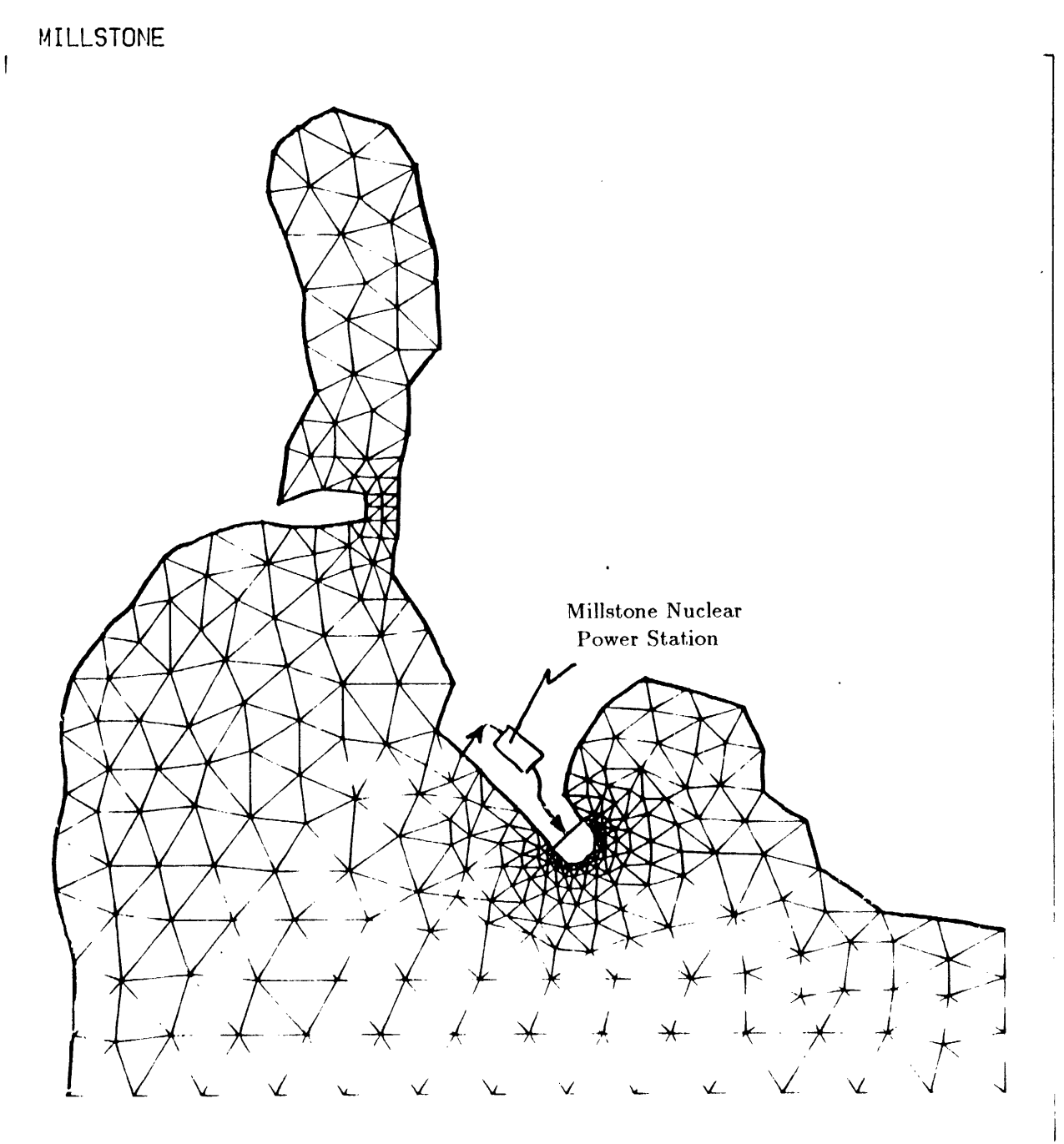

Figure 4.2 Finite element discretization of Long Island Sound near Millstone Nuclear Power Station

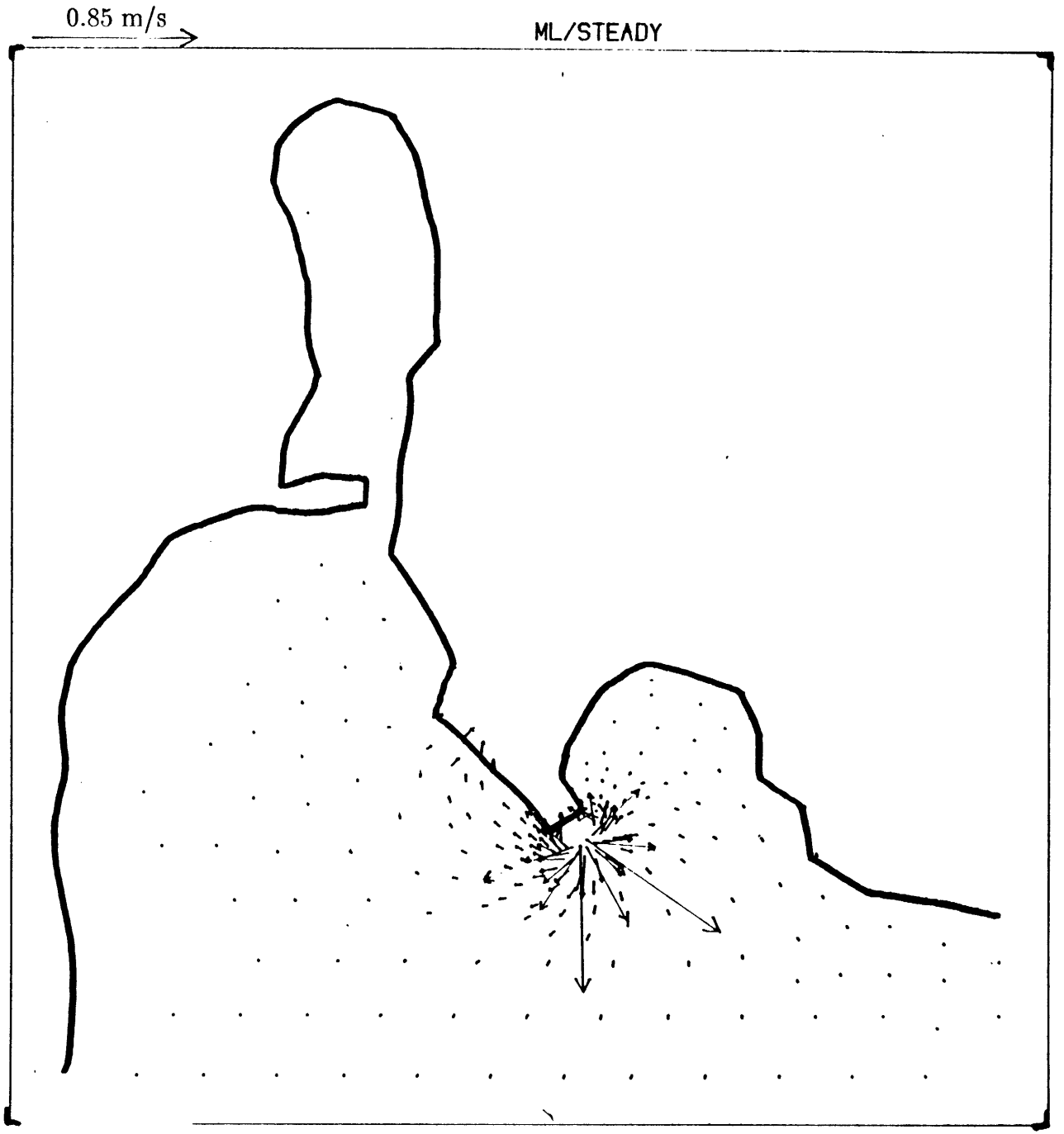

Figure 4.3 Computed surface velocities (2-unit plant operation only, no tides)

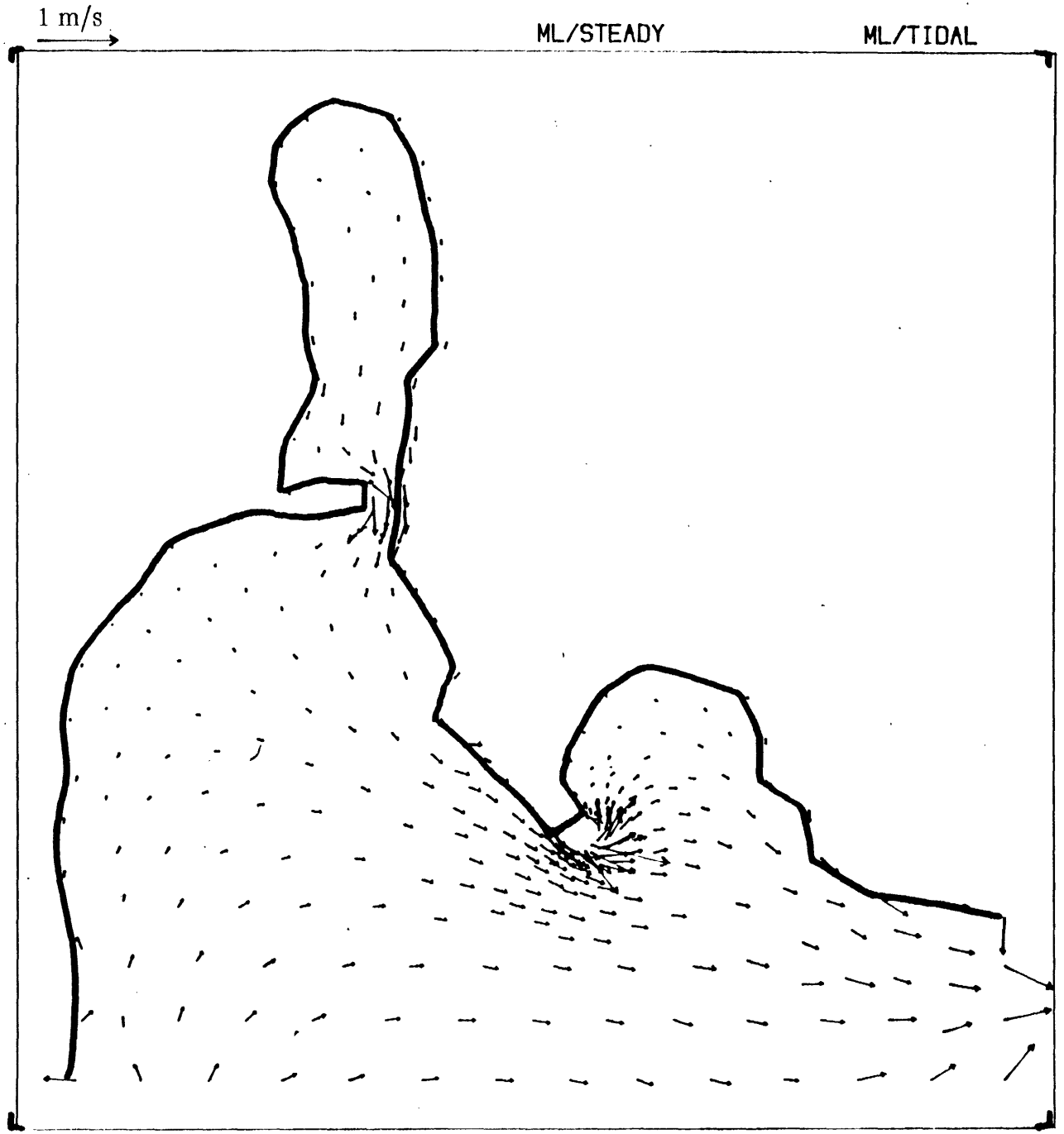

Figure 4.4 Computed surface velocities (tidal plus plant induced) for two units
a) Maximum ebb

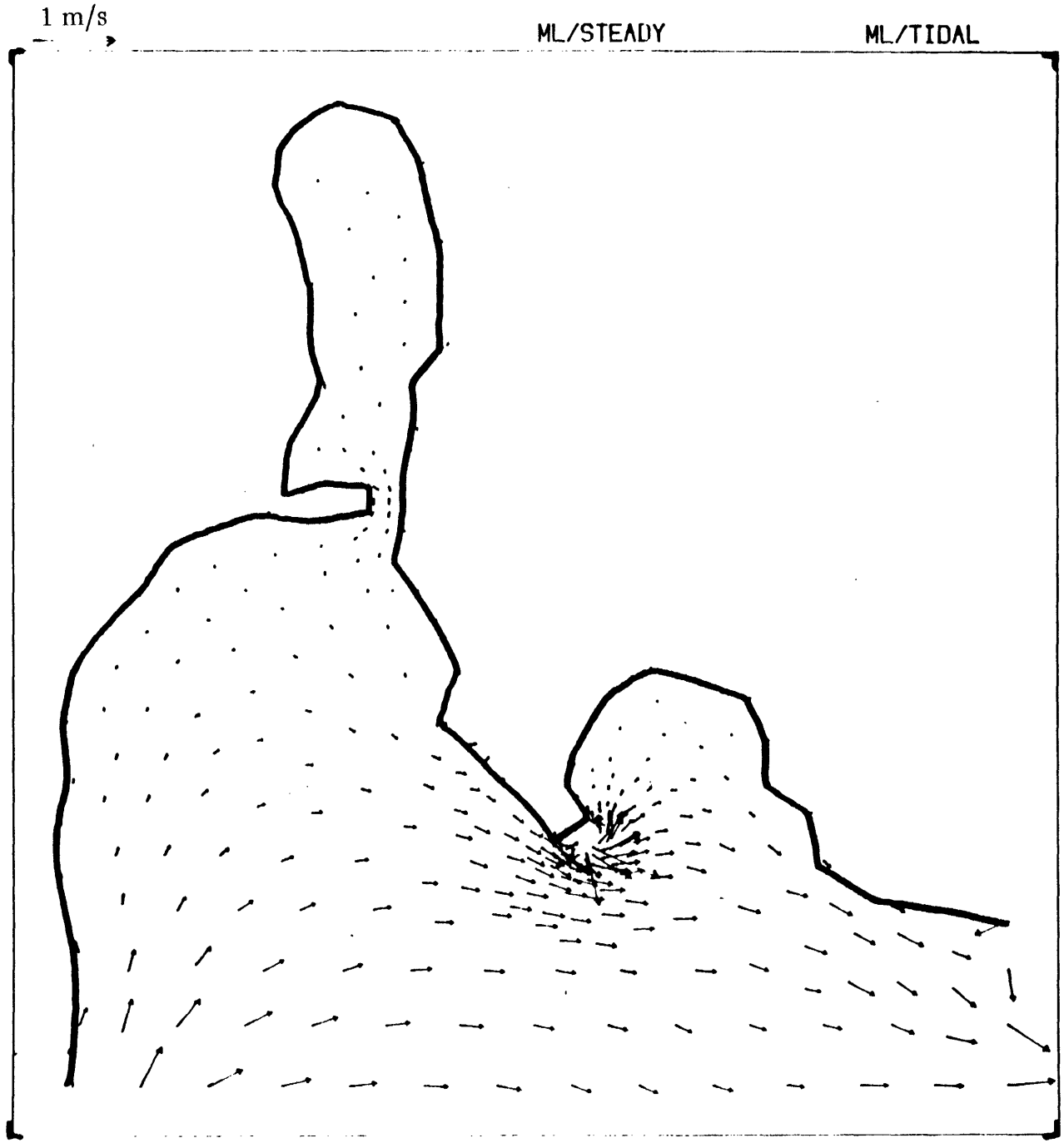

Figure 4.4b Low slack

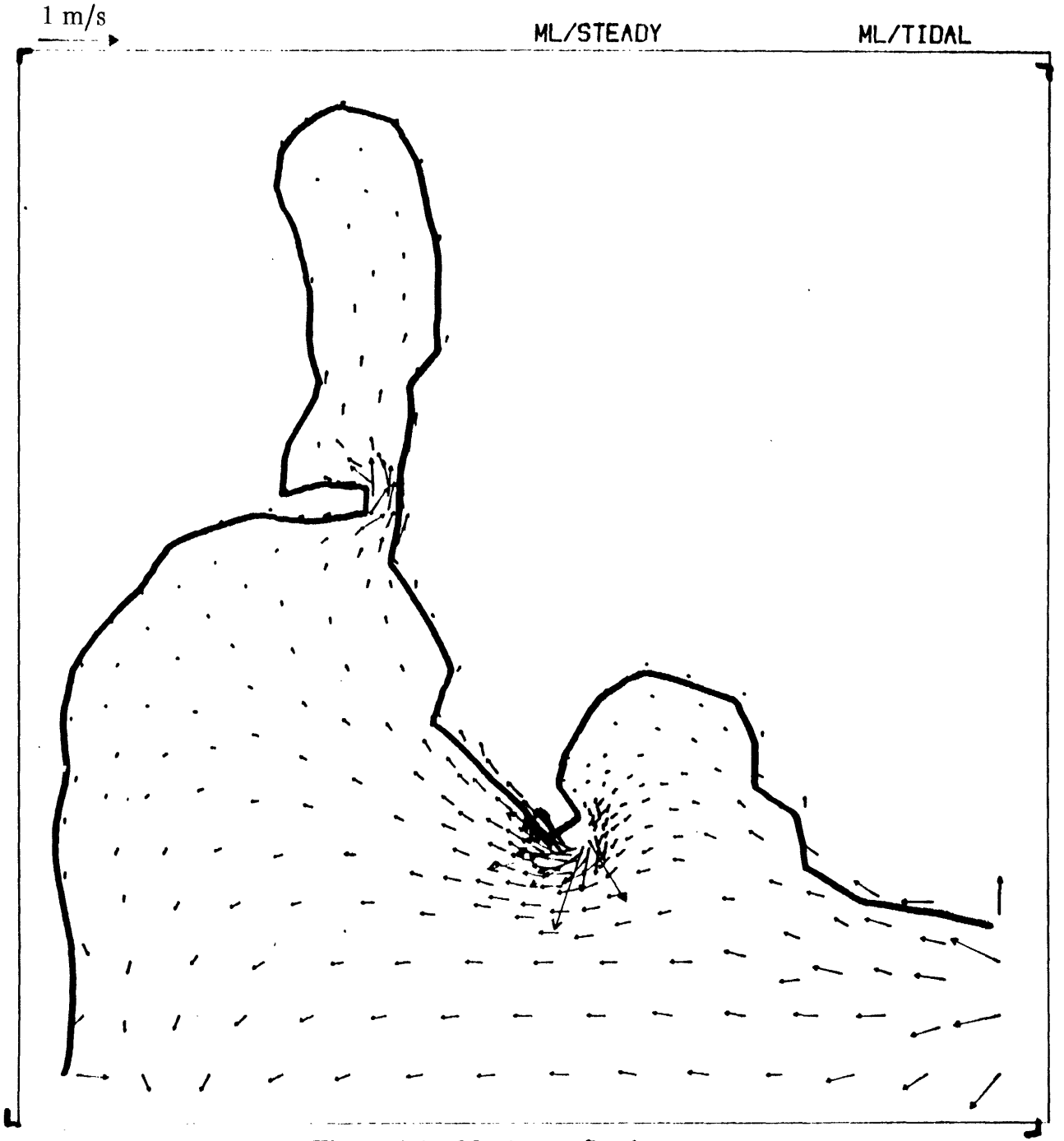

Figure 4.4c Maximum flood

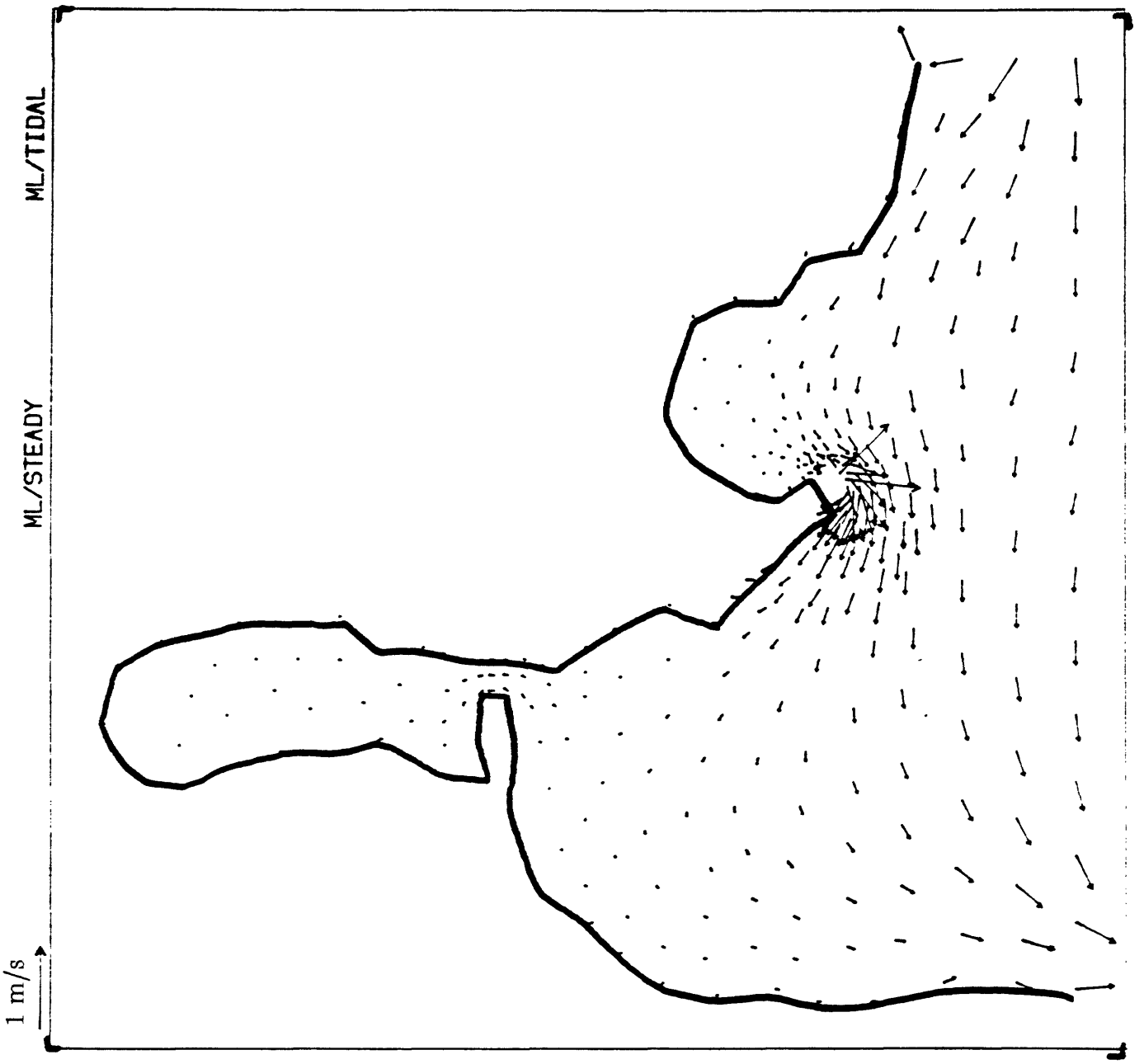

Figure 4.4d High slack

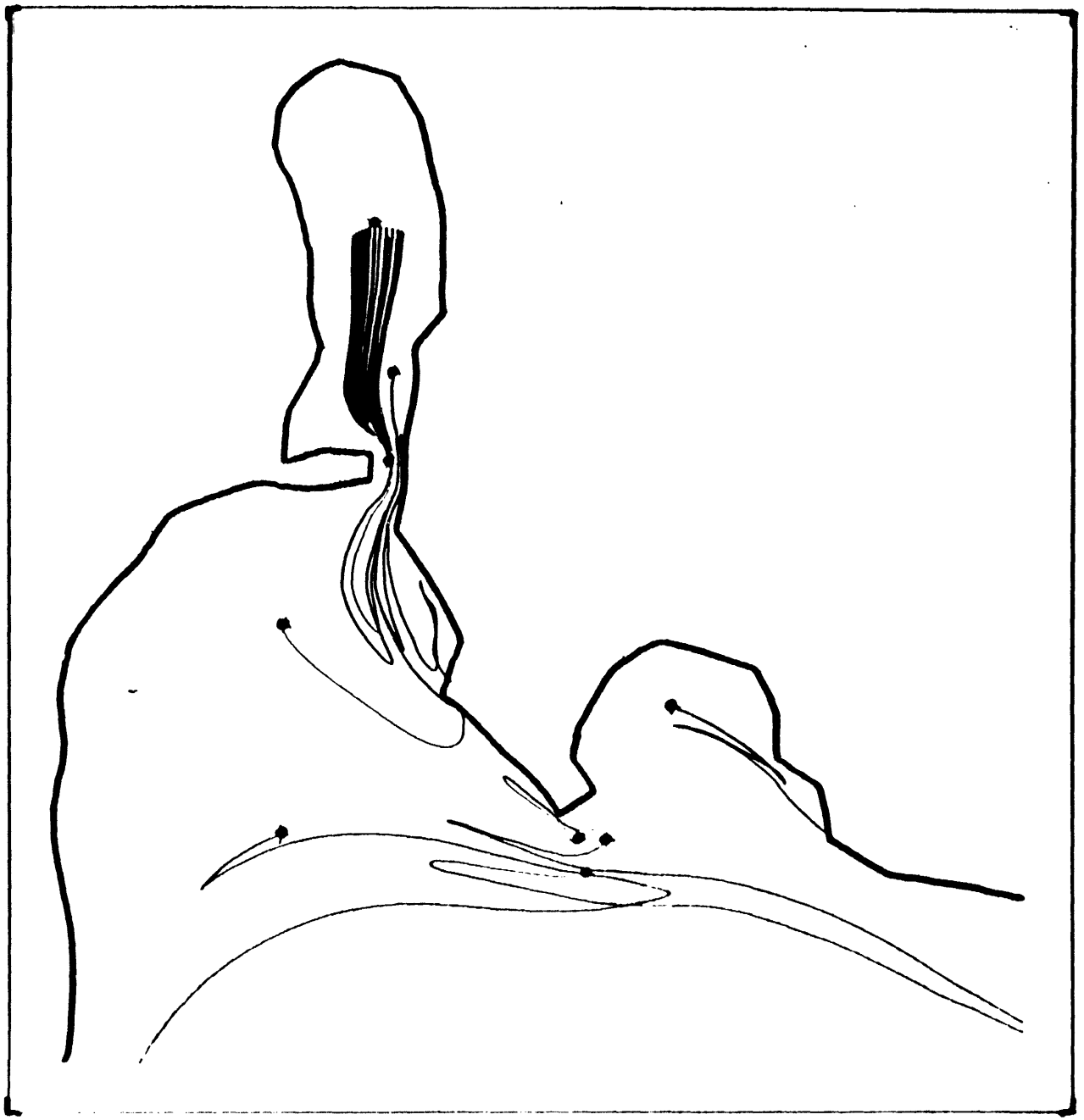

Figure 4.5 Simulated pathlines of particles released at high slack in vicinity of Millstone Nuclear Power Plant

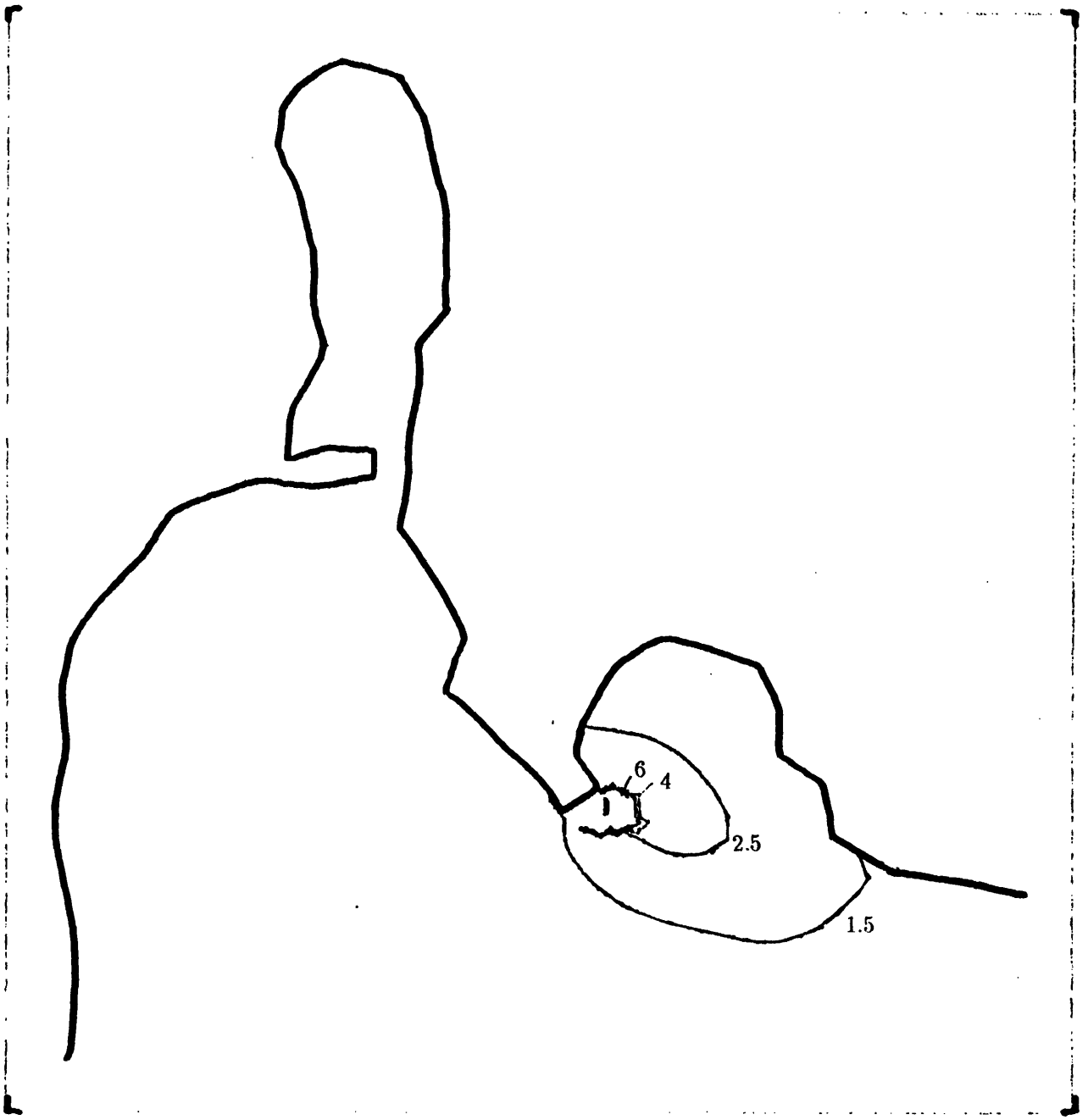

Figure 4.6 Surface layer excess temperatures (°F) for 2 units
a) Maximum cbb

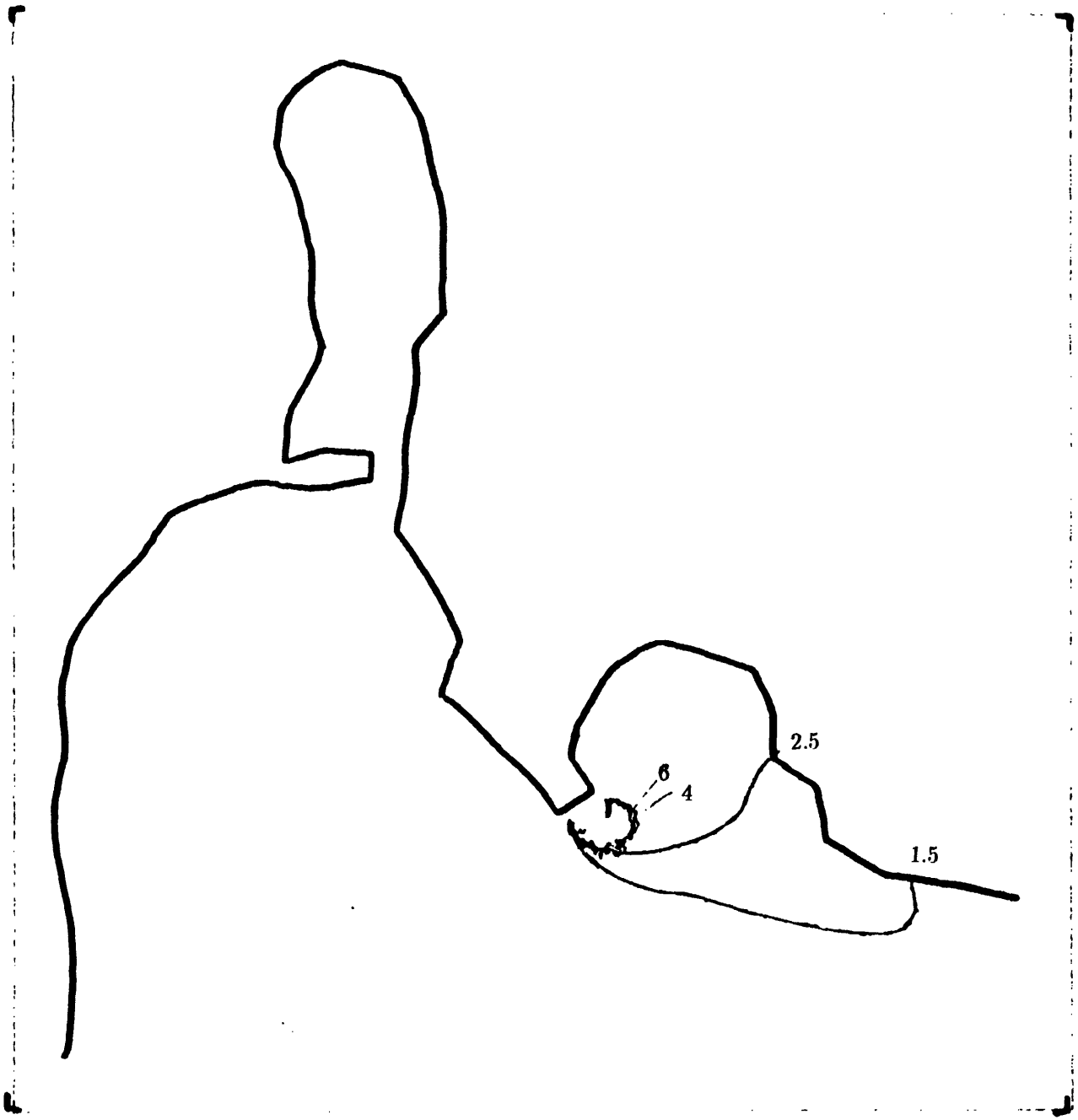

Figure 4.6b Low slack

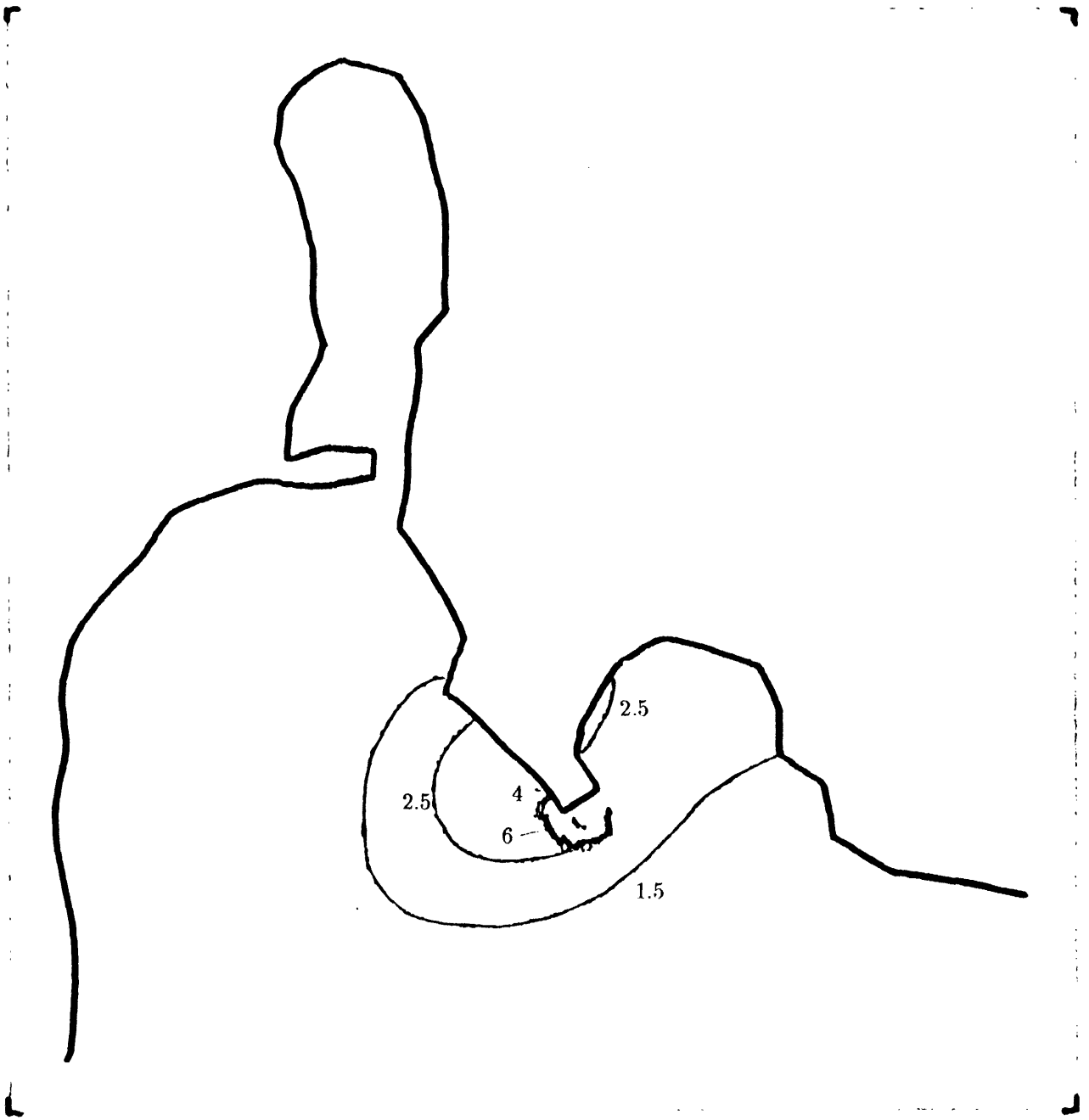

Figure 4.6c Maximum ebb

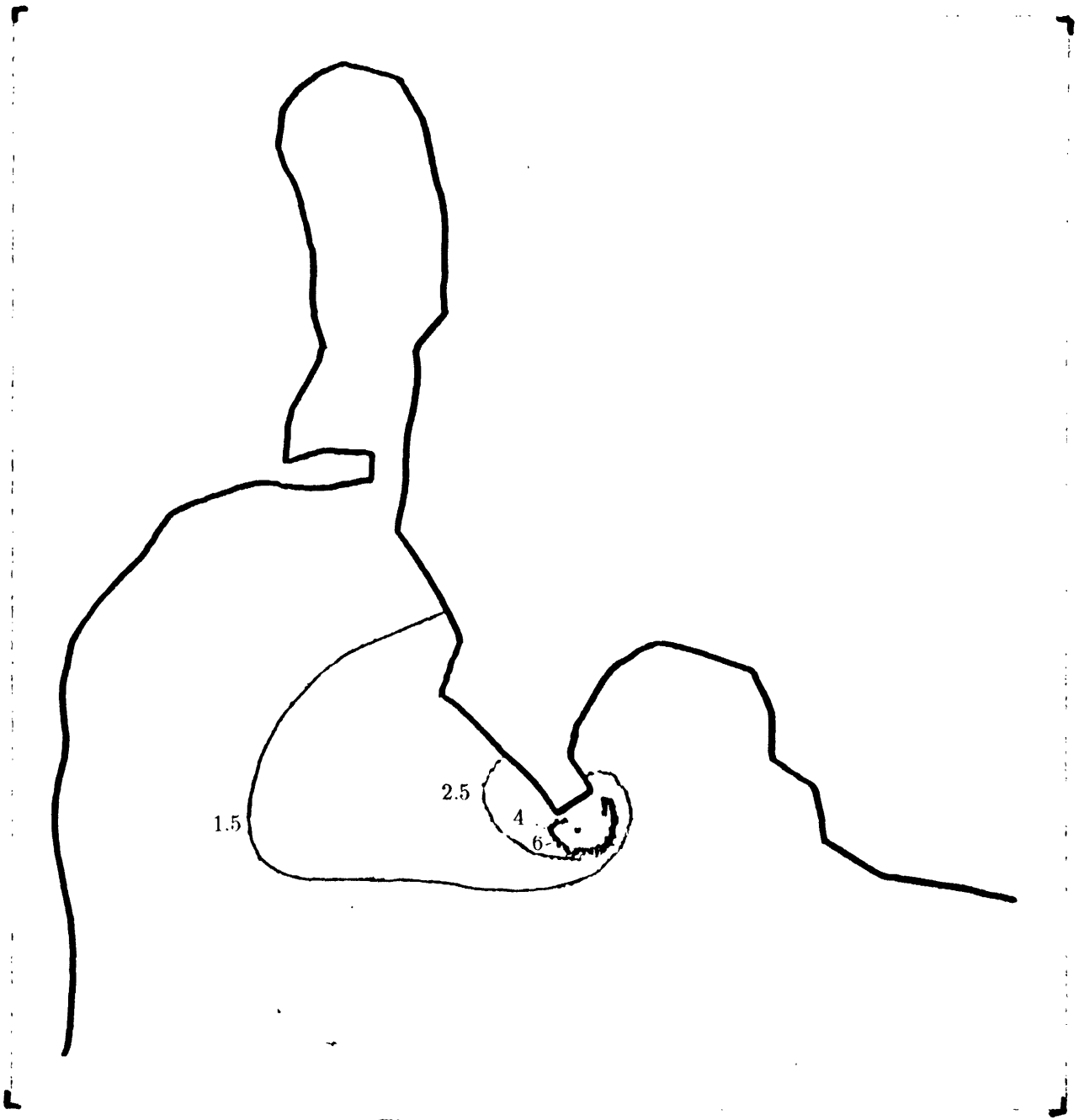

Figure 4.6d High slack

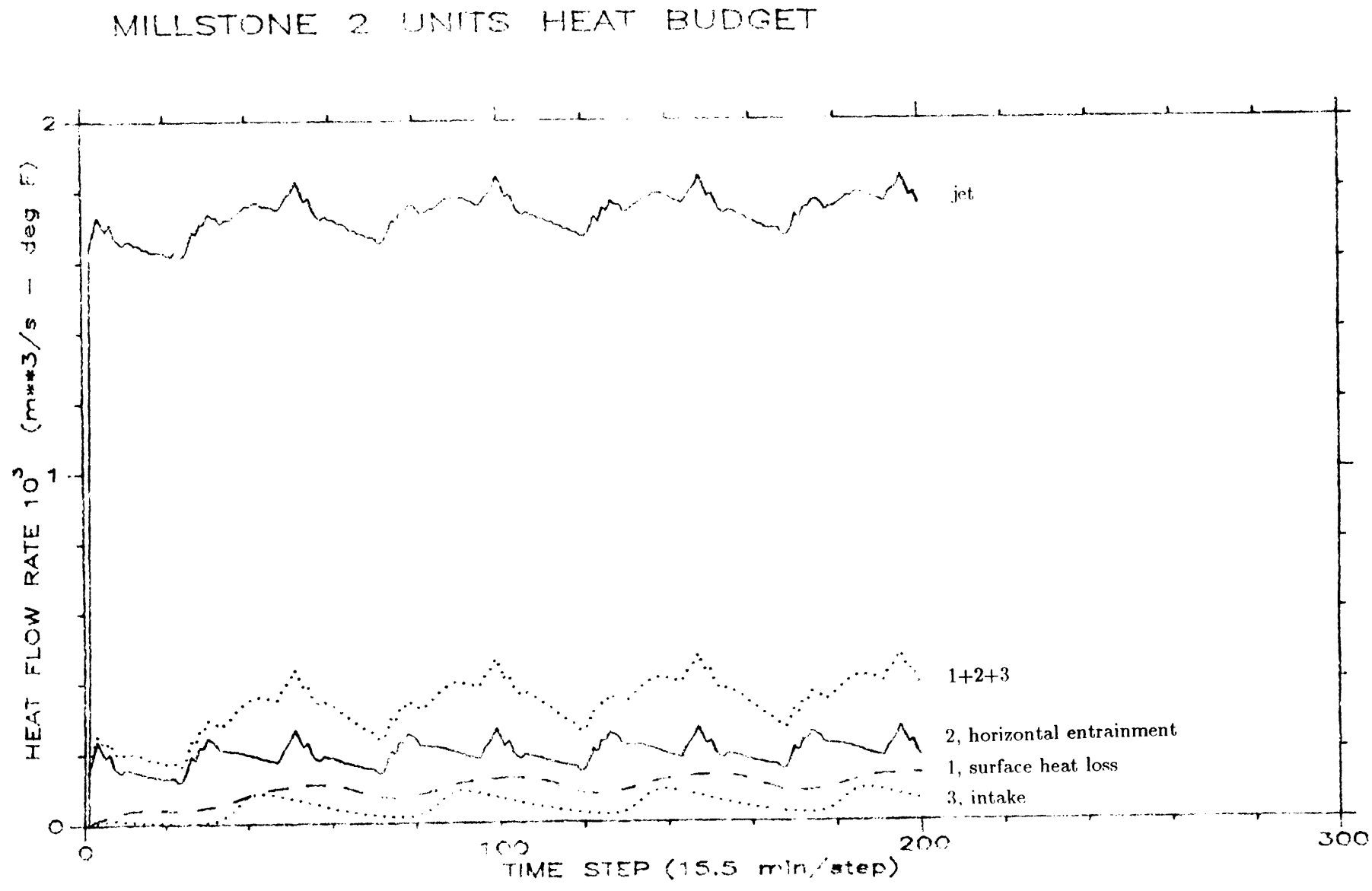

Figure 4.7 Time-varying parameters for dynamic heat budget calculations for two units
a) Various heat fluxes

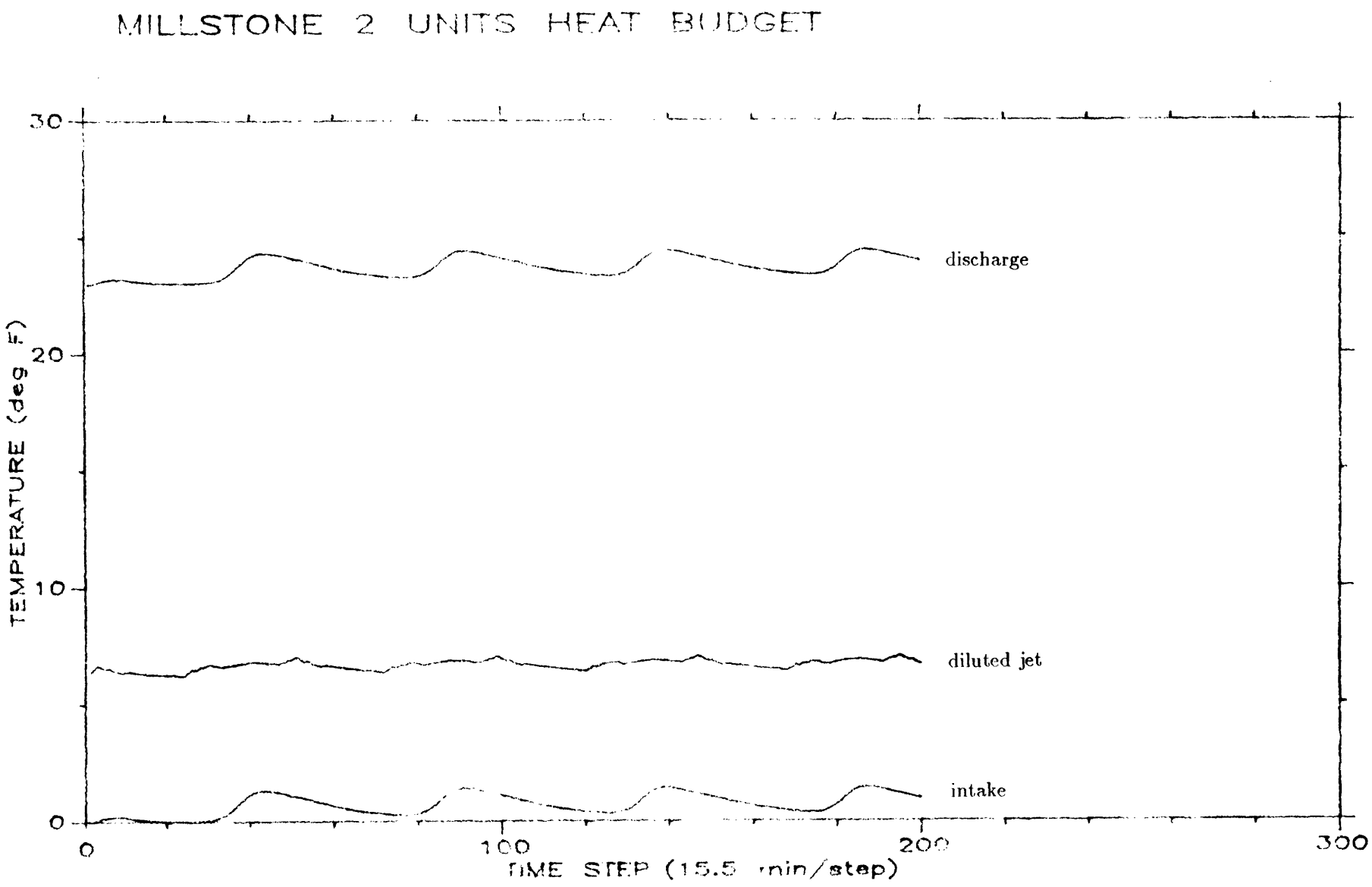

Figure 4.7b Discharge, intake, and diluted jet temperatures

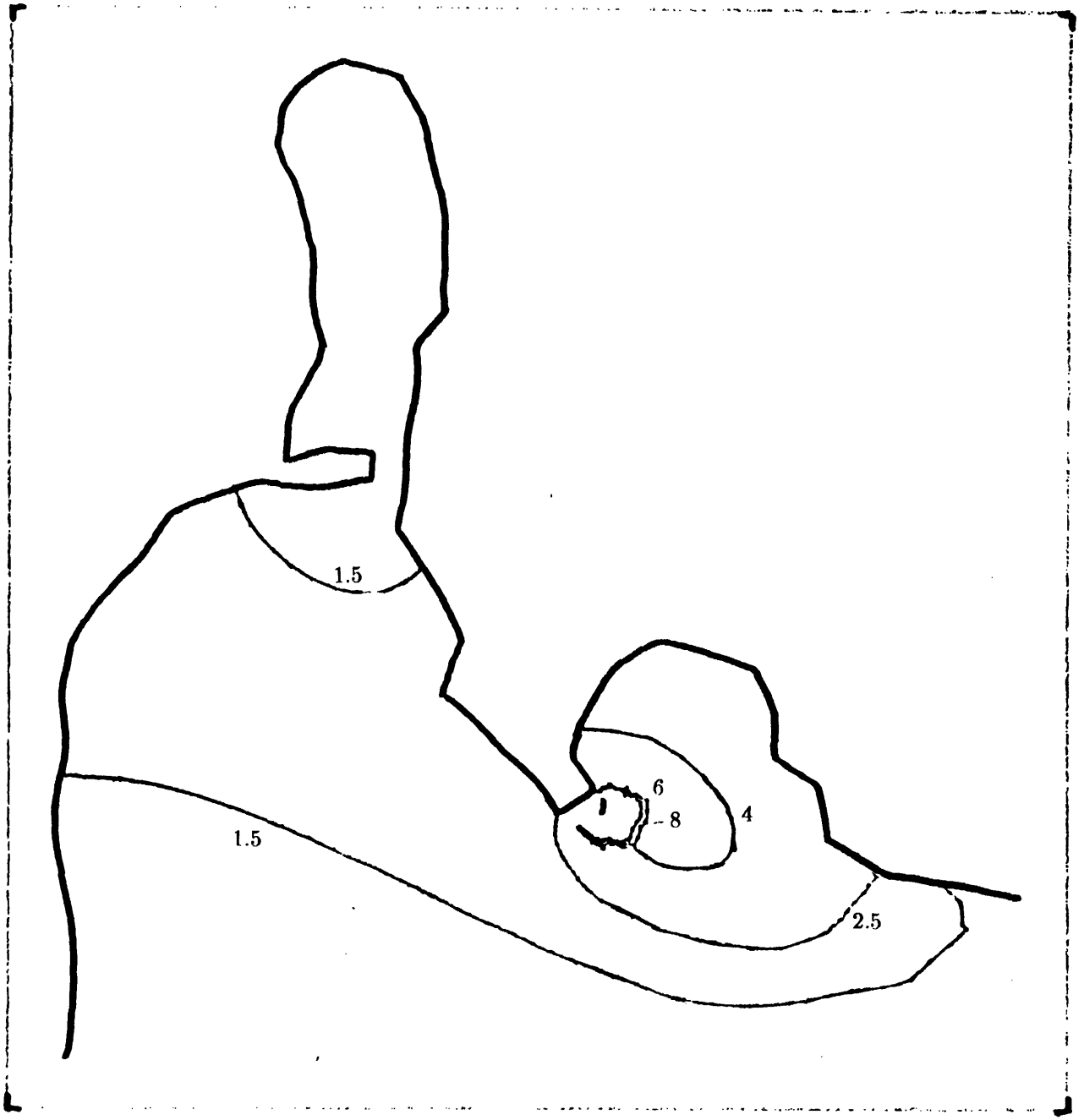

Figure 4.8 Surface layer excess temperatures (°F) for three units at maximum ebb
a) Simulation

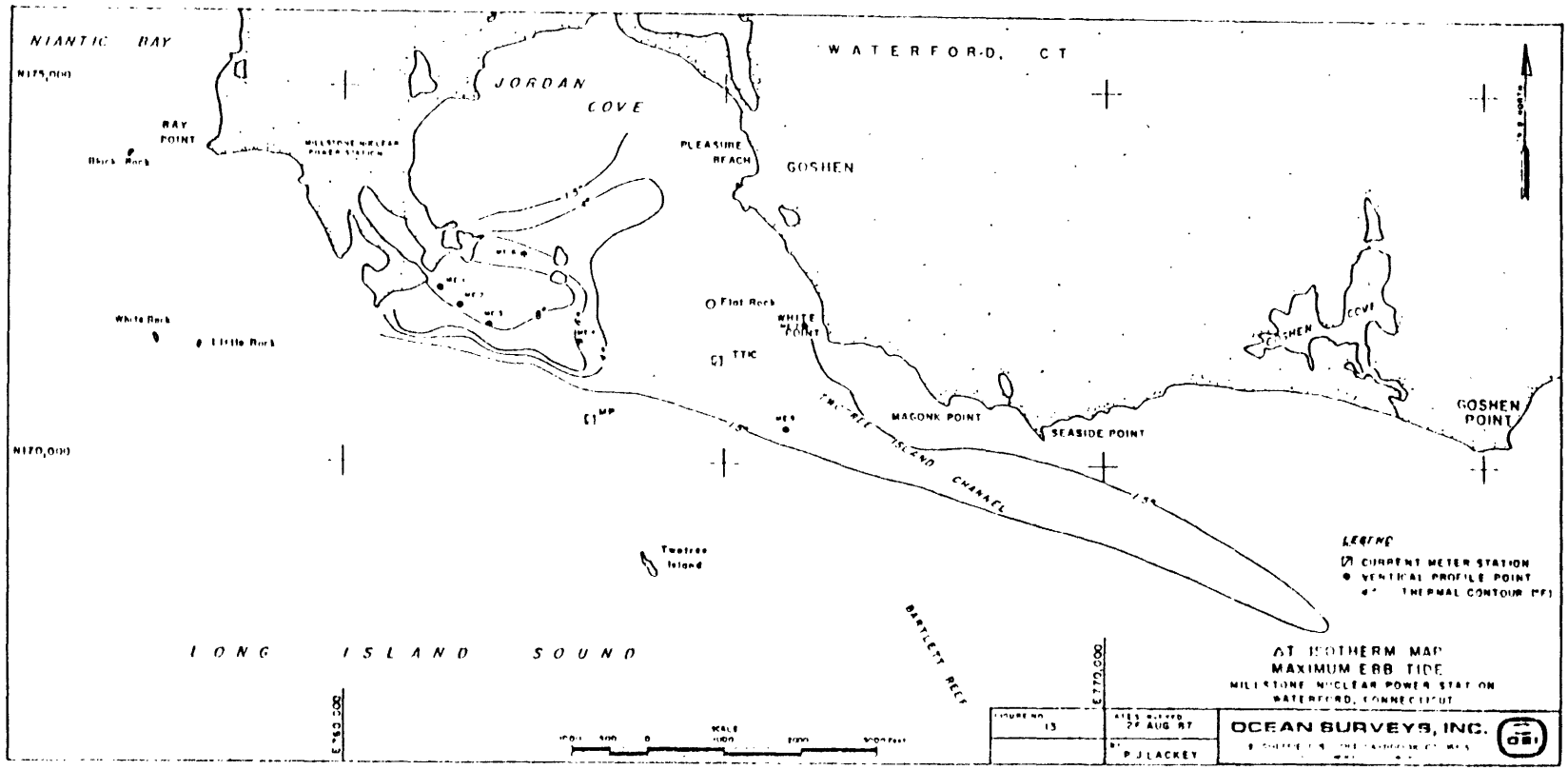

Figure 4.8b) Measurements on Aug. 26, 1987

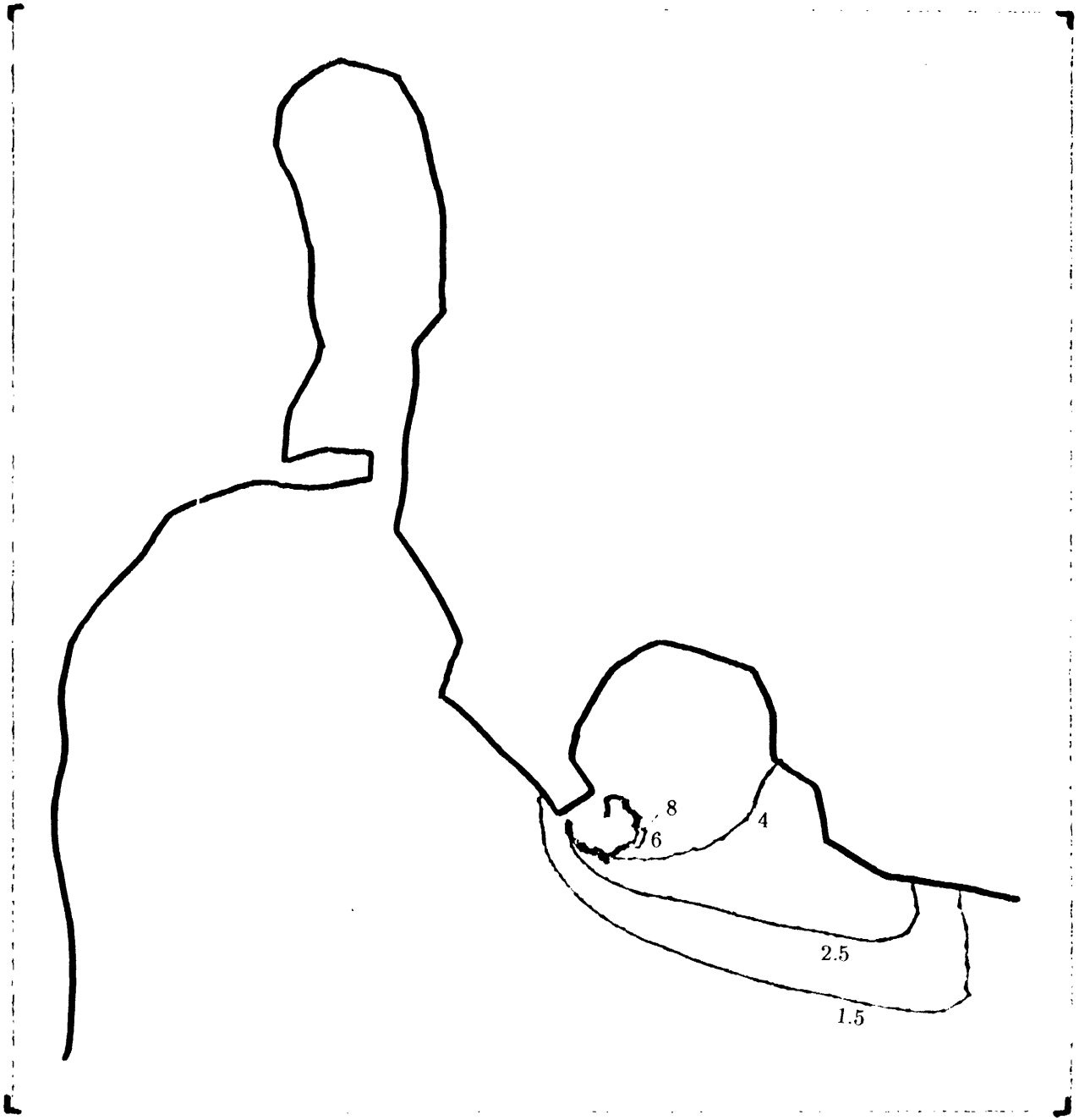

Figure 4.9 Surface layer excess temperatures (°F) for three units at low slack
a) Simulation

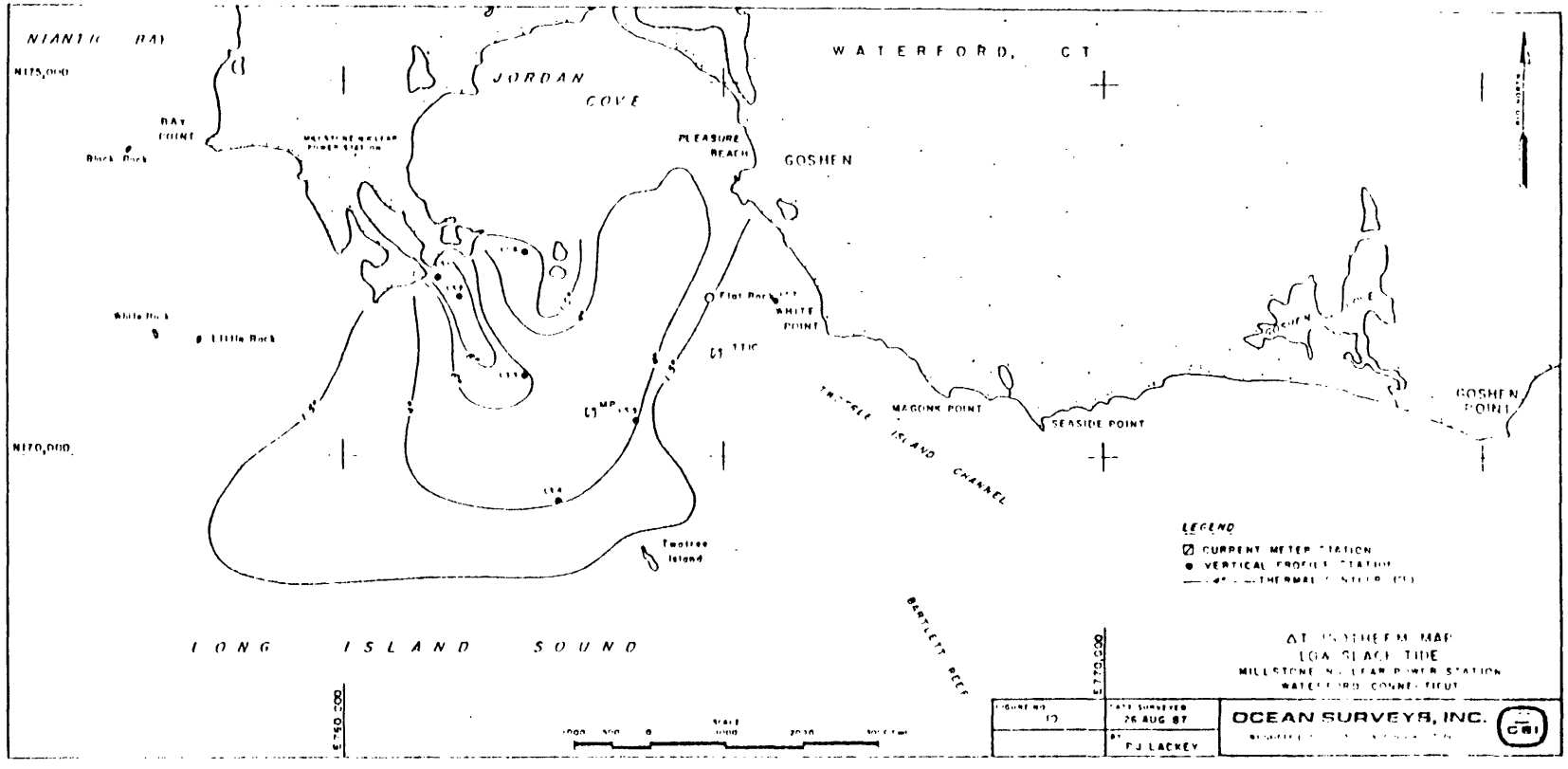

Figure 4.9b) Measurements on Aug. 26, 1987

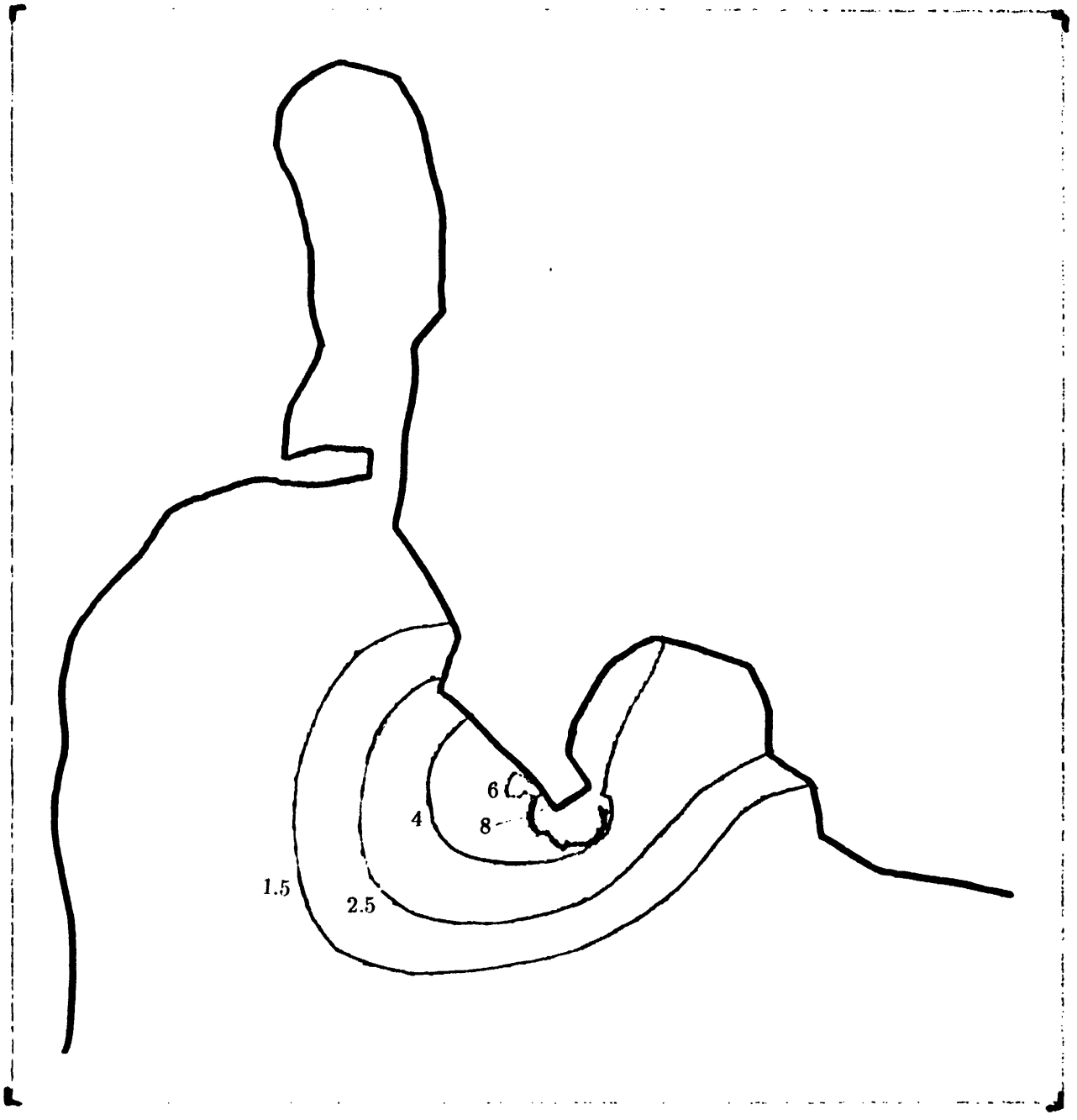

Figure 4.10 Surface layer excess temperatures (°F) for three units at maximum flood
a) Simulation

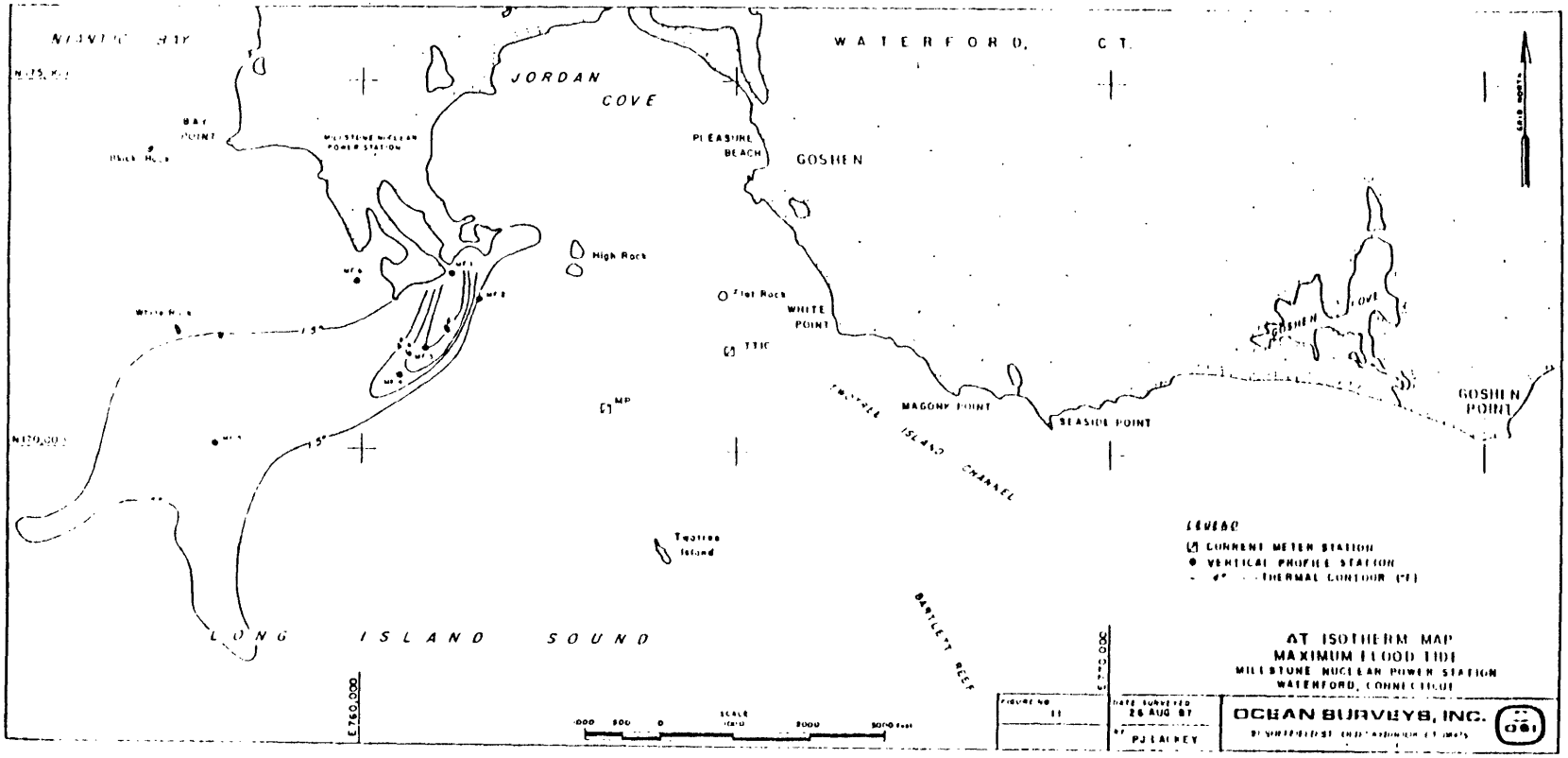

Figure 4.10b) Measurements on Aug. 26, 1987

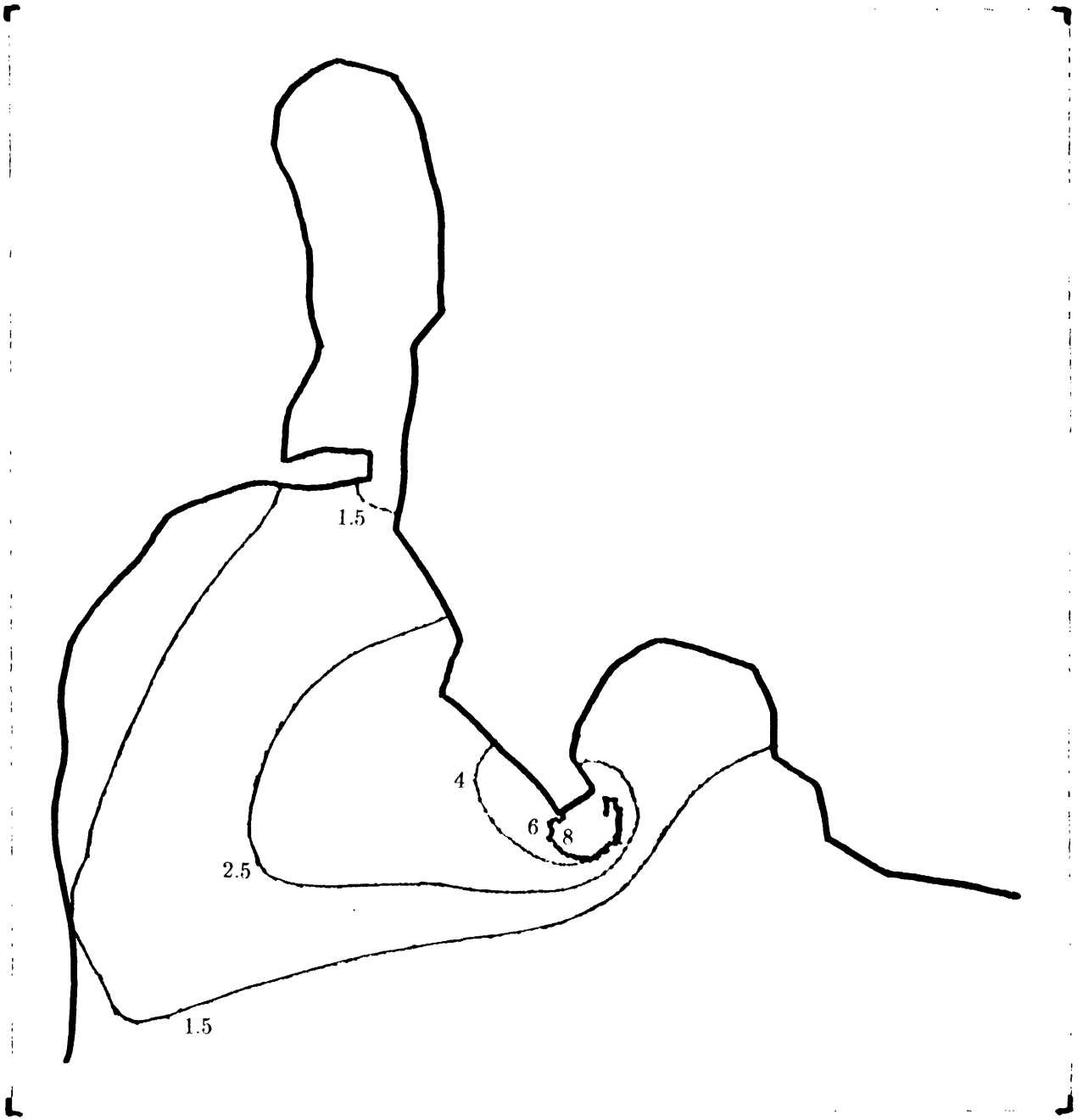

Figure 4.11 Surface layer excess temperatures (°F) for three units at high slack
a) Simulation

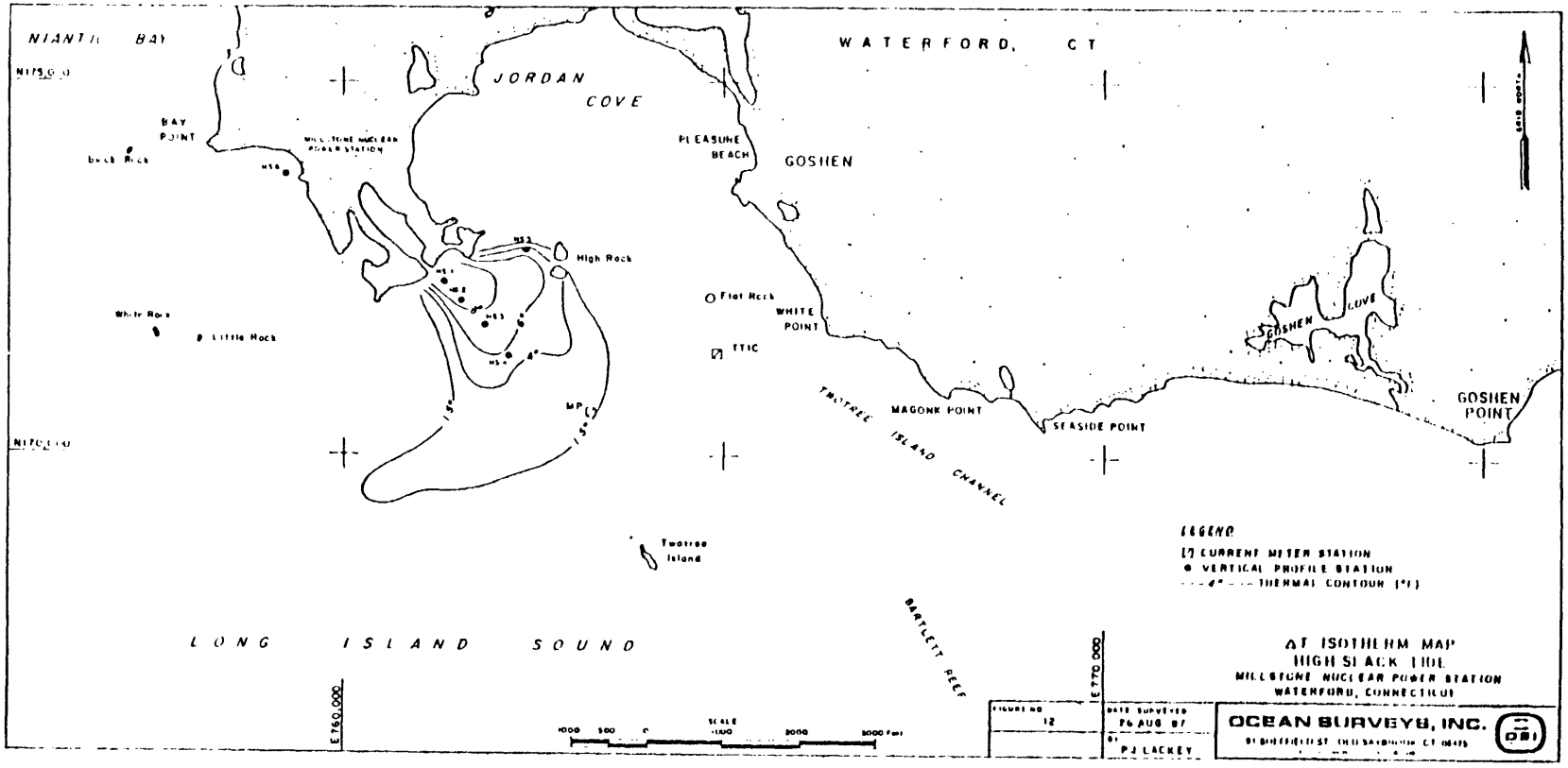

Figure 4.11b) Measurements on Aug. 26, 1987

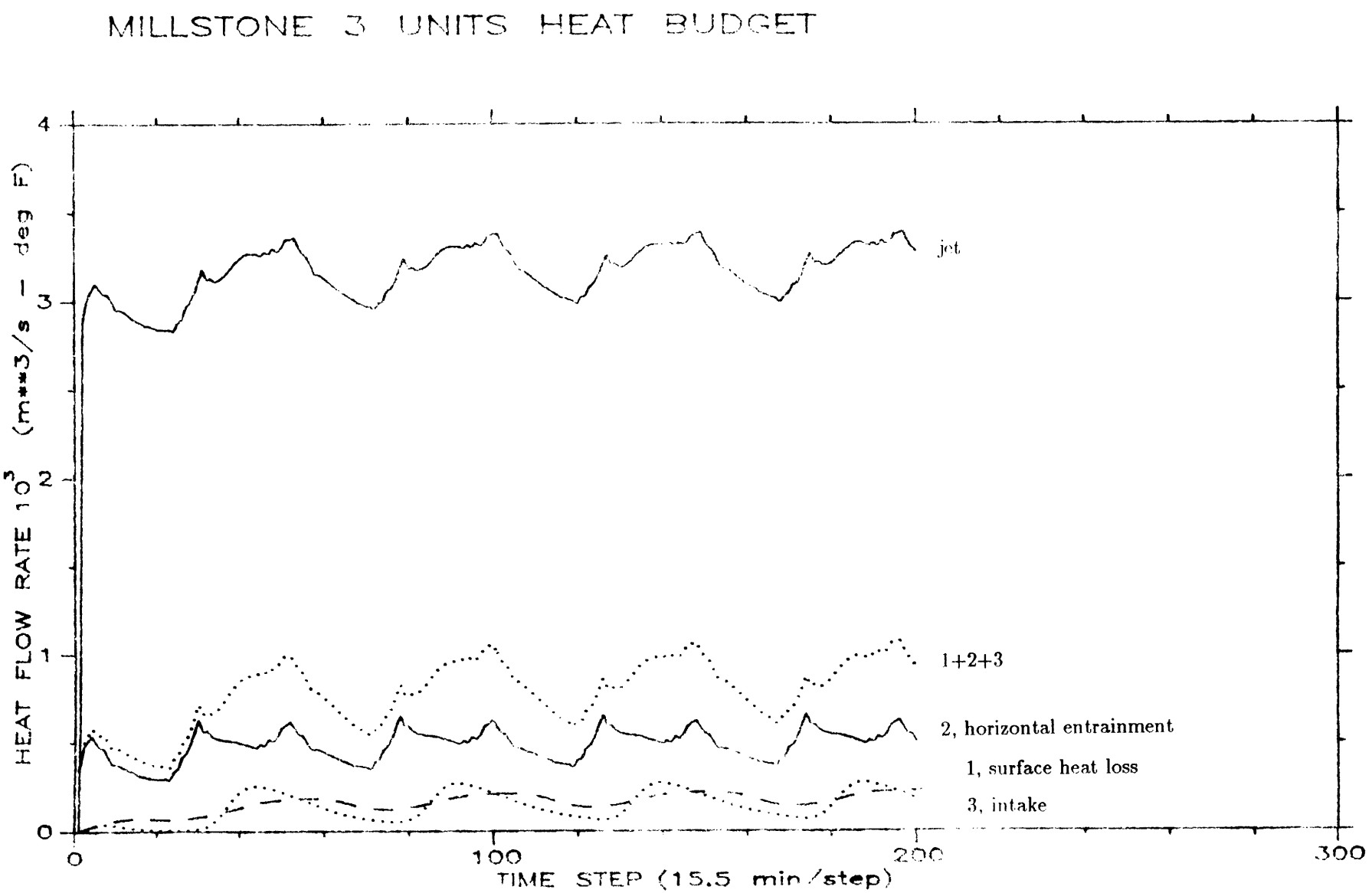

Figure 4.12 Time-varying parameters for dynamic heat budget calculations for three units

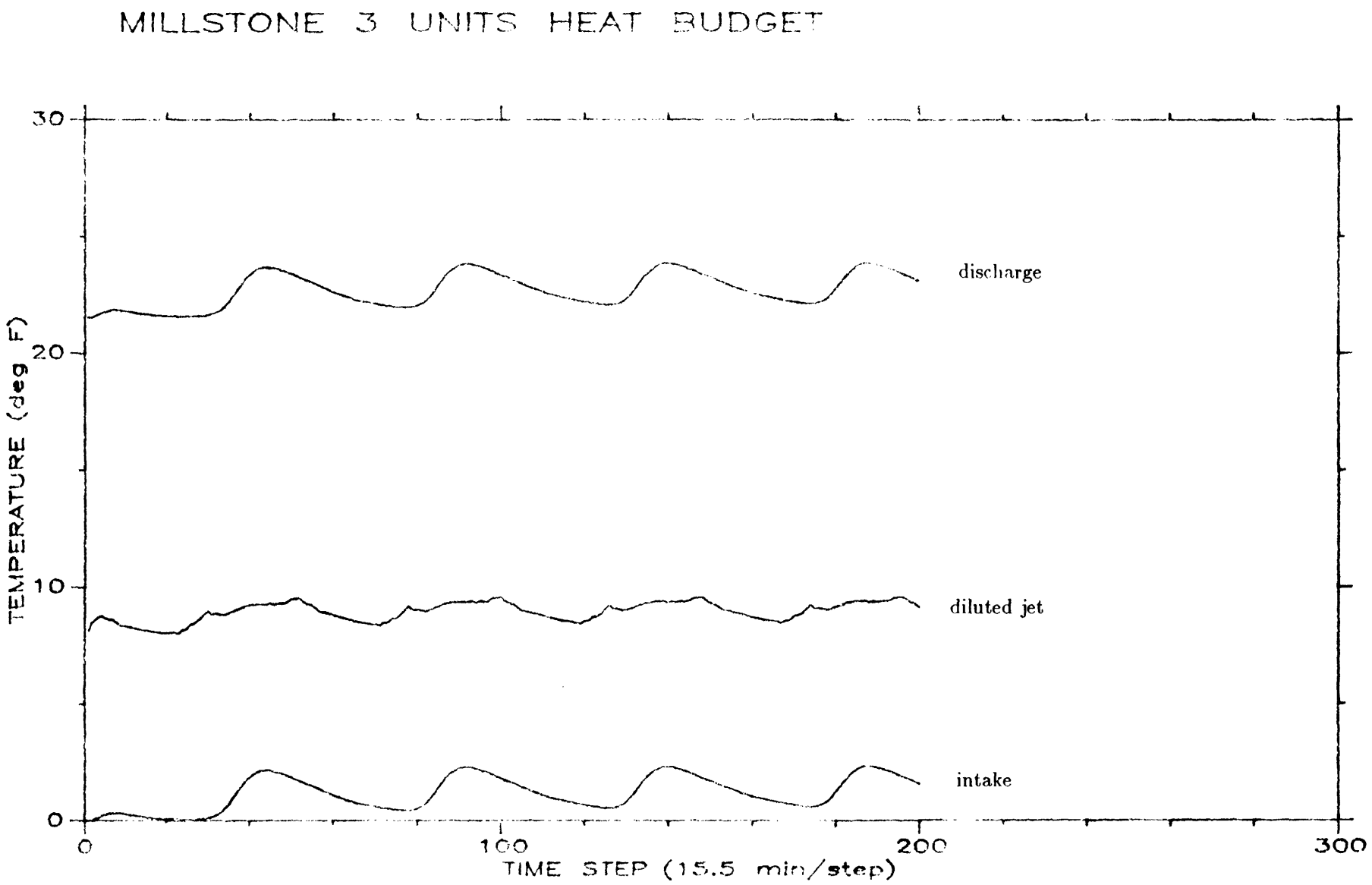

Figure 4.12b Discharge, intake, and diluted jet temperatures

V SUMMARY

This report describes how a pair of two-dimensional numerical models—a harmonic circulation model TEA and an Eulerian-Lagrangian transport model ELA—have been coupled to simulate thermal plume dynamics in the vicinity of coastal power plants. These simulations follow previous study by Kaufman and Adams (1981), but differ from most previous studies in that near field mixing is represented explicitly by specifying entrainment and mixed discharge fluxes (obtained from a separate near field model) as model boundary conditions. Combined with the near field simulations, the technique allows realistic simulation of time-varying temperature throughout the entire receiving water domain. The programs also allow particles to be tracked and provide a time history of various heat fluxes, discharge temperature, intake recirculation, etc. Additional model features added in this study allow simulation of surface wind drift and three-dimensional spreading due to vertical diffusion.

The models have been applied to two sites—Brayton Point Generating Station on Mt. Hope Bay in Massachusetts and Millstone Nuclear Power Station on Long Island Sound in Connecticut. At Brayton Point, simulations were made with both three- and four-unit operation and the former were compared with field measurements. At Millstone, calculations were made for both two- and three-unit operation and the latter were compared with field measurements. In both cases reasonable agreement was achieved.

Computational expense was found to be reasonable, requiring about two CPU hours on a MicroVax II to perform simulations to quasi steady state in a periodic (tidal) flow field. This is significantly less expensive than earlier calculations by Kaufman and Adams (1981) who used more traditional time-stepping models.

In the course of the study, several areas were identified for future research. Regarding the circulation model TEA, the linear version used in these calculations omits the

convective acceleration terms in the momentum equation which leads to excess circulation between discharge and intake. The non-linear version of TEA includes these terms, but was found to be numerically unstable for these applications. It would also be desirable to allow the near field boundary fluxes (both the magnitude and their location along the transition circle) to vary with tidal phase. An initial foray suggested that this was possible in a harmonic circulation model by introducing periodic boundary fluxes at both the dominant (tidal) frequency and two times the dominant frequency.

Calculations with the transport model ELA revealed strong sensitivity to the model time step. In the present formulation, with diffusion and advection computed in that order, the model overestimates temperatures (concentrations) near inflow boundaries, and the magnitude of error increases with Δt. In view of the computational advantages of using large Δt (and the fact that ELA is otherwise well suited for large Δt; Baptista, 1987), it is recommended that the formulation be changed such that the diffusion calculations follow advection and that, for locations near an inflow boundary, the time of travel from the boundary be incorporated in the diffusion matrix. It is also recommended that, in order to realistically simulate the build-up of background temperatures, outer boundaries be located as far away from the discharge as possible.

VI REFERENCES

Baptista, A., E. Adams, K. Stolzenbach. 1984. The solution of the 2-D unsteady, convective diffusion equation by the combined use of the FE method and the method of characteristics. Report No. 296, R. M. Parsons Laboratory, MIT.

Baptista, A. M., E., Adams, K. Stolzenbach. 1985. Comparison of several Eulerian-Lagrangian models to solve the advection-diffusion equation. *Proc. of Int'l Symp. on Refined Flow Modeling and Turbulence Measurements*, U. of Iowa, Iowa City, Iowa.

Baptista, A., E. Adams, K. Stolzenbach. 1986. Accuracy analysis of the backwards method of characteristics. 6th Int'l Conf. on Fin. Elem. in Wat. Res., Lisbon.

Baptista, A. 1987. Solution of advection-dominated transport by Eulerian Lagrangian methods using the backwards method of characteristics. Ph.D. thesis, Dept. of Civil Engineering, MIT.

Jirka, G. H., E. E. Adams, K. D. Stolzenbach. 1981. Properties of buoyant surface jets. *Journal of Hydraulics Division, ASCE* 107.

Kaufman, J. T., E. E. Adams. 1981. Coupled near and far field thermal plume analysis using finite element techniques. Report No. MIT-EL 81-036, MIT Energy Laboratory.

Kossik, R. F, et al. 1987. User's manual for ELA: A two-dimensional Eulerian-Lagrangian transport model. MIT Dept. of Civil Engineering.

Marine Research, Inc. 1978. Brayton Point investigations, Aug.-Oct. 1977. Quarterly Progress Report, Falmouth, Mass.

Northeast Utilities Environmental Lab (NUEL). 1987. Monitoring the marine environment of Long Island Sound at Millstone Nuclear Power Station, Waterford, Connecticut: Summary of studies prior to Unit 3 operation. Northeast Utilities Environmental Lab, Waterford, Connecticut.

Northeast Utilities Environmental Lab (NUEL). 1988. Monitoring the marine environment of Long Island Sound at Millstone Nuclear Power Station, Waterford, Connecticut: Three-unit post-operational studies, 1986-1987. Northeast Utilities Environmental Lab, Waterford, Connecticut.

Ryan, P. J., D. R. F. Harleman, and K. D. Stolzenbach. 1979. Surface heat loss from cooling ponds. *Water Resources Research* 10(5):930-938.

Stolzenbach, K., and E. Adams. 1979. Thermal plume modeling at the Millstone Nuclear Power Station. Report to Northeast Utilities Service Company.